

**Diagenesis of middle Ordovician rocks from the
Lake Simcoe area, south-central Ontario**

by

Laura Mancini

A thesis
presented to the University of Waterloo
in fulfillment of the
thesis requirement for the degree of
Master of Science
in
Earth Sciences

Waterloo, Ontario, Canada, 2011
© Laura Mancini 2011

AUTHOR'S DECLARATION

I hereby declare that I am the sole author of this thesis. This is a true copy of the thesis, including any required final revision, as accepted by my examiners.

I understand that my thesis may be made electronically available to the public

ABSTRACT

Middle Ordovician carbonates in the Lake Simcoe area, south-central Ontario were examined to determine if: (1) The $\delta^{18}\text{O}$ values of early-stage calcite cement in hardgrounds are useful proxies for Ordovician seawater $\delta^{18}\text{O}$ values; (2) a regional hydrothermal event affected middle Ordovician strata in the Lake Simcoe area. Whole rock samples of middle Ordovician hardgrounds and immediately overlying limestones containing early calcite cement have $\delta^{13}\text{C}$ values ranging from -1.7 to +2.9‰ (PDB) and $\delta^{18}\text{O}$ values ranging from -6.9 to -2.9‰ (PDB). Hardground $\delta^{18}\text{O}$ values and the similarity of the isotopic composition between the hardgrounds and overlying limestones are consistent with diagenetic alteration during shallow burial, which indicates the hardgrounds are not useful proxies. Late-stage calcite cements have $\delta^{13}\text{C}$ values from -8.4 to +2.9‰ (PDB) and $\delta^{18}\text{O}$ values from -11.4 to -6.0‰ (PDB). Late-stage microcrystalline dolomites have $\delta^{13}\text{C}$ values from -3.9 to +0.4‰ and $\delta^{18}\text{O}$ values from -10.7 to -7.6‰. Late-stage saddle dolomites have $\delta^{13}\text{C}$ values from -1.7 to 1.9‰ and $\delta^{18}\text{O}$ values from -13.8 to -8.5‰. The late-stage carbonate $\delta^{18}\text{O}$ values are more negative than the early-stage carbonate $\delta^{18}\text{O}$ values and are interpreted to reflect progressively deeper burial diagenesis.

Four types of fluid inclusions were identified in late-stage calcite, saddle dolomite, barite, and quartz. Type 1 inclusions are aqueous liquid-rich with very consistent low to very low vapour-liquid ratios and are of primary, secondary pseudosecondary and indeterminate origins. Type 2 inclusions are aqueous liquid-only and are of primary and secondary origins. Type 3 inclusions are oil-bearing, liquid-rich with low to medium vapor-liquid ratios and are of secondary origin. Type 4 inclusions are vapour-only and are of indeterminate origin. The type 4 inclusions analyzed did not yield any microthermometric data suggesting they are empty cavities that have lost all their fluid.

Fluid inclusions of primary, secondary and pseudosecondary origins in calcite, dolomite and quartz have overlapping homogenization temperatures ranging from 43 to 188°C. Fluid inclusions of indeterminate origin in calcite and barite have homogenization temperatures from 80 to greater than 200°C. Petrographic and microthermometric evidence indicates that fluid inclusion homogenization temperatures greater than 150°C most likely are caused by stretching or leaking; therefore, are discounted. Fluid inclusion types 1 and 2 represent two fluid inclusion assemblages (FIA) based on final ice melting temperatures. The high salinity (10 to 30 wt%_{CaCl₂}) inclusions in FIA 1 are of primary, secondary, pseudosecondary and indeterminate origin in calcite, dolomite, barite and quartz. Fluid inclusions in FIA 1 are interpreted as reflecting saline basin brines from which the host minerals precipitated during burial diagenesis. The low salinity (0 to 2.7 wt%_{CaCl₂}) inclusions in FIA 2 are of secondary and indeterminate origin in calcite. Fluid inclusions in FIA 2 may reflect a meteoric origin such as in a vadose or phreatic environment based on inclusions containing different phases and variable vapor-liquid ratios. Alternatively the low salinity inclusions may reflect alteration from an influx of meteoric fluids that migrated through basement faults and fractures during periods of uplift and erosion.

Early and late-stage carbonates from this study precipitated from ¹⁸O-depleted pore fluids and/or at progressively higher temperatures accompanying deeper burial. The FIA 1 homogenization temperatures support burial diagenesis at 66 to 80°C if it is assumed the rocks were buried 2 km, the surface temperature was 20°C and the geothermal gradient was between 23 to 30°C/km.

An alternative interpretation is mineral precipitation during a regional hydrothermal event. Burial diagenesis does not explain the fluid inclusion homogenization temperatures of 90°C and greater unless geothermal gradients are higher than 35°C/km or burial depth is increased to 3 km or more. However, thermal maturity of organic matter in the Michigan Basin suggests Ordovician strata were never buried more than 2 km. Four models for regional hydrothermal fluid migration are: (1) gravity-driven flow; (2)

‘squeegee-type’ fluid flow; (3) convection cell fluid flow; and (4) structurally-controlled fluid flow. The gravity-driven model relies on continental heat flow and an influx of meteoric water from basin catchment areas. For the ‘squeegee, convection cell and structurally controlled models, hot fluids could have entered the region from several conduits concurrently during episodic reactivation of basement faults and fracture systems in response to intracratonic stresses created by the continuous interaction of tectonic plates. Determining which of the models best explains regional hydrothermal fluid flow in the Michigan Basin is difficult for several reasons; (1) surface temperatures and maximum burial temperatures at the time of mineral precipitation in the Michigan Basin during the Ordovician are unknown; (2) the timing of mineral precipitation in relation to tectonic pulses is undetermined; (3) there is as yet no known deep-seated heat sources in the Michigan Basin for convection to occur; and (4) it is unknown whether advection is a major process in the Michigan Basin. A collaborative multi-disciplinary research project covering geology, geophysics and hydrogeology would provide much more integrated data than is currently available from stable isotopes, fluid inclusions and organic matter.

ACKNOWLEDGEMENTS

The author would like to thank Dr. Mario Coniglio for his unending patience, assistance, support and insight he provided during this research project, also Dr. Robert Linnen for all his advice and patience in explaining and re-explaining certain topics. Thank you to Gordon Wood, from the petrography lab at the University of Western Ontario, for the high quality polished sections and speedy job, and to Derek Armstrong from the OGS and Jim Reimer for their knowledge and input. Thanks to Hagit Blumenthal and Corina McDonald for their moral support and jokes. Thank you to Tom Savage for his GIS expertise. Lastly thanks to Charlie, Niki and Fio for tolerating shorter walks in the park, no trail rides and very little grooming during this time.

TABLE OF CONTENTS

	Page
AUTHOR'S DECLARATION	ii
ABSTRACT	iii
ACKNOWLEDGEMENTS	vi
TABLE OF CONTENTS	vii
LIST OF FIGURES	x
LIST OF TABLES	xii
CHAPTER 1: GEOLOGY OF THE LAKE SIMCOE AREA	
Introduction	1
Previous Work	2
Regional Geology	7
Stratigraphy	9
Objective	16
Methodology	17
CHAPTER 2: PETROGRAPHY OF THE SIMCOE GROUP CARBONATES	
Introduction	19
Hardground Morphology	19
Petrography of Hardgrounds, Early Diagenetic Calcite and Early Replacive Dolomite	25
Petrography of Late-stage Carbonate	29
CHAPTER 3: EARLY CARBONATE CEMENTS AND HARDGROUNDS AS POSSIBLE PROVIDERS OF LOCAL MARINE BASELINE $\delta^{18}\text{O}$	
Introduction	34
Results of Stable Isotope Analyses of Early Diagenetic Calcite and Early Replacive Dolomite	35

Discussion	36
CHAPTER 4: LATE-STAGE CARBONATES OF THE SIMCOE GROUP	
Introduction	43
Isotope and Fluid Inclusion Analyses	43
<i>Late-stage Mineral Precipitate Isotope Data</i>	44
Fluid Inclusion Petrography	45
<i>Late-stage Mineral Precipitate Fluid Inclusion Data</i>	50
Microthermometry	52
<i>Homogenization Temperatures</i>	52
<i>First Ice Melting Temperatures</i>	56
<i>Final Ice Melting Temperatures and Salinity of Fluid Inclusions</i>	58
Homogenization Temperatures and Salinity	61
Discussion	65
Conclusion	70
CHAPTER 5: INTERPRETATION AND DISCUSSION OF STABLE OXYGEN ISOTOPE AND MICROTHERMOMETRIC RESULTS	
Introduction	72
Burial Diagenesis	72
<i>Evaluation of homogenization temperatures in support of burial diagenesis</i>	74
<i>Support for estimated geothermal gradients, burial depths and temperatures</i>	76
Hydrothermal Event	81
<i>Support for a Regional Hydrothermal Event</i>	82
<i>Proposed Models for Regional Fluid Flow Systems</i>	85
Discussion	89

Potential Paragenetic Sequence of Events in the Lake Simcoe Area	91
CHAPTER 6: CONCLUSIONS	94
Future Work	96
REFERENCES	97
APPENDIX A <i>Stable carbon and oxygen isotope data</i>	103
APPENDIX B <i>Fluid inclusion microthermometry data</i>	109

LIST OF FIGURES

	Page
Figure 1. Satellite image of the Lake Simcoe area	2
Figure 2. Location of Lake Simcoe in the Western St. Lawrence Platform	8
Figure 3. Stratigraphic column of the Simcoe Group of south-central Ontario	9
Figure 4. Hardground morphologies	21
Figure 5. Rolling hardground in the Moore Hill bed of the Bobcaygeon Formation	23
Figure 6. Hummocky hardground in the Moore Hill bed of the Bobcaygeon Formation	24
Figure 7. Undercut hardground at the contact between the Gull River and Bobcaygeon formations	24
Figure 8. Smooth hardground at the contact between the Gull River and Bobcaygeon formations	25
Figure 9. Hardground composed of fine-grained peloidal bioclastic grainstone	27
Figure 10. Hardground composed of crinoidal-peloidal grainstone	27
Figure 11. Hardground composed of packstone	28
Figure 12. Hardground composed of peloidal bioclastic grainstone	28
Figure 13. Fracture-fill coarse-calcite	30
Figure 14. Fracture-fill calcite associated with barite	30
Figure 15. Chalcedony cement	30
Figure 16. Fracture-fill coarse-calcite	31
Figure 17. Saddle dolomite with coarse crystalline calcite	31
Figure 18. Saddle dolomite with coarse crystalline calcite and quartz	31
Figure 19. Stable isotope geochemistry of bulk rock samples from the Lake Simcoe area, Ontario	36
Figure 20. Graph of Ordovician seawater $\delta^{18}\text{O}$ values	40
Figure 21. Graph of stable isotope geochemistry of late-stage calcite cement and late-stage dolomite from the Lake Simcoe area	45

Figure 22. Type 1 vapor-liquid fluid inclusion. Sample LM-9A	47
Figure 23. Type 1 vapor-liquid fluid inclusion cluster. Sample LM-5.1	47
Figure 24. Small cluster of type 1 and type 2 fluid inclusions. Sample LM-10B	47
Figure 25. Type 2 liquid-only fluid inclusions. Sample 99-101	47
Figure 26. Type 2 liquid-only fluid inclusions. Sample 99-132	48
Figure 27. Type 3 oil inclusions. Sample LM-6	48
Figure 28. Type 3 oil inclusion (close-up). Sample LM 6	48
Figure 29. Type 3 oil inclusions in fracture in barite. Sample LM-6	48
Figure 30. Fluorescence photomicrograph of oil inclusion. Sample LM-6	48
Figure 31. Type 3 oil inclusions in saddle dolomite. Sample 99-120	49
Figure 32. Type 4 vapor-only fluid inclusions. Sample LM-4	49
Figure 33. Saddle dolomite and calcite. Sample 99-120	52
Figure 34. Histogram of homogenization temperatures of all types and origins of fluid inclusions	55
Figure 35. Histogram of homogenization temperatures of inclusions in calcite, dolomite, barite, and quartz	56
Figure 36. First ice melting temperatures of inclusions in calcite, dolomite, barite, and quartz	58
Figure 37. Salinities of inclusions in calcite, dolomite, barite, and quartz	61
Figure 38. Fluid inclusions in saddle dolomite. Sample 99-120	62
Figure 39. Homogenization temperatures vs. salinity graph	63
Figure 40. Inclusions of various phases and variable vapor-liquid ratios	66
Figure 41. Satellite image of the Lake Simcoe area with fluid inclusion types and sample numbers	69
Figure 42. Graph of stable carbon and oxygen isotope geochemistry for early and late-stage carbonates	74
Figure 43. Paragenetic sequence of the Simcoe Group in the Lake Simcoe area, south-central Ontario	93

LIST OF TABLES

	Page
Table 1: Petrographic description of late-stage carbonates and associated minerals	31
Table 2: Petrographic description of fluid inclusions	50
Table 3: Microthermometric data for type 1 and type 2 fluid inclusions	64
Table 4: List of calculated burial temperatures for Ordovician carbonates of southern Ontario using surface temperatures of the Ordovician tropical seawater environment	75
Table 5: List of calculated burial temperatures for Ordovician carbonates of southern Ontario using surface temperatures of the Ordovician temperate seawater environment	76
Table 6: Comparison of geothermal gradients and burial depths	81

CHAPTER 1: GEOLOGY OF THE LAKE SIMCOE AREA

Introduction

The focus of this study is the middle Ordovician rocks in the area east of Lake Simcoe between latitudes 44° 31' N and 44° 45' N and between longitudes 79° 20' W and 78° 36' W (Fig. 1). These strata, which are important for aggregate and building stones, have been correlated with carbonates elsewhere in Ontario that are significant hydrocarbon reservoirs, such as in eastern Essex County and southern Kent County (Carter and Trevail, 2000; Sangster et al., 2008). Hydrocarbon reservoirs in Ontario produced 13.8 million cubic meters of crude oil and 35.6 billion cubic meters of natural gas by the end of 2006 (MNR, 2011). There are an estimated 14 million cubic meters of oil and 36 billion cubic meters of natural gas resources remaining in Ontario (MNR, 2011). The producing reservoirs and estimated resources are associated with diagenetic dolomitization in the Black River and Trenton limestones (Carter and Trevail, 2000; Sangster et al., 2008); therefore the carbonates in this study could provide new insight into the diagenetic evolution of the carbonates in southwestern and south-central Ontario. Understanding the diagenetic evolution of these carbonates may help establish timing relationships between mineral precipitation, hydrocarbon formation, and basement structural features as conduits for fluid flow.

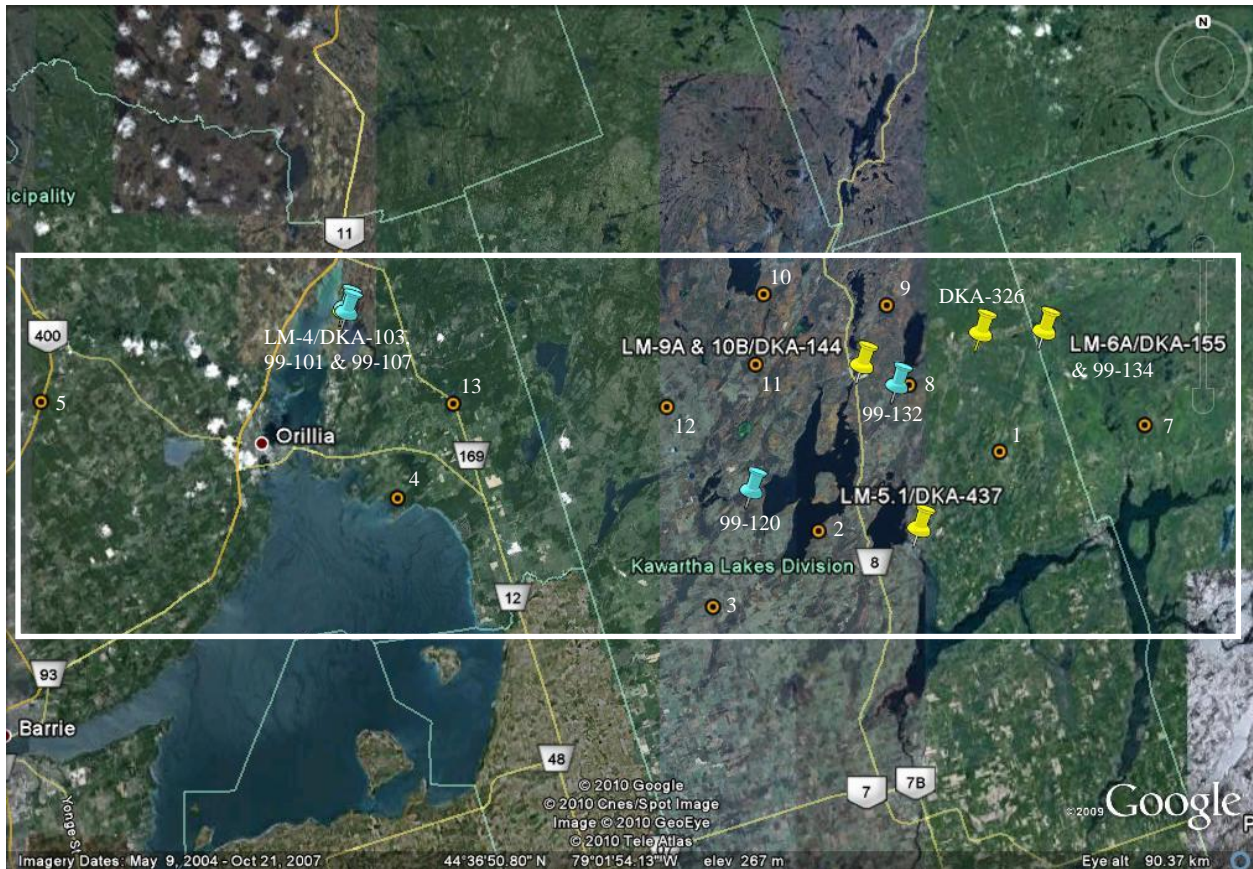


Fig. 1 Satellite image of the Lake Simcoe area. The study area is outlined in white. Yellow pins are LM-series outcrop sample areas for samples collected by the author in 2008, turquoise pins are 99-series outcrop sample areas for samples collected by Mario Coniglio in 1999, and orange markers are OGS core locations for core drilled in 1992-1993 (Table 1). Image from Google Earth, 2009.

Previous Work

The Ordovician rocks in south-central Ontario have been studied by geologists and paleontologists for 150 years (Armstrong, 2000). One of the earliest geological reports on the Lake Simcoe area was done by Alexander Murray in 1842 (Liberty, 1969). Johnston published the first maps of the Lake Simcoe area between 1906 and 1912 (Liberty, 1969; Melchin et al., 1994). From the 1950s to the early 1990s the Ontario Geological Survey (OGS) produced reports and maps of the Lake Simcoe area. Liberty (1969) proposed several changes to the organization of the strata to reduce confusion regarding the nomenclature. In 1990 the OGS

began an extensive study of the Lake Simcoe area. The study included the drilling of 12 boreholes in an east-west trend across the northern Lake Simcoe area. The cores were used by Armstrong and Anastas (1992) and Armstrong and Rheume (1993) to create the most recent maps of the Lake Simcoe area.

Besides mapping, many other studies have been carried out on the sedimentary and depositional aspects of Ordovician strata in southern and south-central Ontario. Brett and Brookfield (1984), Brookfield and Brett (1988), and Brookfield (1988) examined facies and diagenesis of Ordovician rocks in southern Ontario. Brett and Brookfield (1984) examined facies and stratigraphic sequences to determine the environments of formation of different types of hardgrounds. Brookfield and Brett (1988) investigated facies recognized in the previous study in more detail to support their hypothesis of a shoal-basin model for mid-Ordovician deposition. Brookfield (1988) looked at several different factors such as depositional rates, grain type, mineralogy and geochemistry and found mid-Ordovician limestones of southern Ontario to be more compatible with deposition in temperate seas rather than the generally assumed tropical seas. Noor (1989) examined lithostratigraphy of the mid-Ordovician in southern Ontario and suggested the Shadow Lake Formation be reassigned from the Basal Group, where Liberty (1969) placed it, into the Simcoe Group. Noor (1989) based the proposed reclassification on genetic similarities between the Shadow Lake Formation and Simcoe Group. Grimwood (1998) examined storm sedimentation, hardgrounds and lithofacies of the Black River Group in the Lake Simcoe area. Grimwood (1998) agreed with Brookfield (1988) that the Black River Group (Simcoe Group) in the Lake Simcoe area indicated a change from tropical to temperate water conditions during time of deposition. Grimwood et al. (1999) performed petrographic analyses of

samples from the 12 cores drilled by the OGS mentioned above. Grimwood et al. (1999) identified seven lithofacies from the Shadow Lake, Gull River, and Bobcaygeon formations that showed an overall transgressive sequence in a low energy ramp environment.

Coniglio et al. (1990), Melchin et al. (1994), and Brookfield and Elgadi (1998) produced fieldtrip guidebooks for south-central Ontario related to the Ontario Petroleum Institute, Geological and Mineralogical associations of Canada, and Geological Society of America annual conferences, respectively. LeBaron and Williams (1990) reported on carbonate building stone resources and Armstrong (2000) examined the OGS cores from the 1990 investigation mentioned above using petrography, geochemistry and aggregate quality analysis for a study on alkali-reactive limestone.

Diagenesis of Ordovician strata in southwestern and southern Ontario has been the topic of several studies. Mukherji and Young (1973) investigated the diagenetic history of the Black River Group in southern Ontario. They proposed the Black River Group underwent two stages of diagenesis (early and late) with most of the alterations having occurred during the early stage under a thin layer of sediment. Mukherji and Young (1973) also suggested late-stage alteration occurred mainly during subaerial exposure. Wilkinson et al. (1982) suggested that middle Ordovician hardgrounds from Kirkfield, Ontario remained unaltered since their original formation and that these hardgrounds were cemented by low Mg-calcite based on the similarity of these interparticle cements to Holocene low Mg-calcites. Coniglio and William-Jones (1992) performed petrographic and geochemical analyses on Ordovician rocks from the Manitoulin Island area. Coniglio and William-Jones (1992) suggested the Manitoulin Island carbonates are

very similar to Trenton reservoir rocks elsewhere in the Michigan Basin. They also concluded that fractures and hydrothermal fluids were important factors in the diagenesis of the Manitoulin Island carbonates. Middleton et al. (1993) investigated dolomitization of Trenton and Black River carbonate reservoirs in southwestern Ontario and identified two types of dolomite in the Trenton Group: 1) cap dolomite formed from compactional dewatering of the overlying Blue Mountain shale, and 2) fracture-related dolomite formed from dolomitizing fluids that flowed through fracture systems connecting the Precambrian basement rocks to the Black River and Trenton strata (Middleton et al., 1993). Expanding on the previous two studies, Coniglio et al. (1994) concluded dolomitization of the Black River and Trenton strata occurred during burial diagenesis under the influence of hydrothermal fluids. This conclusion was based on fluid inclusion homogenization temperatures elevated beyond those anticipated during deep burial.

Several fluid inclusions studies of the Simcoe Group and correlative rocks in Michigan, Indiana, and Wisconsin were done to determine whether dolomite is burial or hydrothermal in origin. Simo et al. (1994) looked at fluid inclusions, $\delta^{18}\text{O}$ and $^{87}\text{Sr}/^{86}\text{Sr}$ values for dolomites of the Glenwood Formation located in the central part of the Michigan Peninsula. Simo et al. (1994) found variable homogenization temperatures and $\delta^{18}\text{O}$ values, which were interpreted to reflect either variable temperatures of the dolomitizing fluid or post-entrapment alteration. After correcting homogenization temperatures for pressure (0.5 kilobar correction) Simo et al. (1994) concluded the trapping temperatures were consistent with dolomitization in a deep burial setting. Yoo et al. (2000) studied dolomitization and dolomite neomorphism in the Trenton and Black River Limestones along the Kankakee Arch, Northern Illinois using stable isotopes, fluid inclusions and mineral associations. From final ice melting temperatures Yoo et al. (2000)

determined that the dolomitizing fluid was saline brine with a composition of 30.2 to 15.2 wt% NaCl equivalent. Based on variable stable isotope composition, fluid inclusion homogenization temperatures and salinities, Yoo et al. (2000) suggested the dolomite precipitated from late saline diagenetic fluids that ascended from fractures and faults in the basin bottom during deep burial. This is supported by the fact that the dolomite was found mainly along pre-existing linear fault zones (Yoo et al., 2000).

Luczaj (2006) investigated dolomitization of Ordovician carbonates near the Wisconsin Arch in the Michigan Basin. From petrographic and geochemical analysis Luczaj (2006) identified 3 types of regional dolomite: 1) early stage; 2) middle stage; and 3) late stage. Types 2 and 3 are found to be closely associated with Mississippi Valley Type (MVT) Fe, Pb, and Zn sulphide mineralization. Luczaj (2006) interpreted two-phase aqueous fluid inclusion assemblage homogenization temperatures, regional and stratigraphic dolomite distribution, and oxygen isotope data as reflecting a hydrothermal origin for the dolomite rather than deeper burial and/or elevated paleogeothermal gradients. Luczaj (2006) suggested the rocks were dolomitized by ¹⁸O-depleted high temperature fluids while there was an active hydrothermal system in the Michigan Basin.

Despite the abundance of research done in southern and southwestern Ontario, there are still many questions needing to be addressed. Coniglio (2000) pointed out several questions, for example, what stratigraphic controls allowed late-stage dolomitization and reservoir development along fracture systems in Michigan Basin strata but not in equivalent fractured strata in the Lake Simcoe area? Is the late-stage dolomitization and reservoir development in

Michigan Basin strata related to unspecified basinal controls? Why were these controls not a factor in later diagenesis as evidenced by the similar suite of later diagenetic minerals (e.g., ferroan saddle dolomite, fluorite, etc.) in the Lake Simcoe area and Michigan Basin? Coniglio (2000) stressed the importance of addressing these questions to further understand what factors control hydrocarbon reservoir development in some Ordovician carbonates.

Regional Geology

The long history of stratigraphic and sedimentological studies in southern Ontario has resulted in a comprehensive understanding of the regional geology.

The Lake Simcoe area is part of the Western St. Lawrence Platform (Fig. 2), which consists of Cambrian to upper Devonian strata (Johnson et al., 1992). In southern Ontario the Paleozoic succession covers approximately 70,000 km² extending southwest from the Ontario-Quebec border to Lake Huron and to the northeastern end of Lake Erie (Johnson et al., 1992; Melchin et al., 1994). The stratigraphic succession in the Lake Simcoe area consists of Ordovician rocks unconformably overlying Precambrian basement (Armstrong, 2000). The Ordovician succession reaches a maximum 100 m thickness in the southern part of the Lake Simcoe area (Armstrong, 2000).

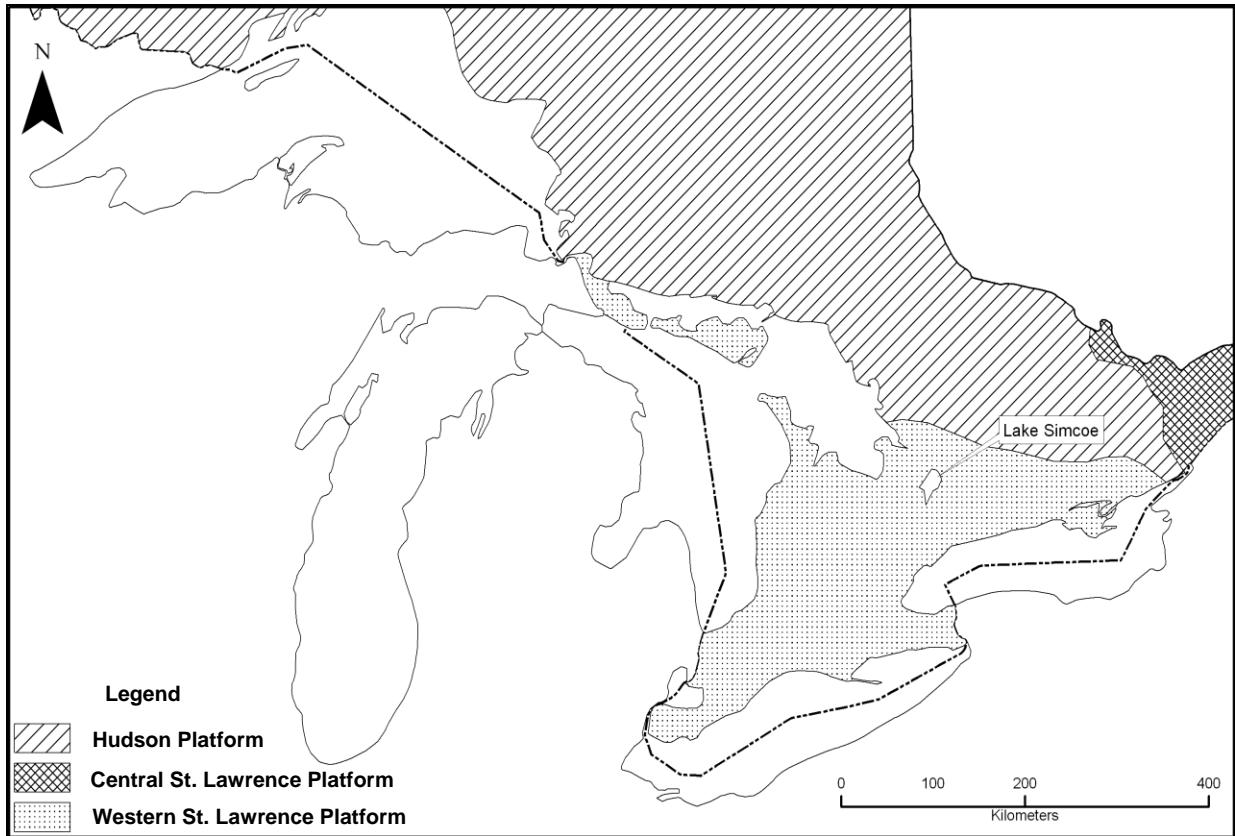


Fig. 2 Location of Lake Simcoe in the Western St. Lawrence Platform (dotted area) in relation to the Hudson and Central St Lawrence platforms

The Ordovician strata in the Lake Simcoe area were deposited in a shallow epicontinental sea formed from the Tiptecanoe transgression that occurred during Blackriverian time (Johnson et al., 1992; Armstrong, 2000). The transgression is seen as an overall deepening-upward trend (Fig. 3) of basal nearshore siliclastics to intertidal limestone and dolostone to shoal and subtidal lagoonal limestone to a deep shelf limestone and shale mix (Armstrong, 2000). Three major structural intracratonic features were present and periodically active during deposition of the Paleozoic strata on the Western St. Lawrence Platform: the Michigan Basin, the Appalachian Basin, and the intervening Algonquin Arch (Johnson et al., 1992).


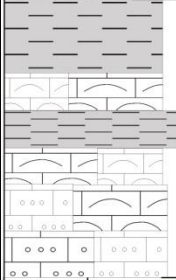
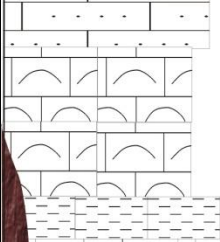
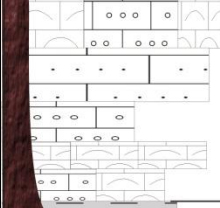

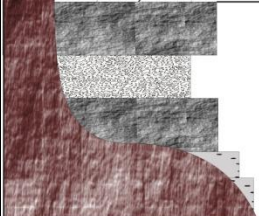
Simcoe Group south-central Ontario		Depositional Environment and Lithologies
	Collingwood member	Deep shelf Petroliferous, argillaceous lime mudstone
	L Lindsay Formation	Deep shelf Bioclastic lime mudstone-wackestone Shallow shelf Bioclastic wackestone-packstone, bioclastic grainstone
	U L Verulam Formation	Shallow shoal intra-bioclastic grainstone Shoal-shallow shelf Bioclastic packstone-grainstone Deep shelf Bioclastic wackestone-grainstone calcareous shale
	U M L Bobcaygeon Formation	Shallow shelf Bioclastic grainstone Shallow shelf wacke-grainstone + shale Shoal Intra-peloidal wacke-grainstone bioclastic wackestone
	U L Gull River Formation	Lagoon-tidal flat Lime mudstone Dolostone
	Shadow Lake Formation	Nearshore-supratidal Arkosic siltstone, argillaceous sandstone conglomerate

Fig. 3 Stratigraphic column showing deepening-upward trend in the rocks of the Simcoe Group of south-central Ontario (Modified from Armstrong, 2000).

Stratigraphy

The shallow-water marine carbonates and craton-derived clastic rocks in the Lake Simcoe area are part of the Simcoe Group (Fig.3). The Simcoe Group was deposited on top of the

eroded surface of the Precambrian basement during the Ordovician (Johnson et al., 1992). The Lindsay Formation and Collingwood member (Fig. 3) in the uppermost Simcoe Group are not seen in the study area therefore they are not included in the stratigraphic descriptions below.

Shadow Lake Formation

The Shadow Lake Formation (Fig. 3) contains the oldest Paleozoic rocks in south-central Ontario and unconformably overlies Precambrian Grenville basement (Armstrong, 2000). The Shadow Lake Formation is composed of non-fossiliferous argillaceous arkosic sandstone and conglomerate, siliclastic mudstone and siltstone, and some argillaceous dolostone and limestone (Armstrong, 2000). The rocks range in thickness from 0 to 10 m and are red, maroon, green, brown to buff, and green and brownish-grey in color (Melchin et al., 1994; Armstrong, 2000). Sedimentary structures include ripple-marks, planar and cross-lamination, burrows, and mud-cracks (Melchin et al., 1994). The different rock types are often interbedded and contacts between beds are gradational. The deposits are interpreted as being near-shore marine transgressive lag sediments (Melchin et al., 1994). The Shadow Lake Formation is conformably overlain by the Gull River Formation (Armstrong, 2000).

Gull River Formation

The Gull River Formation is informally subdivided into a lower and upper member based on lithostratigraphy:

lower member

The lower member (Fig. 3) is up to 15 m thick with light green, grey, and brown beds (Armstrong, 2000). The lower member is composed of limestone, dolostone, and fine-grained argillaceous dolomitic limestone (Armstrong, 2000) and is interpreted as having been deposited in a restricted intertidal to supratidal environment based on desiccation cracks and evaporite minerals and nodules, and its low fossil content (Armstrong, 2000). The lower member also contains subtidal lagoonal beds consisting of peloidal bioclastic packstone and grainstone, oolitic grainstone, and brown, burrow-mottled, fossiliferous wackestone and packstone (Armstrong, 2000). Fossils in the lower member consist of ostracods, cephalopods, gastropods, bivalves, brachiopods, and trilobites (Armstrong, 2000). The top of the lower member has a light green argillaceous dolomitic limestone bed (1.5 m thick) which has been informally called the “green marker bed” (GMB). The GMB is interpreted as having been deposited in a supratidal environment and its widespread occurrence suggests a regional regression at time of deposition (Armstrong, 2000).

upper member

The upper member (Fig. 3) is up to 10 m thick and is composed of thin intraclastic packstone and grainstone, and lime mudstone (Armstrong, 2000). The few fossils found in the upper member include ostracods, trilobites, and brachiopods. The upper member is interpreted as having been deposited in a tidal flat to shallow subtidal environment (Armstrong, 2000). Intraformational conglomerate, mudcracks, and fenestral fabric and vertical burrows containing sparry calcite are all found in the upper member (Armstrong, 2000). In the eastern part of the

study area the upper member contains wackestone, packstone, sandy peloidal and intraclastic lime mudstone, minor grainstone, siliclastic clay, silt, and minor sand grains (Armstrong, 2000). The lower contact of the upper member is sharp with the GMB. The upper contact of the upper member is gradational with the lower Bobcaygeon Moore Hill beds (Armstrong, 2000).

Bobcaygeon Formation

The Bobcaygeon Formation (Fig. 3) has a confusing history of nomenclature due to the use of both lithostratigraphic and biostratigraphic terms and to regional facies variations (Melchin et al., 1994). The Bobcaygeon Formation is subdivided informally into lower, middle, and upper members. The lower member is further informally subdivided into the Moore Hill beds (MHB) and an upper part (Armstrong, 2000). All subdivisions are based on lithostratigraphy (Melchin et al., 1994, and Armstrong, 2000).

lower member – Moore Hill beds

The MHB (Fig. 3) are typically 1 to 5 m thick, dark brown, medium to thickly bedded, and very fine-grained. The rocks are composed of bioclastic peloidal wackestone (Armstrong, 2000). The MHB are bioturbated and fossils found in these rocks include bivalves, brachiopods, bryozoans, cephalopods, gastropods, tabulate corals, and trilobites (Armstrong, 2000). The bioturbation and types of fossils indicate a subtidal depositional environment; the fine grain size indicates a more protected lagoonal environment compared to the Gull River Formation (Armstrong, 2000). The MHB also contains a k-bentonite layer less than 10 cm thick. The

lower contact with the Gull River Formation is sharp and often defined by hardgrounds which frequently form on bed surfaces within the MHB. The upper contact of the MHB with the upper part of the lower member is either sharp, expressed as a hardground or gradational (Armstrong, 2000).

lower member – upper part

The upper part (Fig. 3) of the lower member is up to 7 m thick, grey-brown in color and fine to coarse-grained. The rock is composed of fossiliferous, bioclastic, peloidal grainstone and packstone (Armstrong, 2000). The upper part of the lower member has a semi-nodular appearance from bioturbation and contains sedimentary structures such as hardgrounds, and planar, ripple and trough cross-stratification (Armstrong, 2000). The fossils found in the upper part are brachiopods, bryozoans, calcareous algae, cephalopods, echinoderm fragments, gastropods, stromatoporoids, tabulate corals, and trilobites (Armstrong, 2000). This part of the lower member is interpreted as having been deposited in a shallow, agitated, normal marine environment, possibly shoals on a shallow marine shelf (Armstrong, 2000). The contact with the middle member is sharp.

middle member

The middle member (Fig. 3) is more argillaceous than the lower member and consists of interbedded shale and limestone (Melchin et al., 1994; Armstrong, 2000). The limestone beds are 5 to 30 cm thick with shaly partings and consist of fine to medium-grained, grey-brown peloidal grainstone with planar laminations and few fossils (Melchin et al., 1994; Armstrong,

2000). The middle member is interpreted as having been deposited in a storm-influenced, deeper and more open marine shelf than the lower member. The contact with the upper member is gradational (Melchin et al., 1994; Armstrong, 2000).

upper member

The upper member of the Bobcaygeon Formation (Fig. 3) consists of light grey-brown, fine to coarse-grained, bioclastic, bioturbated packstone and grainstone with decreased argillaceous content (Melchin et al., 1994, Armstrong, 2000). The fossils are mostly echinoderm fragments and brachiopods, and some bryozoans, trilobites and gastropods. Sedimentary structures include ripples, cross-lamination and graded bedding (Melchin et al., 1994; Armstrong, 2000). The upper member contains k-bentonite layers that have been genetically linked with a suite of middle Ordovician volcanic ash deposits correlated across North America (Armstrong, 2000). The upper member is interpreted as having been deposited on a deepening storm-influenced shelf in an intershoal and shoal environment (Armstrong, 2000). Contact with the overlying Verulam Formation is gradational with increasing shale content upwards into the Verulam Formation (Melchin et al., 1994).

Verulam Formation

The Verulam Formation is informally subdivided into a lower and upper member based on lithostratigraphy:

lower member

The lower member (Fig. 3) is more than 40 m thick and consists of coarse-grained bioclastic grainstone and packstone and a nodular micritic lime mudstone (Armstrong, 2000). These beds are lenticular, discontinuous and interbedded with grey-green calcareous shale (Armstrong, 2000). Fossils include brachiopods, domal and branching bryozoans, echinoderms, gastropods, and trilobites (Armstrong, 2000). The lower member is interpreted as having been deposited in a storm-influenced shoal and shelf environment (Armstrong, 2000). Evidence for this interpretation is storm generated basal shelf lags, lenticular bedding, normal grading, scoured bases, and wave-rippled upper surfaces (Armstrong, 2000). The lower member also contains hardgrounds, bioturbated nodular bedding and burrows (Armstrong, 2000). The contact with the upper member is gradational.

upper member

The upper member (Fig. 3) is up to 10 m thick and consists of coarse-grained, bioclastic grainstones and rudstones that display trough cross-stratification (Armstrong, 2000). The most abundant fossils are echinoderms, brachiopods, and bryozoans. The upper member is interpreted as having been deposited in a shallow shoal environment and is indicative of regression during the latter part of Verulam deposition (Armstrong, 2000).

Objective

The objective of this study is to better understand the diagenetic evolution of the middle Ordovician rocks in the Lake Simcoe area by discerning the factors that controlled the post-depositional alteration of these carbonates. This study focuses on the Gull River and Bobcaygeon formations because of their widespread exposure and accessibility in the Lake Simcoe area.

The investigation will consider seafloor alteration, seen mainly as hardgrounds, as well as processes that were important during the burial history of the rocks. Therefore the focus is on early diagenetic calcite and early replacive dolomite in limestone sediments immediately above hardgrounds and in hardgrounds (all from OGS cores) as well as late-stage fracture dolomite and calcite (all from outcrop).

Questions to be addressed in this thesis are: (1) whether hardgrounds are useful indicators for local marine baseline $\delta^{18}\text{O}$? (2) Is a regional hydrothermal event supported by $\delta^{18}\text{O}$ and fluid inclusions? The answer to the first question may provide a clearer picture of the marine environmental conditions at time of seafloor lithification (earliest stage of diagenesis). More importantly the local baseline marine $\delta^{18}\text{O}$ can be used for interpretation of oxygen isotopes in late-stage carbonates which are from the same rocks as the hardgrounds. Answering the second question may give a better understanding as to whether the factors that controlled fluid migration and hydrocarbon reservoir formation in the Michigan and Appalachian basins also affected Lake Simcoe area carbonates.

A better understanding of these controlling factors will add to the knowledge already gained by earlier studies on correlative carbonates in other areas of Ontario including those in the Michigan Basin that form significant hydrocarbon plays.

Methodology

Fieldwork and sample collection at the study site was carried out by Dr. Mario Coniglio in the summer of 1999 to compliment earlier Ontario Geological Survey studies conducted from 1990 to 1993. Dr. Coniglio performed petrographic and cathodoluminescence analyses on thin sections, as well as analyzed selected samples for their stable carbon and oxygen isotopic compositions. Carbonate samples for stable isotope analysis were collected using a modified dental drill. Powders were analyzed at the Stable Isotope Laboratory at the University of Windsor. Evolved gas was extracted from ~30 mg of untreated powder reacted with 100% phosphoric acid. The reaction occurred for approximately 4 hours at 25°C for calcite and 50°C for dolomite. The gas was analyzed for $^{18}\text{O}/^{16}\text{O}$ and $^{13}\text{C}/^{12}\text{C}$ using a Finnigan-Mat Delta Plus mass spectrometer. Results are reported in conventional per mil notation with respect to VPDB, utilizing standard correction procedures. Acid fractionation corrections for dolomite are based on Rosenbaum and Sheppard (1986). The $\delta^{13}\text{C}$ and $\delta^{18}\text{O}$ values are accurate to better than 0.03‰ and 0.04‰, respectively. Accuracy was determined by replication of international and internal standards and from duplicates of the samples collected in 1999.

Cathodoluminescence microscopy, using a Reliotron Cathodoluminescence instrument mounted on a Nikon binocular microscope, was done to identify growth zones. Thin sections

were stained with Alizarin Red S and potassium ferricyanide to differentiate between calcite and dolomite as well as ferroan and non-ferroan growth zones in these carbonates.

Five doubly polished sections from the samples collected in 1999, and eight doubly polished sections from samples collected for the present study in the summer of 2008 were used for fluid inclusion analysis at the University of Waterloo, using a LINKAM THMSG 600 stage calibrated between $-56.6^{\circ}\text{C} \pm 0.1^{\circ}\text{C}$, $0.0^{\circ}\text{C} \pm 0.1^{\circ}\text{C}$ and $374^{\circ}\text{C} \pm 1^{\circ}\text{C}$ using SYNFLINC synthetic fluid inclusion standards. Homogenization temperatures were determined prior to melting temperatures to avoid stretching the inclusion during freezing. Final ice melting temperatures were used to calculate salinities which are reported as weight percent CaCl_2 (wt% CaCl_2). Salinity calculations were done using the equations and computer program of Bakker et al. (1996). Composition of the fluids was determined from Oakes et al. (1990) $\text{NaCl-CaCl}_2\text{-H}_2\text{O}$ ternary phase diagram. Hydrocarbon-bearing fluid inclusions were identified using an ultraviolet light fluorescing microscope with a mercury lamp and blue (365 nm) filter (McLimans, 1987; Burruss, 1991; Hutton, 1991).

CHAPTER 2: PETROGRAPHY OF SIMCOE GROUP CARBONATES

Introduction

This study examines seafloor alteration based on examination of hardgrounds and overlying limestone as well as late-stage carbonates and sulphates (all from the Simcoe Group) to better understand the diagenetic evolution of mid-Ordovician carbonates in the Lake Simcoe area. These hardgrounds were evaluated to determine their potential as mid-Ordovician seawater $\delta^{18}\text{O}$ proxies because they are from the same rocks as the late-stage carbonates and sulphates, therefore have gone through the same diagenetic processes. If these hardgrounds retain an original mid-Ordovician seawater $\delta^{18}\text{O}$ signature they can be used as an internal baseline for $\delta^{18}\text{O}$ values to interpret the late-stage carbonates discussed later.

Hardground Morphology

Hardgrounds are defined as horizons of continuous to discontinuous lithified seafloor sediments that form at the seafloor sediment-water interface or up to 50 cm below the sediment surface (Brett and Brookfield, 1984; Melchin et al., 1994). Hardground surfaces commonly show evidence of encrusting and boring organisms which is indicative of exposure on the seafloor (Brett and Brookfield, 1984). Hardgrounds are thought to form during periods of low or no sedimentation allowing greater quantities of seawater to interact with and cement the sediment (Melchin et al., 1994).

Brett and Brookfield (1984) identified six different hardground morphologies in the Lake

Simcoe Area:

1) Smooth hardgrounds (Fig. 4) have very few burrows and little erosion. Smooth hardgrounds are found to occur in distal facies where there is minimal disruption to sedimentation (Brett and Brookfield, 1984).

2) Rolling hardgrounds (Fig. 4) are also found in distal environments and are created by the erosion of nodular or burrowed beds.

3) Hummocky hardgrounds (Fig. 4) result from further erosion of rolling hardgrounds where sediments are removed from between nodules and burrows (Brett and Brookfield, 1984).

4) Undercut/pebbly hardgrounds (Fig. 4) form from continued erosion of hummocky hardgrounds which eventually collapse. These hardgrounds are found in coarse beds at the bases of proximal cycles (Brett and Brookfield, 1984).

5) Reworked hardgrounds (Fig. 4) occur when pebbly hardgrounds are transported and redeposited elsewhere.

6) Planar hardgrounds (Fig. 4) are the result of heavy erosion and occur where sediments in burrows lithify contemporaneously and to the same hardness as the rest of the bed (Brett and Brookfield, 1984).

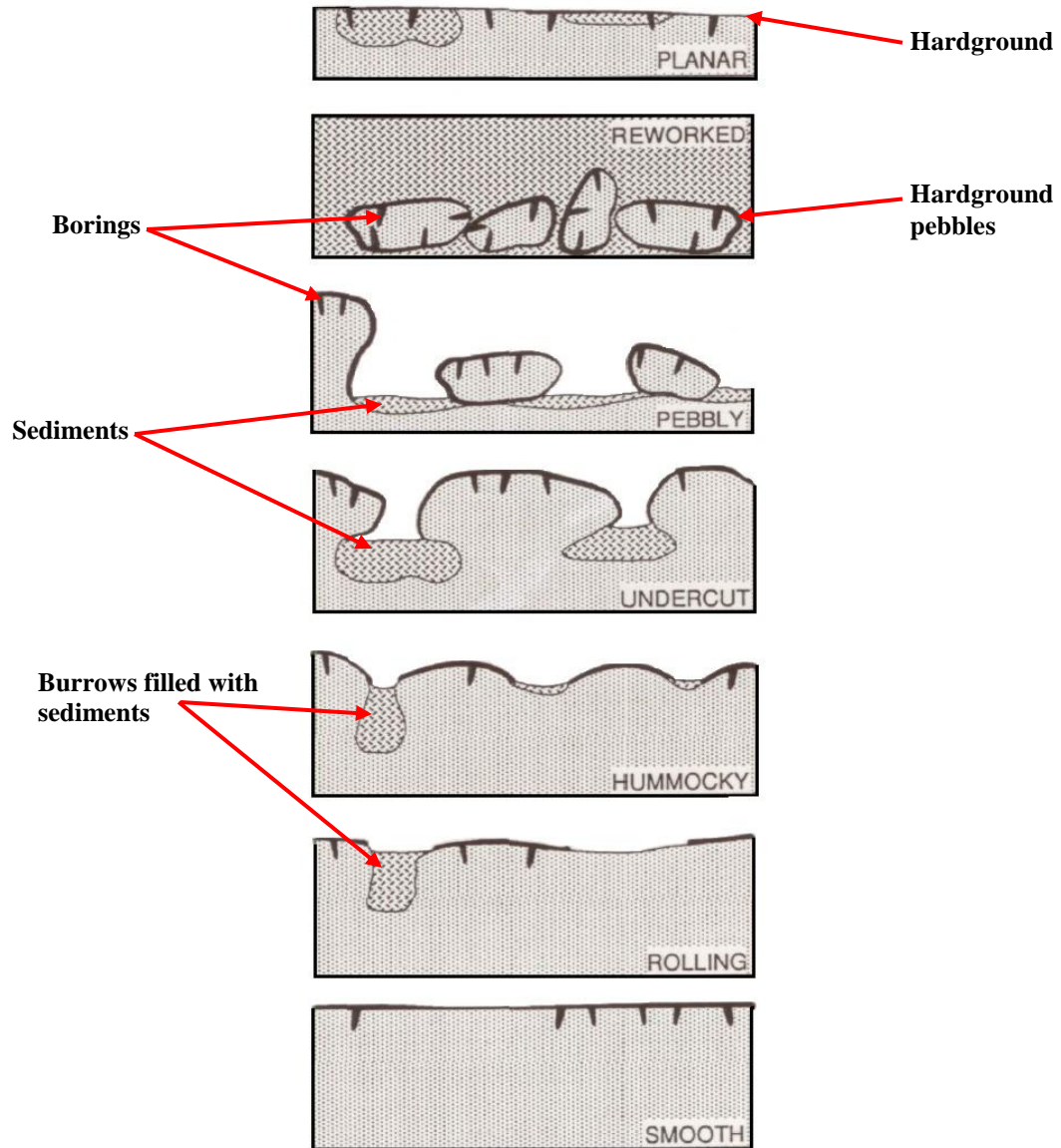


Fig. 4 Hardground morphologies of Brett and Brookfield (1984). The amount of turbulence decreases from top to bottom (Modified from Melchin et al., 1994)

Toole (2001) investigated the Trenton and Black River formations in the Lake Simcoe Area and recognized five of the morphologies identified by Brett and Brookfield (1984). Toole (2001) interpreted smooth and planar hardgrounds to have formed in a lagoonal setting in grainstone, packstone, wackestone and mudstone. Rolling hardgrounds are commonly found in deep shelf

settings in a variety of lithologies from coarse-grained grainstone to very fine-grained lime mudstone and are bioturbated and burrowed (Toole, 2001). Hummocky hardgrounds are extensively burrowed, bioturbated and eroded, and are found in grainstone, mudstone and wackestone in a crinoidal shoal/shallow shelf environment. Undercut hardgrounds are found in fine-grained mudstone, wackestone and grainstone in high energy crinoidal shoal/shallow shelf areas (Toole, 2001). Pebbly hardgrounds are found in high energy and/or storm affect intertidal areas in fine-grained wackestone and packstone (Toole, 2001).

Brett and Brookfield (1984) identified 25 different species of encrusting and boring organisms. Smooth hardgrounds are found to contain some microborings and encrusting bryzoans (possibly *Prasopora*). Rolling hardgrounds have encrusting red algae (*Solenopora?*) and bryzoa (*Prasopora?*). Hummocky hardgrounds do not have many microborings but have complex burrow systems (Brett and Brookfield, 1984). Undercut hardgrounds are heavily bioturbated with complex burrow systems, and pebbly hardgrounds have no boring or encrusting organisms and very little bioturbation or burrows (Brett and Brookfield, 1984). *Trypanites*, *Prasopora*, algae and/or bacteria are the most common microboring organisms with *Prasopora* making up 90% of encrusting organisms (Melchin et al., 1994). Pelmatozoan holdfasts from a variety of echinoderms are also identified as well as a variety of loosely attached and free-living organisms like gastropods and brachiopods (Melchin et al., 1994).

Hardgrounds seen in outcrops during summer 2008 field work were mainly rolling (Fig. 5) and hummocky (Fig. 6). Undercut and smooth hardgrounds were also found (Figs. 7 and 8).

Many of the hardgrounds showed evidence of burrowing, microboring and encrusting organisms similar to those described by Brett and Brookfield (1984).



Fig. 5 Rolling hardground in the Moore Hill bed of the Bobcaygeon Formation. Arrow points to hardground surface; pen for scale.

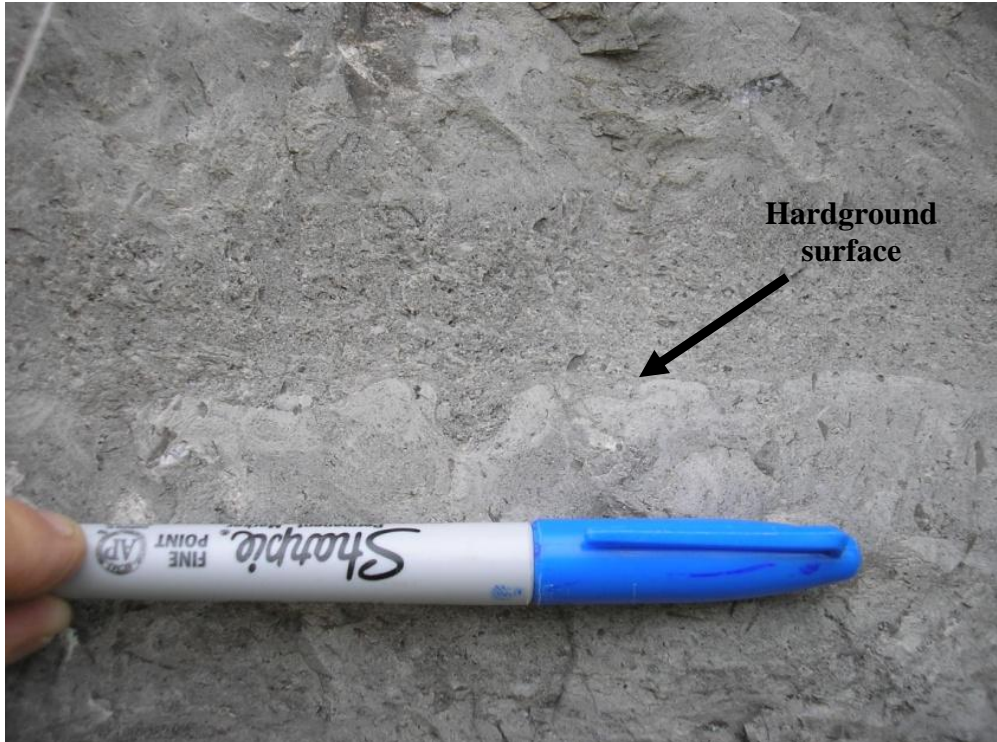


Fig. 6 Hummocky hardground in the Moore Hill bed of the Bobcaygeon Formation. Arrow points to hardground surface; pen for scale

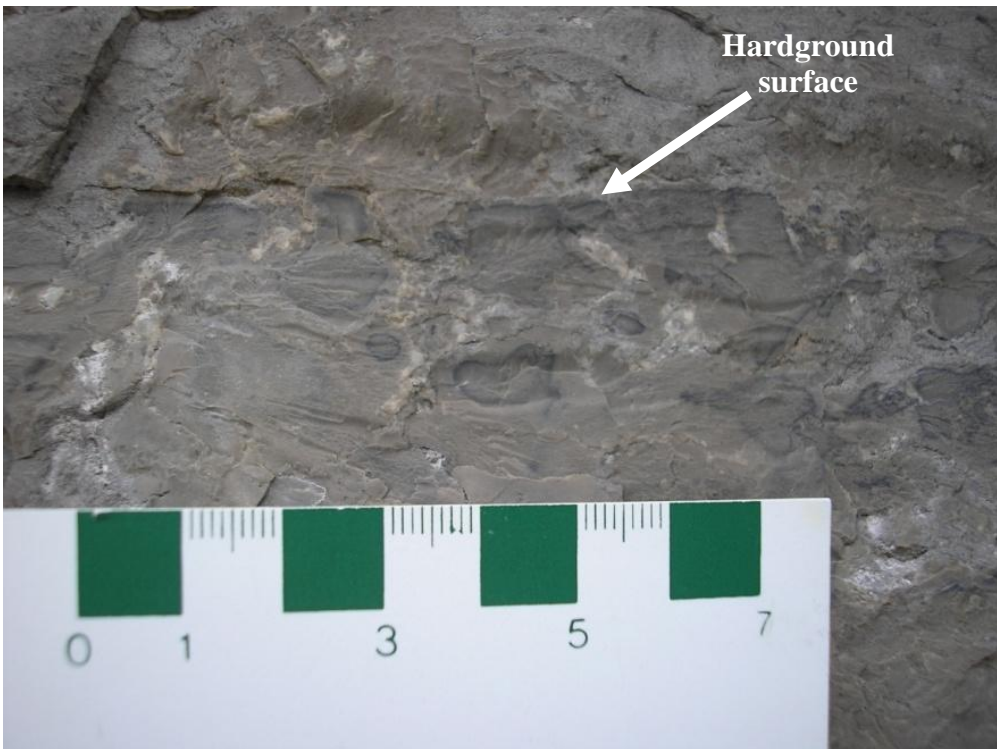


Fig. 7 Undercut hardground at the contact between the Gull River and Bobcaygeon formations. Arrow points to the hardground surface that helps define the contact between the two formations; scale is in cm.



Fig. 8 Smooth hardground at the contact between the Gull River and Bobcaygeon formations. Arrow points to hardground surface; scale is 5 cm.

Petrography of Hardgrounds, Early Diagenetic Calcite and Early Replacive Dolomite

The terms early diagenetic calcite and early replacive dolomite are petrographic terms referring to the timing of calcite and dolomite precipitation in the paragenetic succession determined by petrographic analysis of the Lake Simcoe carbonates.

The majority of hardgrounds examined in this study are composed of fine-grained peloidal microbioclastic grainstone (Fig. 9). Some hardgrounds are composed of coarse-grained crinoidal and peloidal grainstone (Fig. 10), micropeloidal wackestone-packstone, ooid grainstone, or packstone with a mud matrix (Fig. 11).

Sediments immediately above the hardgrounds are mainly composed of microbioclastic peloidal grainstone (Fig. 9) and crinoid-rich microbioclastic grainstone (Fig. 12). Some sediments are composed of micropeloidal grainstone, oolitic peloidal grainstone, or siliclastic-rich microbioclastic peloidal grainstone-packstone.

Thin section petrography and staining revealed most of the early diagenetic calcite found in the hardgrounds and overlying sediments is ferroan to slightly ferroan interparticle cement with crystals sizes of ≤ 10 to 20 μm . A couple of peloidal bioclastic grainstone samples contain ferroan coarse-crystalline calcite cement with anhedral calcite crystals ranging in size from 20 to 50 μm .

Thin section petrography and staining showed the early dolomite found in the sediments overlying the hardgrounds is ferroan and non-ferroan microcrystalline sucrosic dolomite replacing a lime mud matrix. The replacive dolomite crystals are euhedral to anhedral and range in size from 20 to 60 μm .

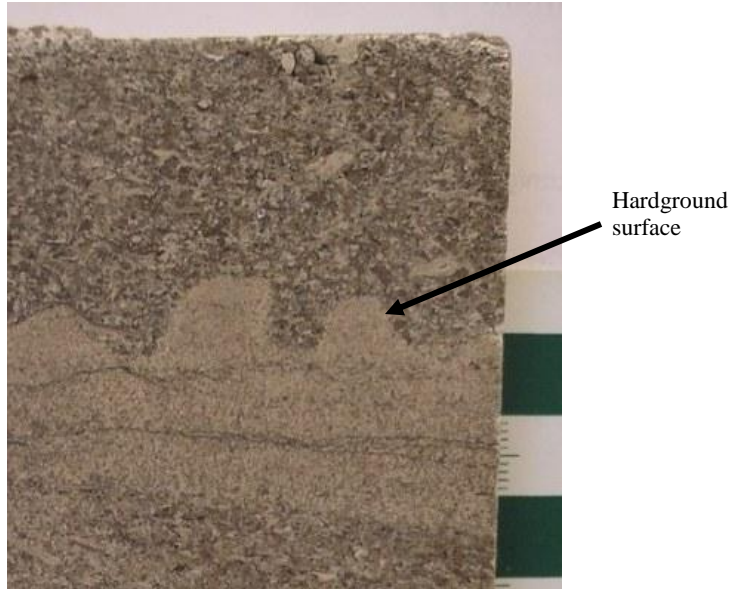


Fig. 9 Hardground composed of fine-grained peloidal microbioclastic grainstone. Overlying sediment is coarser-grained microbioclastic peloidal grainstone. Surface of hardground is intensively burrowed. Scale is in cm. Lower Bobcaygeon Formation, OGS core 93-11-8.10.

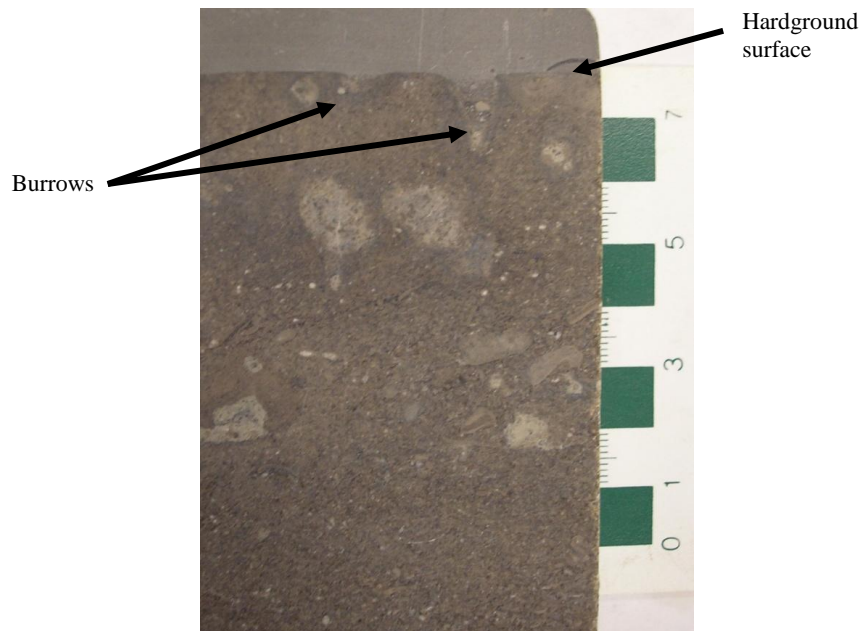


Fig. 10 hardground composed of crinoidal-micropeloidal grainstone. Hardground surface is burrowed. Overlying sediment is composed of micritic microbioclastic grainstone. Scale is in cm. Lower Bobcaygeon Formation, OGS core 93-12-22.72.

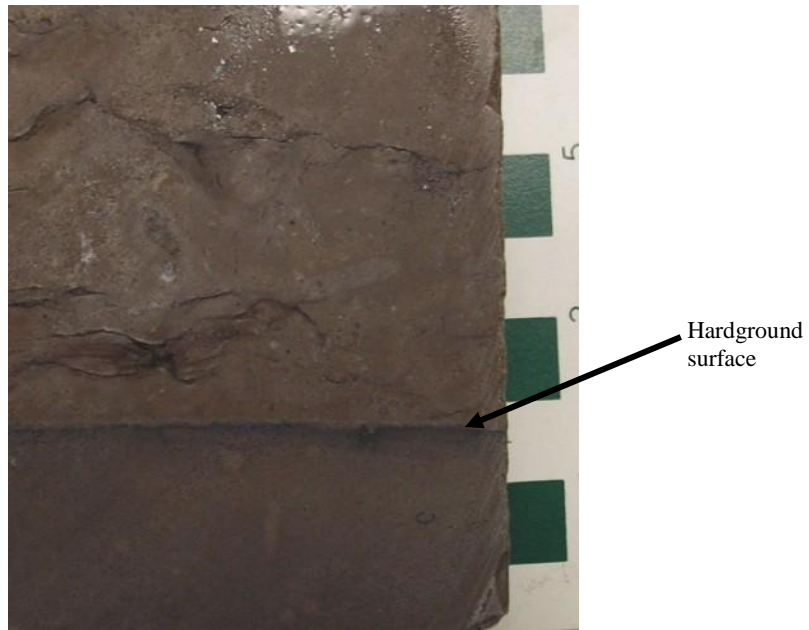


Fig. 11 Hardground composed of packstone with micritic calcite cement. Sediment above hardground is fine-grained micropeloidal-microbioclastic grainstone. Scale is in cm. Upper Gull River Formation, OGS core 93-4-21.09.



Fig. 12 Sediment is coarse-grained crinoid-rich microbioclastic grainstone. Hardground is composed of fine-grained micropeloidal bioclastic grainstone. Hardground surface is intensively burrowed (black lines highlight part of the overhang). Holes are from sample extraction for stable isotope analyses. Scale is in cm. Moore Hill Beds, Bobcaygeon Formation, OGS core 93-11-13.99.

Petrography of Late-Stage Carbonate

The term late-stage is a petrographic term referring to the timing of calcite and dolomite precipitation in the paragenetic succession of the Lake Simcoe carbonates analyzed in this study.

Four types of calcite were found in fractures and vugs. The types are based on textures and mineral associations:

- 1) Coarse-crystalline calcite with straight intercrystalline boundaries.
- 2) Coarse-crystalline calcite with extensive twinning (Fig. 14) associated with subhedral to anhedral barite laths and/or aggregates of fibrous barite (Figs. 13 and 14). Some calcites have poikilotopic texture (Fig. 13).
- 3) Euhedral to subhedral elongated calcite crystals replaced by chalcedony (Fig. 15).
- 4) Coarse-crystalline calcite with later fine-grained chalcedony rimming fractures and vugs (Fig. 16).

Several samples contain ferroan and non-ferroan saddle dolomite associated with calcite cement and quartz (Figs. 17 and 18). The saddle dolomite crystals are euhedral to subhedral and range in size from 0.2 to 8 mm. A couple of samples contained ferroan and non-ferroan microcrystalline dolomite with crystals ranging in size from 20 to 50 μm . Full descriptions of the late-stage minerals used for both stable isotope analyses and microthermometry are provided in Table 1 below.

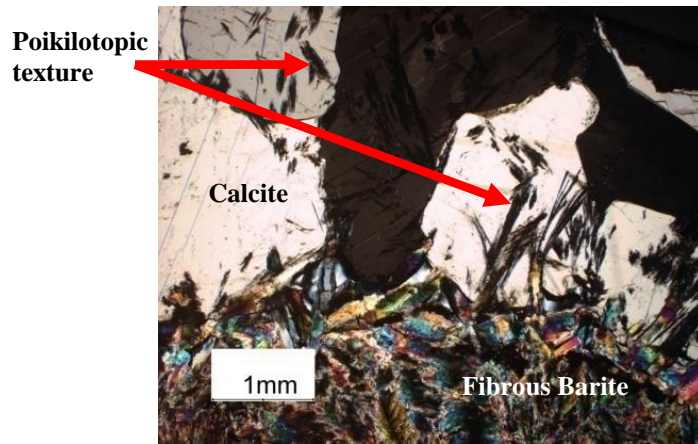


Fig. 13 Fracture-fill coarse-calcite that has overgrown barite seen by the poikilotopic texture of the calcite. Photomicrograph is in cross-polarized light (cpl). Sample 99-132.

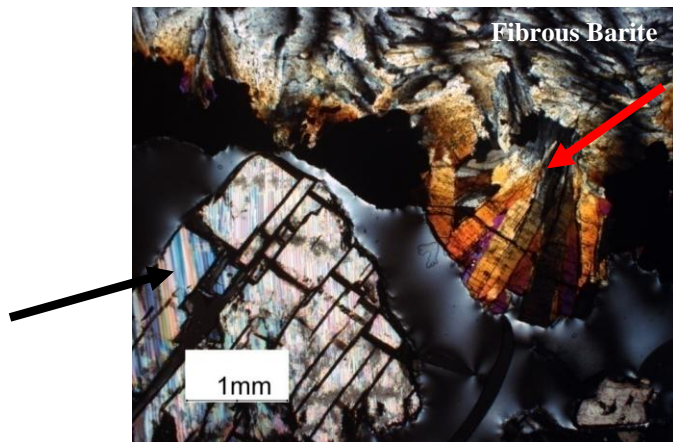


Fig. 14 Black arrow points to extensive twinning in fracture-fill calcite associated with barite (red arrow points to barite laths). Photomicrograph is in cpl. Sample 99-134.

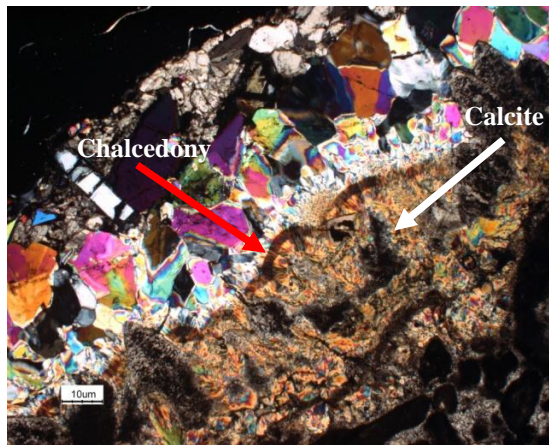


Fig. 15 Chalcedony (red arrow) cement rimming calcite (white arrow). Photomicrograph is in cpl. Sample LM-5.1

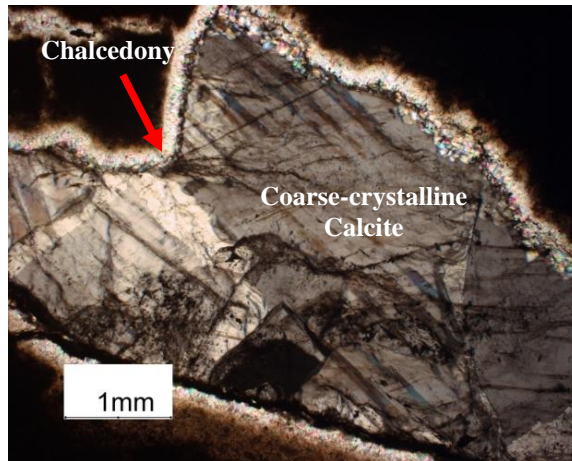


Fig. 16 Fracture-fill coarse-calcite rimmed by fine-grained chalcedony (red arrow). Photomicrograph is in cpl. Sample 99-107.

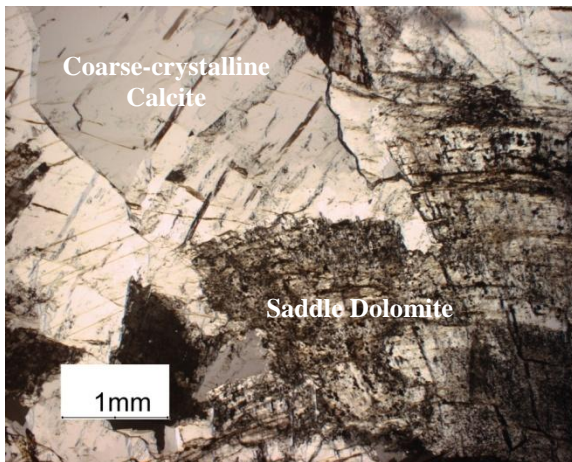


Fig. 17 Saddle dolomite with coarse-crystalline calcite. Photomicrograph is in cpl. Sample 99-120.

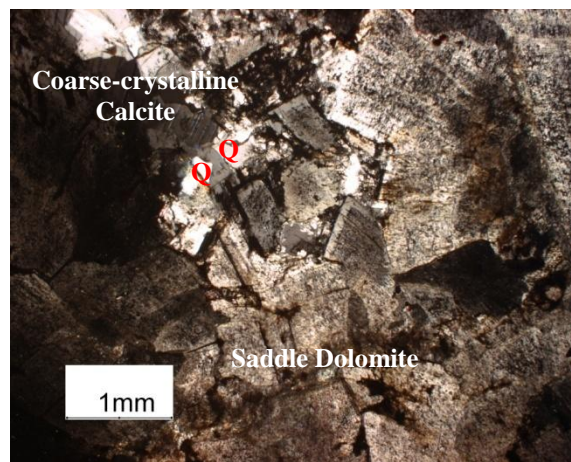


Fig. 18 Saddle dolomite with coarse-crystalline calcite and quartz (Q). Photomicrograph is in cpl. Sample 99-120.

Table 1 Petrographic description of late-stage carbonates and associated minerals in samples collected in 1999 (99- series) and 2008 (LM- series) from outcrops in the Lake Simcoe area. These samples were used for stable isotope analysis (99-series) and microthermometry (99- and LM-series). Cathodoluminescence was performed on 99-series samples.

Sample No.	Setting	Major Minerals	Crystal Sizes	Crystal Habits	Other Minerals	Notes
LM-4 uBob	Local fracture ~ 7 cm long and up to 2 cm wide	Sparry calcite	0.2 to 2 mm	Subhedral to anhedral	None apparent	Calcite becomes increasingly inclusion rich toward center of fracture.

LM-5.1 and 5.2 uBob	Biomoldic pore (brachiopod?). Pore in LM-5.1 is ovoid ~ 2.5 cm long, 1.5 cm at widest point and ~ 1 cm at narrowest point. Pore in LM-5.2 is ~ circular with ~ 1 cm diameter	Sparry calcite	0.1 to 4.5 mm. Most ~ 0.5 mm	Subhedral to euhedral	Fibrous radiating chalcedony crystals up to 0.5 mm in length	Calcite in LM-5.2 is elongated (cut parallel to c-axis). Chalcedony lines the pores and replaces calcite.
LM-6 uGR	Exposed fracture wall on road cut. Extent of fracture unknown	Barite (Ba) and sparry calcite (SC)	Ba: up to 3 mm long SC: 0.3 to 5 mm	Ba: euhedral to subhedral laths SC: anhedral to subhedral	Sulfides (trace pyrite) and possibly bitumen present	Barite postdates calcite. Some calcite has irregular boundaries.
LM-9A lBob MH	Vug ~circular ~ 1.4 cm in diameter	Sparry calcite	0.2 to 4 mm. Most 0.5 to 2 mm	Subhedral to anhedral with irregular grain boundaries	None apparent	Uniform extinction on most crystals. Some crystals exhibit strain (undulose extinction).
LM-10B lBob MH(?)	Biomoldic (nautiloid) 7 cm in length	Two populations of sparry calcite	Pop 1: 50 um to 1mm Pop 2: 1 to 4 mm	Pop1: subhedral Pop 2: anhedral	None apparent	Several crystals exhibit strain (undulose extinction)
DKA-103AA uBob	Fracture fill in brecciated zone in LS quarry wall. Extent unrecorded	Sparry calcite and microspar in fractures in breccia	0.2 to 5 mm most are 0.5 to 1 mm	Subhedral	~ 3% pyrite	Microspar rims sparry calcite.
DKA-326AA GR	Fracture, extent unrecorded	Two populations of sparry calcite	Pop 1: 0.2 to 1 mm Pop2: 1 to 5 mm	Pop 1: anhedral Pop 2: subhedral	None apparent	Pop 1 found in smaller fracture off of the main fracture containing Pop 2.
99-101 uGR	Fracture fill in brecciated zone in limestone quarry wall. Extent unrecorded	Sparry calcite ferroan to non-ferroan	0.2 to 10 mm most ~1 mm	Subhedral	Some pyrite	Strain evident in some crystals (undulose extinction) Cathodoluminescenc (CL): weak to moderately bright orange.
99-107 GR	Fracture 25 mm long and up to 3 mm wide	Sparry calcite slightly ferroan (early) to non-ferroan	0.2 to 9 mm most are ≤1 mm	Anhedral	Megaquartz ≤ 0.2 mm in size subhedral Dolomite rhombs (seen in thin section) ferroan 15 to 200 um euhedral	Quartz lines fracture and postdates non-ferroan calcite. Dolomite found in limestone host. CL: sparry calcite is bright orange, rest is non-luminescent.

99-120A uBob	Fracture, extent unrecorded	Saddle dolomite (SD) slightly ferroan to ferroan and sparry calcite non-ferroan to slightly ferroan	SD: 0.2 to 2 mm SC: 0.5 to ~1.5 mm	SD: subhedral to euhedral SC: anhedral to subhedral	Quartz <1 mm in size	Quartz lines fractures and rims dolomite and calcite. CL: saddle dolomite is non-luminescent. Sparry calcite is bright orange. Saddle dolomite has very cloudy centers.
99-132 lBob	Fracture, extent unrecorded (in photo appears to be of outcrop scale)	Sparry calcite	0.5 to 6 mm most 3-5 mm	Anhedral to subhedral	Fibrous barite and barite laths up to 1.5 mm in length. Trace manganese oxide found in calcite lamellae (in polished section)	Calcite replaces barite (relict barite in calcite). CL: sparry calcite is moderate to bright orange. Barite is non-luminescent.
99-134 lBob MH	Fracture, extent unrecorded (in photo appears to be of outcrop scale)	Slightly ferroan sparry calcite with barite	SC: 0.5 to 18 mm Ba: laths up to 2 mm	SC: subhedral to anhedral Ba: spherulites grading into laths and splaying aggregates	Goethite and marcasite (reflected light)	Barite overgrown by calcite CL: sparry calcite bright orange. Barite blue luminescence

CHAPTER 3: EARLY CARBONATE CEMENTS AND HARDGROUNDS AS POSSIBLE PROXIES OF LOCAL MARINE BASELINE $\delta^{18}\text{O}$

Introduction

An important question asked in the present study is whether the Lake Simcoe hardgrounds make good proxies for marine carbonate $\delta^{18}\text{O}$ values. How well is the marine $\delta^{18}\text{O}$ isotopic signature preserved in these ancient marine sediments? Despite thirty years of research on the geochemistry of ancient seawater there is still disagreement on its isotopic composition (Muehlenbachs et al., 2003). An obvious problem is there are no ancient seawater samples for direct analysis. Marine fossil calcite and calcite cements are used as proxies instead, but these are prone to diagenetic alteration which changes their geochemistry (Muehlenbachs et al., 2003). Hardgrounds are not the usual carbonate marine proxy. Most studies, such as Tobin and Walker (1997) discussed later, use apparently unaltered fibrous marine calcite cement (FMCC) as proxies because they are low magnesium calcite and are more stable than high magnesium calcite or aragonite which are susceptible to diagenetic alteration (Tobin and Walker, 1997). This stability allows FMCC to potentially retain original $\delta^{18}\text{O}$ seawater signatures to a greater extent than other carbonate phases.

Fibrous marine calcite was not found in the Lake Simcoe study site, therefore hardgrounds were chosen as potential proxies in this study because they are cemented close to the seafloor and may possibly retain an original mid-Ordovician $\delta^{18}\text{O}$ seawater signature. The limestones directly above the hardgrounds were analyzed for comparison of their $\delta^{18}\text{O}$ values with the

hardgrounds. If the hardgrounds retain an original $\delta^{18}\text{O}$ seawater signature, their $\delta^{18}\text{O}$ values should be more positive than those of the overlying limestones because hardgrounds were cemented prior to burial. A well preserved mid-Ordovician seawater signature in these hardgrounds will allow them to be used as an internal baseline $\delta^{18}\text{O}$ for interpreting late-stage carbonates analyzed in this study.

Results of Stable Isotope Analyses of Early Diagenetic Calcite and Early Replacive Dolomite

Stable carbon and oxygen isotope values were determined from 54 bulk rock samples containing early diagenetic calcite cement associated with hardgrounds and 12 bulk rock samples containing microcrystalline replacive dolomite. The term “bulk rock” is used here because depositional and diagenetic components of the rock were analyzed together. Individual components could not be separated due to their microscopic size. All 66 samples are from the OGS cores. The bulk rock samples containing early diagenetic calcite cement (Fig. 19) show a narrow range of $\delta^{13}\text{C}$ values from -1.7 to +2.9‰ (PDB) and a narrow range of $\delta^{18}\text{O}$ values from -6.9 to -2.9‰ (PDB). The bulk rock samples containing early replacive dolomite (Fig. 19) also shows a narrow range of $\delta^{13}\text{C}$ values from -2.3 to +0.3‰ and a wide range of $\delta^{18}\text{O}$ values from -11.1 to -1.6‰. Early replacive dolomite has a more restricted $\delta^{13}\text{C}$ range and a slightly wider range of $\delta^{18}\text{O}$ values than the early calcite cement.

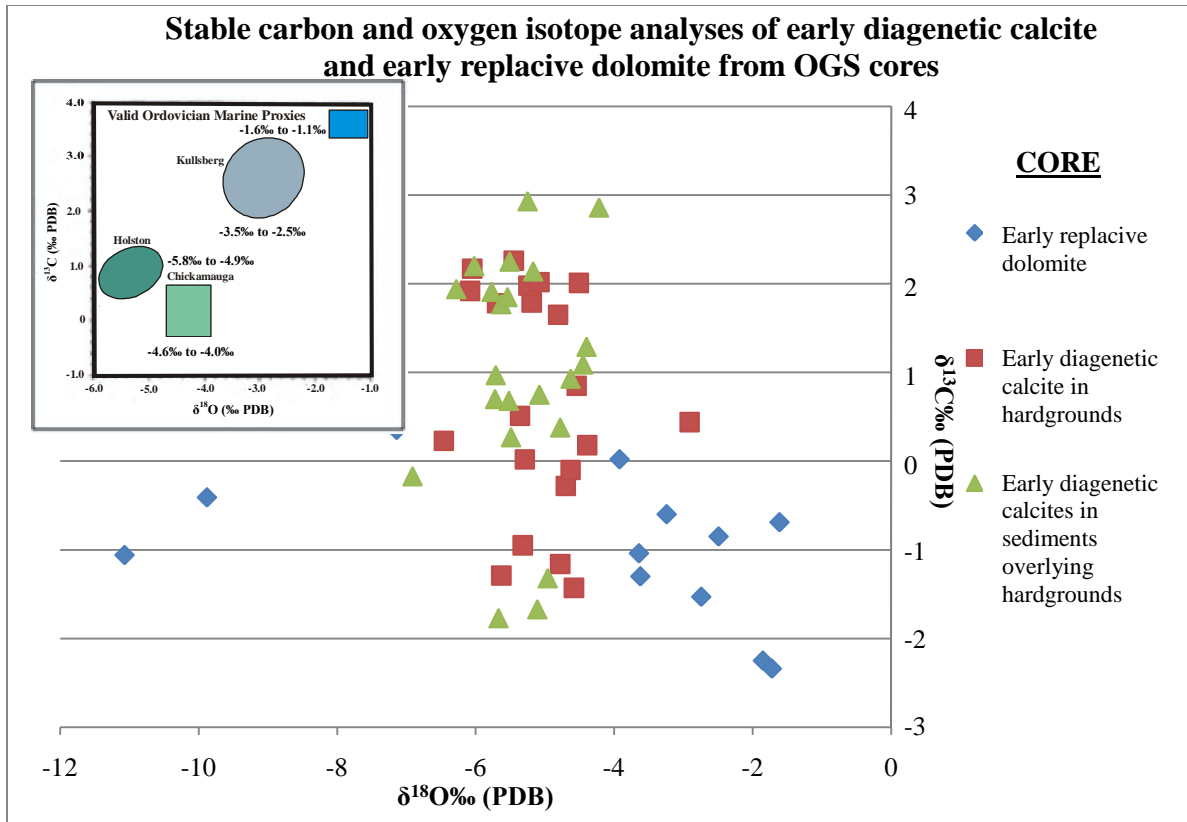


Fig.19 Stable isotope geochemistry of bulk rock samples from the Lake Simcoe area, Ontario. The hardgrounds and overlying limestones show very similar isotopic compositions whereas the dolomite extends to more negative $\delta^{13}\text{C}$ values (PDB) but slightly more positive $\delta^{18}\text{O}$ values (PDB) than the limestone and hardgrounds. The inset at left, modified from Tobin and Walker (1997), shows isotopic composition of valid Ordovician marine proxies.

Discussion

The more positive $\delta^{18}\text{O}$ values in the replacive dolomite could reflect contemporaneous dolomite precipitation with the calcite from the same pore fluids (Land, 1985). According to Land (1985) modern marine dolomites have $\delta^{18}\text{O}$ values that are more positive compared to co-existing calcite by $\sim 3\%$ (PDB). In the present study the majority of dolomite appears to have more positive $\delta^{18}\text{O}$ values by ~ 2 to 3% relative to the calcites from the same samples (Fig. 19). This suggests, from an oxygen isotopic perspective, that the calcite and dolomite could be co-

precipitates. Petrographic evidence of co-precipitation was indeterminate due to the tiny crystal sizes. The hardgrounds have the same isotopic signature (Fig. 19) as immediately overlying limestones lacking evidence of early seafloor lithification. Assuming the overlying limestones were not cemented early, the calcite $\delta^{18}\text{O}$ values indicate the hardgrounds have not retained their original mid-Ordovician $\delta^{18}\text{O}$ seawater signature, and therefore hardgrounds are not useful as proxies. For these hardgrounds to be useful proxies their $\delta^{18}\text{O}$ values should be higher relative to the overlying limestone as the hardgrounds were cemented at or near the sediment-water interface prior to burial (Coniglio, 2010 personal communication). Also, hardground $\delta^{18}\text{O}$ values are too negative for mid-Ordovician seawater assuming a precipitation temperature of 20°C and seawater $\delta^{18}\text{O}$ values of -2 to 0‰ (SMOW) as previously suggested by several studies such as Tobin and Walker (1997) and Muehlenbachs et al. (2003) (discussed below).

Tobin and Walker (1997) examined marine equant, bladed and translucent fibrous marine calcite in three Ordovician units from Sweden and the US (Alabama and Tennessee) to determine if they were valid marine proxies for Ordovician seawater $\delta^{18}\text{O}$ values. Validation for these calcites was based on four criteria (Tobin and Walker, 1997):

- 1) The FMCC had intrinsic blue color under cathodoluminescence indicating the FMCC was relatively unaltered.
- 2) Mn and Fe concentrations in the equant, bladed and fibrous marine calcites were close to concentrations in modern marine precipitates formed in oxic conditions.

3) Mg and Sr concentrations in the equant, bladed and fibrous marine calcites were consistent with compositions of abiogenic marine precipitates in a warm Ordovician sea.

4) Very little (<1%) microdolomite was associated with the equant, bladed and fibrous marine calcites, similar to what is seen in unaltered Cenozoic marine cements (Tobin and Walker, 1997).

The unaltered marine calcite $\delta^{18}\text{O}$ values from the three Ordovician units (Fig. 19 inset) ranged from -5.8 to -2.5‰ (PDB) and were more positive with a much more limited range compared to diagenetic calcites from the same units. Tobin and Walker (1997) used the calcite-water paleotemperature equation $10^3 \ln \alpha_{\text{calcite-H}_2\text{O}} = 2.78 * (10^6 T^{-2})$ of Friedman and O'Neil (1977) to calculate paleotemperatures using their unaltered calcite $\delta^{18}\text{O}$ values and previously estimated Ordovician seawater values from published late-Ordovician Hirnantian brachiopod data. Tobin and Walker (1997) constrained Ordovician seawater $\delta^{18}\text{O}$ to -2‰ \pm 1.5‰ (SMOW) by assuming that optimal carbonate precipitation during the Ordovician occurred at similar seawater temperatures as modern carbonates (24 to 28°C). Tobin and Walker (1997) suggested the unaltered marine calcites in their study make good proxies because they are close to equilibrium with Ordovician seawater and meet all four criteria mentioned above.

Muehlenbachs et al. (2003) reviewed several studies on ophiolites as well as studied the Solund-Stavfjord ophiolite complex (SSOC) in Norway to determine if ophiolites are useful proxies for ancient seawater isotopic composition. Muehlenbachs et al. (2003) created a $\delta^{18}\text{O}$ vs. depth profile of the SSOC by analysis of quartz and epidote from late Ordovician (443 Ma)

SSOC ophiolite and Miocene (5.9 Ma) sea floor from Ocean Drilling Program (ODP) Hole 504B from the Costa Rica Rise. Both the Ordovician and Miocene rocks became progressively more negative in $\delta^{18}\text{O}$ values with depth. This profile is very similar to what is seen in modern oceanic crust which implies seafloor alteration processes were the same during the Ordovician as they are today (Muehlenbachs et al., 2003). The increasingly more negative $\delta^{18}\text{O}$ values with increasing depth seen in the SSOC profile could only have occurred if the Ordovician seawater altering the seafloor was $0\text{‰} \pm 2\text{‰}$ SMOW (Muehlenbachs et al., 2003).

According to Muehlenbachs et al. (2003) these results are in agreement with previous studies of other ophiolites from the Paleozoic which suggests that Cambrian, Ordovician, and Silurian seawater $\delta^{18}\text{O}$ values did not change over time and were consistently $\sim 0\text{‰}$ SMOW. Also, ophiolites are good proxies because they record deep ocean geochemistry unlike carbonates which might simply reflect the shallower warmer epicontinental seawater they precipitate from and may have only a tenuous link to the deep ocean (Muehlenbachs et al., 2003).

The hardgrounds in this study were further evaluated as potential proxies by calculating Ordovician seawater $\delta^{18}\text{O}$ values using the calcite-water paleotemperatures equation of Friedman and O'Neil (1977), the $\delta^{18}\text{O}$ values of -7 to -3‰ PDB, which represents the majority of the hardground calcites, and assumed Ordovician seawater surface temperatures from 15 to 30°C. These temperatures were chosen to demonstrate the effect of the hardground $\delta^{18}\text{O}$ values on calculated seawater $\delta^{18}\text{O}$ values through a range of temperatures reflecting temperate to tropical

conditions. The seawater $\delta^{18}\text{O}$ values are graphed along with the hardground $\delta^{18}\text{O}$ values and seawater temperatures in Fig. 20 below.

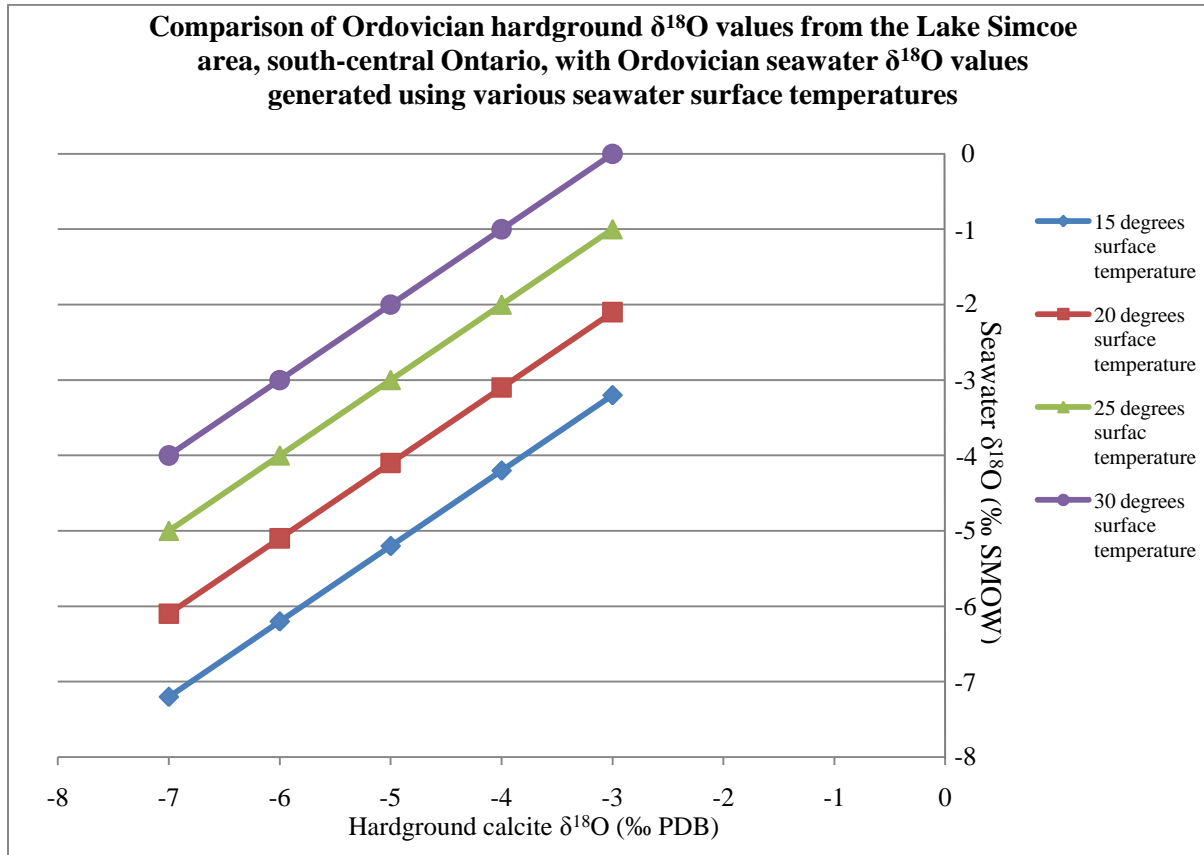


Fig. 20 Graph of Ordovician seawater $\delta^{18}\text{O}$ values calculated using hardground $\delta^{18}\text{O}$ values and assumed Ordovician seawater temperatures from 15 to 30°C. The majority of hardground $\delta^{18}\text{O}$ values generated seawater $\delta^{18}\text{O}$ values that are more negative than the -2 to 0‰ suggested by Tobin and Walker (1997) and Muehlenbachs et al. (2003) for the Ordovician. One hardground $\delta^{18}\text{O}$ value of -3‰ produced a seawater $\delta^{18}\text{O}$ value of -2.1‰ at an assumed surface temperature of 20°C. The rest of the hardground $\delta^{18}\text{O}$ values produce seawater $\delta^{18}\text{O}$ values in the -2 to 0‰ range at seawater temperatures higher (25-30°C) than 20°C. These results indicate the hardgrounds did not retain an original Ordovician seawater $\delta^{18}\text{O}$ signature and are not useful as proxies.

Hardground $\delta^{18}\text{O}$ values are more negative from right to left along the x-axis and seawater $\delta^{18}\text{O}$ values are more negative from top to bottom along the y-axis (Fig. 20). The different colored lines represent different seawater surface temperatures ranging from 15 to 30°C. At 15°C and a hardground $\delta^{18}\text{O}$ value of -3‰, the seawater $\delta^{18}\text{O}$ value is -3.2‰ (SMOW) (Fig. 20). This value is more negative than the -2 to 0‰ suggested by Tobin and Walker (1997) and

Muehlenbachs et al. (2003) for Ordovician seawater $\delta^{18}\text{O}$ values at a constant temperature. The hardground $\delta^{18}\text{O}$ values of -3 and -4‰ do produce seawater $\delta^{18}\text{O}$ values in the -2 to 0‰ range with surface temperatures of 25 and 30°C (Fig. 20). These temperatures are higher than the currently accepted Ordovician seawater surface temperature of 20°C. One hardground $\delta^{18}\text{O}$ value of -3‰ produced a seawater $\delta^{18}\text{O}$ value of -2.1‰ at 20°C. However, the majority of hardground $\delta^{18}\text{O}$ values consistently produce seawater $\delta^{18}\text{O}$ values too negative for an assumed Ordovician $\delta^{18}\text{O}$ seawater signature of -2 to 0‰ suggesting the hardgrounds have not retained an original Ordovician seawater signature.

The hardgrounds do not appear to retain an oxygen isotopic composition that is consistent with precipitation from Ordovician seawater at reasonable shallow marine temperatures (Fig. 20); therefore, the hardgrounds are not good proxies. Hardground $\delta^{18}\text{O}$ values and the similarity of the isotopic composition between the hardgrounds and overlying limestones are consistent with diagenetic alteration during shallow burial.

A previous study (discussed below) on correlative carbonates in the Michigan Basin has yielded similar $\delta^{13}\text{C}$ and $\delta^{18}\text{O}$ values for calcite in hardgrounds and bulk limestones, and came to similar conclusions. Coniglio et al. (1994) examined burial and hydrothermal diagenesis of the Trenton and Black River carbonates in the Manitoulin Island and Chatham Sag areas of the Michigan Basin. Stable isotope analyses of calcite in bulk limestone and hardgrounds from outcrop and core yielded $\delta^{13}\text{C}$ values from -1.6 to +1.5‰ (PDB) and $\delta^{18}\text{O}$ values from -5.7 to -

4.4‰ (PDB) for both. These values indicate diagenetic alteration not an original Ordovician seawater signature.

CHAPTER 4: LATE-STAGE CARBONATES OF THE SIMCOE GROUP

Introduction

Anomalously high homogenization temperatures have been reported in correlative carbonates elsewhere in southwestern Ontario and the United States, however their origin is not agreed upon. Several studies of hydrocarbon reservoirs in the Michigan Basin interpret these high temperature carbonates as having precipitated at maximum burial depth from deep basinal brines (Granath, 1991; Drzewiecki et al., 1995; and Gerard and Barnes, 1995). Other studies of these and correlative carbonates in the Appalachian Basin interpret them as reflecting hydrothermal precipitation or alteration during burial diagenesis (Coniglio et al., 1994; Yoo et al., 2000; Dix and Robinson, 2003; Luczaj, 2006; and Smith, 2006). There is also debate as to whether the hydrothermally precipitated or altered carbonates represent a local or regional high temperature event (Coniglio et al., 1994; Reimer et al, 2001; Luczaj 2006; and Smith 2006). A clearer understanding of the diagenetic evolution of the carbonates in the Lake Simcoe area could shed additional light on their reservoir equivalents in southwestern Ontario and the United States.

Isotope and Fluid Inclusion Analyses

Stable carbon and oxygen isotope values were determined from late-stage calcite, saddle dolomite and microcrystalline dolomite in outcrop samples. Microthermometric data were determined from samples of late-stage calcite, saddle dolomite, quartz and barite from vugs and

fractures from outcrop. Stable isotope and microthermometry data and photomicrographs are included in Appendices A and B, respectively.

Late-stage Mineral Precipitate Isotope Data

Ferroan and non-ferroan late-stage calcite cements (Fig. 21) have a wide range of $\delta^{13}\text{C}$ values from -8.4 to +2.9‰ (PDB) and a narrow range of $\delta^{18}\text{O}$ values from -11.4 to -6.0‰ (PDB). Ferroan and non-ferroan late-stage microcrystalline dolomites (Fig. 21) have a narrower range of $\delta^{13}\text{C}$ values from -3.9 to +0.4‰ and a narrow range of $\delta^{18}\text{O}$ values from -10.7 to -7.6‰. Ferroan and non-ferroan late-stage saddle dolomites (Fig. 21) also have a narrow range of $\delta^{13}\text{C}$ values from -1.7 to +1.9‰ and a narrow range of $\delta^{18}\text{O}$ values from -13.8 to -8.5‰. The late-stage calcite cements are more enriched in ^{13}C and have a wider range of $\delta^{13}\text{C}$ values than the late-stage microcrystalline and saddle dolomites. The late-stage dolomite $\delta^{18}\text{O}$ values are more depleted in ^{18}O than the calcite. Both late-stage carbonates are more depleted in ^{18}O than the early-stage carbonates (Fig. 21).

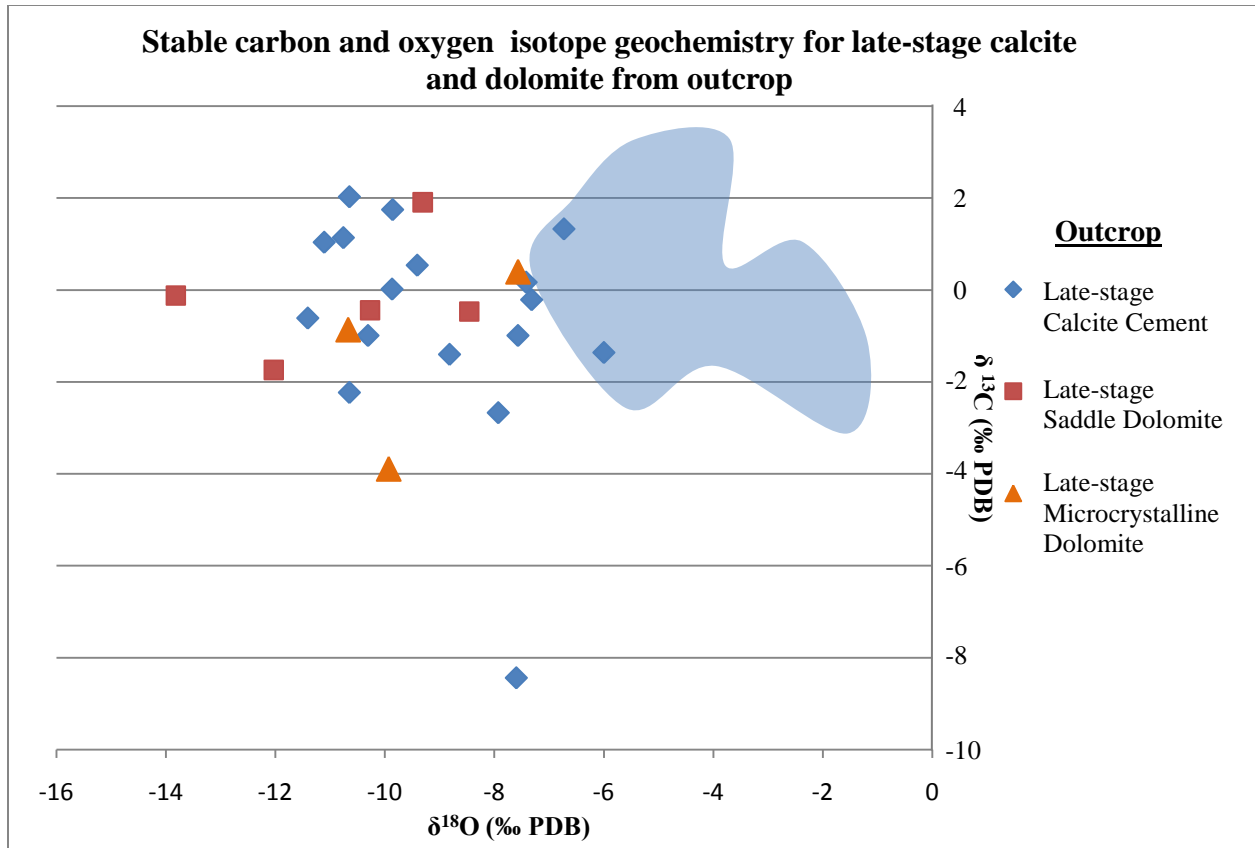


Fig. 21 Graph of stable isotope geochemistry of late-stage calcite cement and late-stage dolomite from the Lake Simcoe area, Ontario. The blue shaded area represents the majority of early-stage carbonates analyzed in this study (Fig. 19). The late-stage dolomites has more negative $\delta^{18}\text{O}$ values than the late-stage calcite. Both late-stage carbonates have more negative $\delta^{18}\text{O}$ values than the early-stage carbonates.

Fluid Inclusion Petrography

Fluid inclusion petrography was completed on twelve polished sections containing late-stage calcite in fractures and vugs. One polished section also contained saddle dolomite. One other polished section contained barite as well as the calcite. Three of the polished sections included megaquartz (Table 1).

Four types of fluid inclusions were identified with sizes ranging from ≤ 2 to ≥ 20 μm . Type 1 inclusions (Figs. 22-24) are found in calcite, dolomite, barite and quartz. Type 1 inclusions are aqueous liquid-rich with very consistent low to very low vapour-liquid ratios (V:L). These inclusions are mainly 5 to 20 μm in size and generally found along healed fractures. They were also observed grouped with types 2 and 4 inclusions along fractures and cleavage planes, (see below). Quartz crystals contain type 1 inclusions that are potentially primary inclusions as they occur as isolated individual inclusions and isolated clusters of inclusions (Fig. 23).

Type 2 inclusions are found in calcite, dolomite, barite and quartz. They are aqueous liquid-only (Figs. 24-26) and are typically 2 to 10 μm in size. Type 2 inclusions were observed in healed fractures and cleavage planes with inclusion types 1 and 4 implying type 2 inclusions potentially are type 1 inclusions that have necked-down.

Type 3 inclusions are oil-bearing, liquid-rich with low to medium V:L (Figs. 27-30). They range in size from ≤ 5 to 16 μm and were observed in healed fractures in barite (Fig. 29) and in the rims of saddle dolomite crystals (Fig. 31) that are adjacent to clear calcite crystals. Some of the type 3 inclusions fluoresce pale orange under ultraviolet light (Fig. 30).

Type 4 inclusions are vapour-only (Fig. 32) and range in size from 5 to ≥ 10 μm . Type 4 inclusions are common to all the polished sections and typically occur with types 1 and 2 inclusions in healed fractures and cleavage planes. Type 4 inclusions are potential type 1 inclusions that have leaked, necked-down or boiled.

Most fluid inclusions of all four types are secondary, lying along cleavage planes and healed fractures that clearly cross grain boundaries. Fluid inclusions that are interpreted as being potentially primary were observed in clear crystals as isolated individual inclusions or in isolated clusters of inclusions. These crystals were either uniformly non-luminescent or uniformly luminescent under cathodoluminescence (CL) therefore it was not determined if potential primary inclusions were trapped in growth zones. Fluid inclusions interpreted as pseudosecondary inclusions were observed in healed fractures within the crystals and did not cross grain boundaries. There were several fluid inclusions of indeterminate origin. A full description of the fluid inclusions is found in Table 2 below.

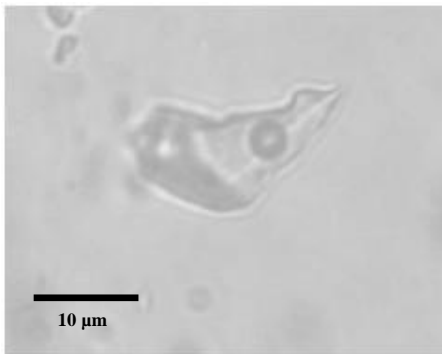


Fig. 22 Type 1 fluid inclusion. Photomicrograph is in ppl. Sample LM-9A.

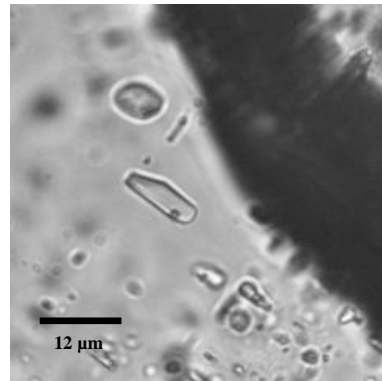


Fig. 23 Type 1 fluid inclusion cluster (ppl). Fluid inclusion sizes range from 5 μm to 12 μm . Sample LM-5.1.

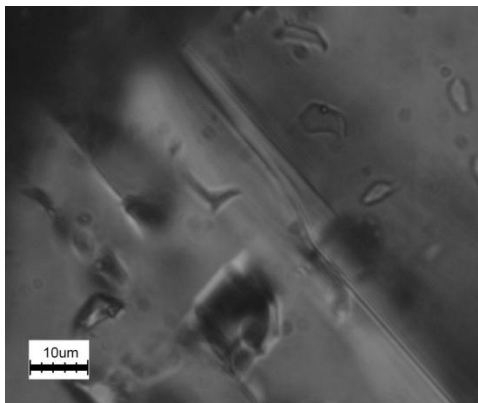


Fig. 24 Small cluster of type 1 and type 2 fluid inclusions (ppl). Sample LM-10B.

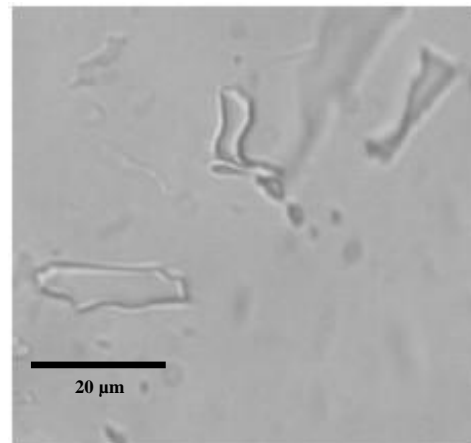


Fig. 25 Type 2 fluid inclusions (ppl) 10 μm to 20 μm in size. Sample 99-101.

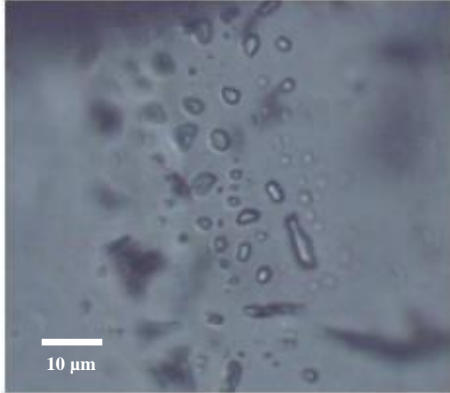


Fig. 26 Type 2 fluid inclusions (ppI). Fluid inclusion sizes range from 2 μm to 10 μm. Sample 99-132.

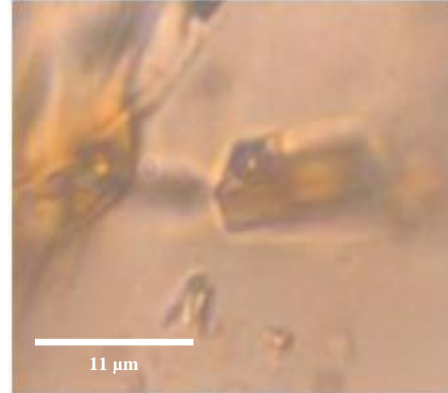


Fig. 27 Type 3 oil inclusions (ppI). Sample LM-6.

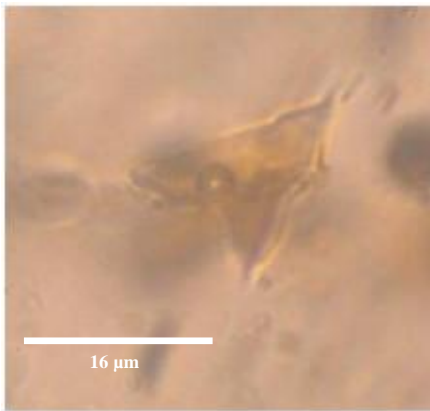


Fig. 28 Type 3 oil inclusion (ppI). Sample LM-6.

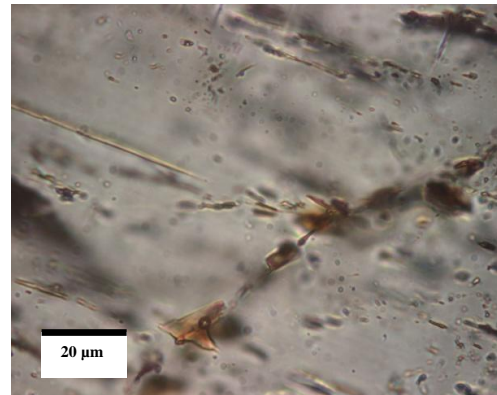


Fig. 29 Type 3 oil inclusions (ppI). Fracture containing secondary inclusions from Figs. 26 and 27. Sample LM-6.

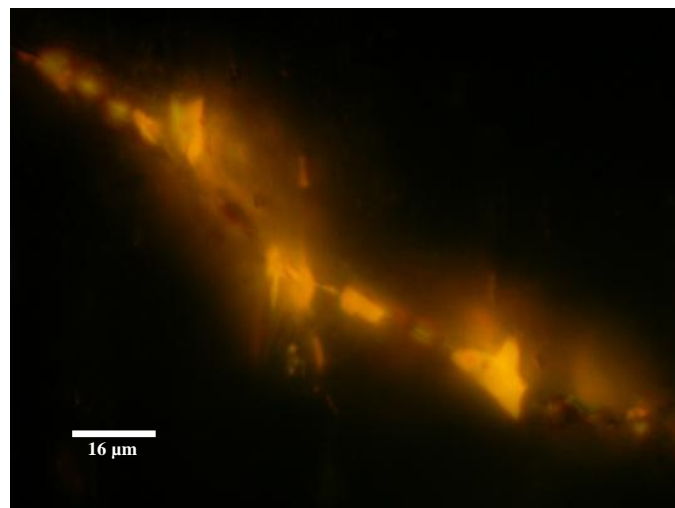


Fig. 30 Type 3 oil inclusions. Fluorescence photomicrograph of the oil inclusions in the fracture in Fig. 29. Pale orange color indicates immature oil and temperatures at the lower end of the oil window from 65 to 150°C. Sample LM-6.

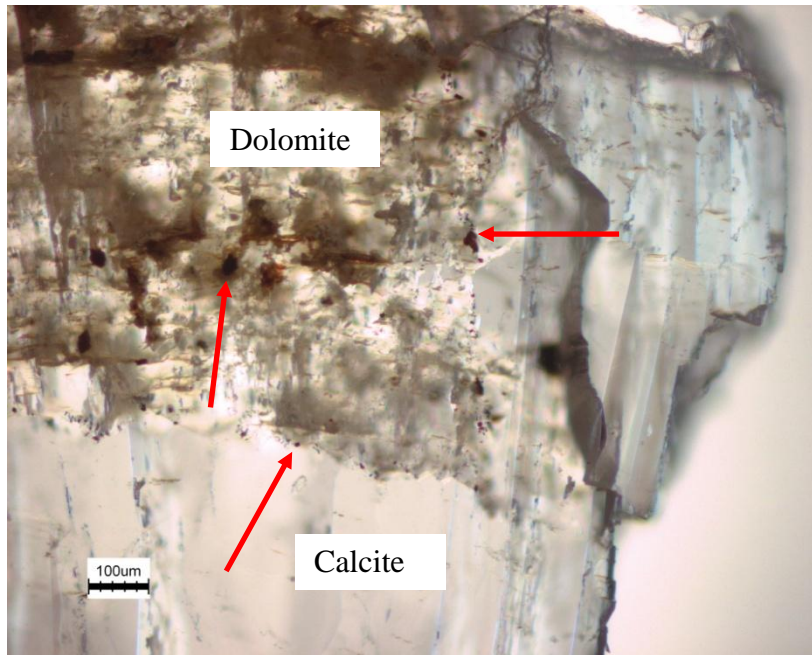


Fig. 31 Type 3 oil inclusions in the rims and interior of saddle dolomite crystals that are associated with clear calcite crystals (ppl). Calcite was identified from its twinning in cpl. Red arrows point to oil inclusions of various sizes. Sample 99-120.

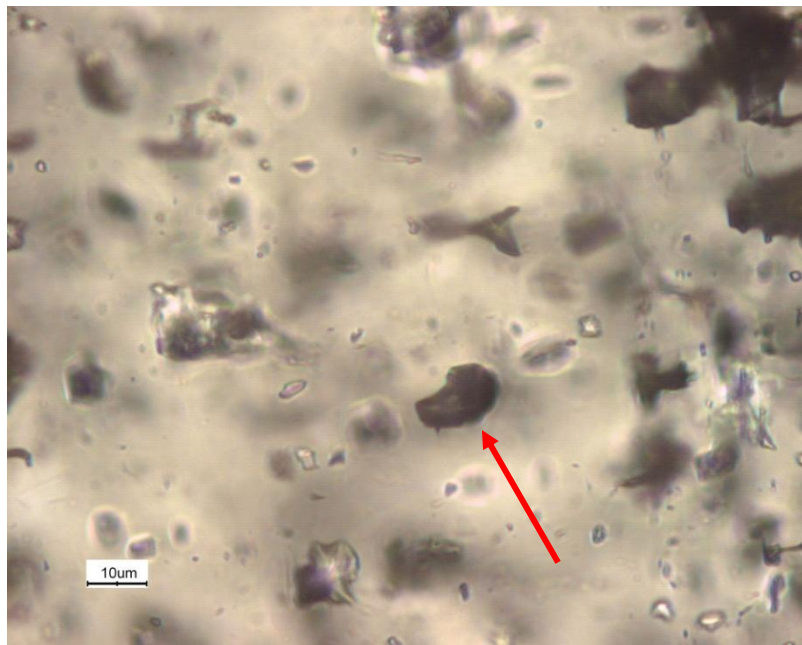


Fig. 32 Type 4 vapour-only inclusion (red arrow) of indeterminate origin in calcite (ppl). Sample LM-4.

Table 2 Petrographic description of fluid inclusions in doubly polished sections (PS) from samples collected in 1999 (99- series) and 2008 (LM- series) from the Lake Simcoe area.

Type	Phases	origin	V:L	Size and shape	Location	Abundance
1	Liquid-rich (low to very low V:L)	Secondary/pseudosecondary, primary and indeterminate	$\geq 40:60$	5 to 20 μm Mainly rounded and negative crystals	Fractures and cleavage. Some found in growth rims	One of the most abundant
2	Liquid-only	Secondary, pseudosecondary (necked down?) and indeterminate		2 to 10 μm Mainly rounded, irregular and elongated	Fractures and cleavage	Least abundant in LM-series PS samples. Dominant in a couple of 99-series PS samples
3	Liquid-rich hydrocarbon-bearing (low to med V:L ratio)	Secondary, pseudosecondary and indeterminate	50:50 to 40:60	≤ 5 to 16 μm Rounded and irregular	Fractures and cleavage	Abundant in a few samples
4	Vapour-only	Secondary, pseudosecondary. Leaked, necked down		Typically larger than other types from 5 μm to ≥ 10 μm . Rounded and irregular	Fractures and cleavage	Common in most PS

Late-stage Mineral Precipitate Fluid Inclusion Data

Approximately 300 fluid inclusions were analyzed, of which 177 yielded useable data. The method used is described in full in the Methodology section of Chapter 1. The majority of fluid inclusions were very difficult to analyze regardless of the mineral host. Homogenization temperatures (T_h) were the easiest to determine, whereas ice freezing, eutectic (T_e) and final ice melting ($T_{m(\text{ice})}$) temperatures were the most difficult to determine and often not observable. Most of the complete data sets (freezing, T_e , $T_{m(\text{ice})}$, and T_h) were obtained from type 1 inclusions. Type 2 inclusions were the most difficult to obtain data for. They were typically smaller than

types 1 and 3 inclusions and most did not nucleate a vapour bubble even after repeated freezing and thawing. Type 3 oil inclusions were analyzed for homogenization temperatures only. Petroleum inclusions have very complex compositions (Munz, 2001). Low temperature phase behavior of petroleum inclusions is different to other types of fluid inclusions (Goldstein, 2001). Freezing of petroleum inclusions is rarely seen even to temperatures as low as -180°C (Burruss, 1981). Type 4 inclusions did not yield any data even when frozen to -196°C suggesting these inclusions are empty cavities that have lost all their fluids. Therefore, type 4 inclusions are not included in the microthermometric results.

Calcite contained the most fluid inclusions ($n=150$) which yielded useable data. There were fifteen clusters that contained in total 123 of the 150 inclusions. The remaining 27 were single inclusions. The cloudiness of saddle dolomite crystals (Fig. 33) limited the visibility of inclusions to only two clear growth rims in a single sample (99-120). Four single inclusions and one cluster with three inclusions in the saddle dolomite showed visible phase changes allowing collection of complete data sets.

Complete data sets for inclusions hosted by quartz were obtained from one cluster ($n=6$) in the only sample (LM-5.1) containing crystals that are large enough to have inclusions with visible phase changes. Eleven single inclusions and one cluster ($n=3$) were analyzed in barite. Stretching of inclusions in barite was tested for by evaluating the consistency in homogenization temperatures in several inclusions by repeated heating and cooling of the inclusions. No stretching of the inclusions was detected. Complete data sets were obtained from seven

inclusions in the barite. The majority of inclusions analyzed in the present study ranged between 2 to 10 μm in size with a few 20 to 30 μm in size. All inclusion clusters analyzed each contained from 3 to more than 50 inclusions.

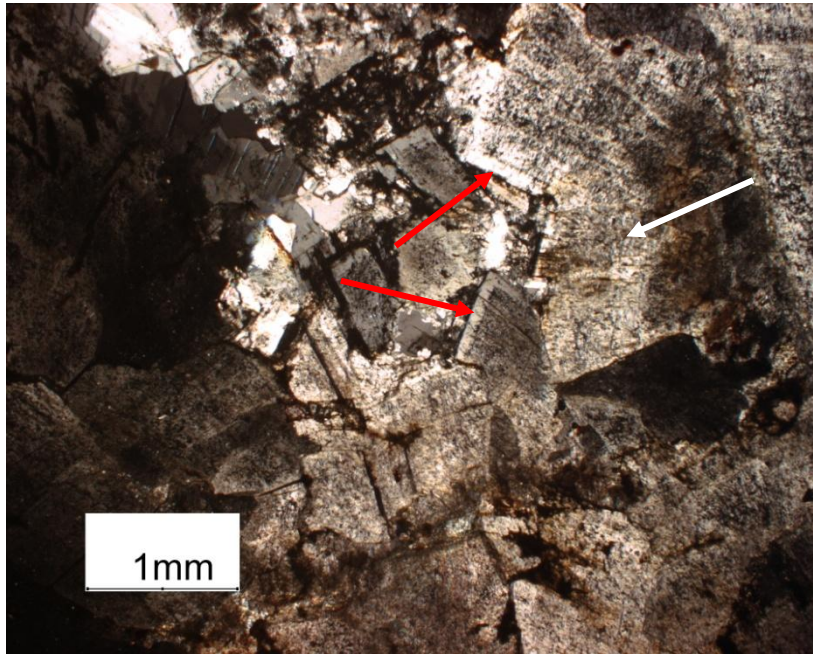


Fig. 33 Red arrows point to the two clear overgrowths where fluid inclusions were found for analyses. The cloudy interiors of the saddle dolomite crystals (white arrow) obscured most inclusions. Photomicrograph taken in cpl. Sample 99-120.

Microthermometry

Homogenization Temperatures

A wide range in homogenization temperatures (T_h) from 43.1°C to >300°C was observed in all mineral hosts (Fig. 34) with calcite having the widest range, followed by barite. There are three populations of T_h values (Fig. 34): 1) >100°C; 2) high 90s°C to mid 70s°; and 3) low 70s°C to low 40s°C. All three populations were clearly seen in calcite (Fig. 34 and 35). A detailed list of microthermometric data is in Table 3 located at the end of the results section.

Type 1:

Type 1 inclusions (n=125) have the widest range in T_h values (Table 3) from 43.1°C to >200°C (Fig. 34). Secondary (n=76) and possible primary (n=21) inclusions have similar ranges of T_h values. The majority of primary inclusions have a narrower range (80 to 92°C) than the secondary inclusions (65 to 95°C). Pseudosecondary inclusions (n=4) have the narrowest range (Fig. 34) possibly because of the small number of pseudosecondary inclusions analyzed. Inclusions of indeterminate origin (n=19) have the widest range in T_h values with six inclusions >200°C (Fig. 34). Given a lack of a distinct histogram peak at high temperatures (Fig. 34) and no evidence of metamorphism, it is likely that all fluid inclusions with homogenization temperatures greater than 150°C represent inclusions that have leaked.

Type 1 inclusions in calcite (n=89) have the lowest homogenization temperatures with the majority ranging from 65-95°C (Fig 35). Saddle dolomite (n=7) and quartz (n=6) have distinctly higher T_h values (90-110°C) than the calcite. Saddle dolomite has one potential primary inclusion located in a relatively clear growth rim and oriented along its c-axis parallel to the crystal boundary. This inclusion has a T_h value of 137°C indicating a high temperature origin. Type 1 inclusions in barite (n=14) all homogenized at temperatures much greater than 100°C and represent the second highest T_h values in this study (Fig. 35). These inclusions all have $T_{m(ice)}$ values within $\pm 8^\circ\text{C}$ of each other (-38 to -30°C) and are in the range of the majority of Type 1 inclusions (Fig. 36). This indicates these inclusions have leaked or necked down (Goldstein and Reynolds, 1994).

Type 2:

Type 2 inclusions (n= 50) are primary (n= 3) and secondary (n=47) in origin (Fig. 34). Only fourteen of the type 2 inclusions nucleated a vapour bubble even after several cooling and heating cycles. Thirteen of these inclusions have a consistent T_h value of 85°C (Table 3) and one inclusion has a T_h value of 92°C (Fig. 34 and 35). All Type 2 inclusions are in calcite.

Type 3:

Type 3 petroleum inclusions in barite are secondary (n=3) in origin. Two inclusions yielded homogenization temperatures of 98.1°C and 104.3°C (Figs. 34 and 35). These temperatures are well within the oil window from 65 to 150°C (Goldstein and Reynolds, 1994). This is supported by the pale orange fluorescence of the oil inclusion (Fig. 30) which indicates immature oil from the low end of the oil window (Goldstein and Reynolds, 1994). One petroleum inclusion in sample LM-6 initially homogenized at 120°C. When the analysis was repeated to confirm the temperature the T_h dropped to 116°C and continued to drop after each run. Analysis was discontinued after the ninth run and a T_h value of 79.6°C. This phenomenon was likely caused by overheating of the sample in the initial run. The overheating may have caused hydrocarbon cracking and compositional changes leading to differences in homogenization temperatures (Robert Linnen personal communication, 2009).

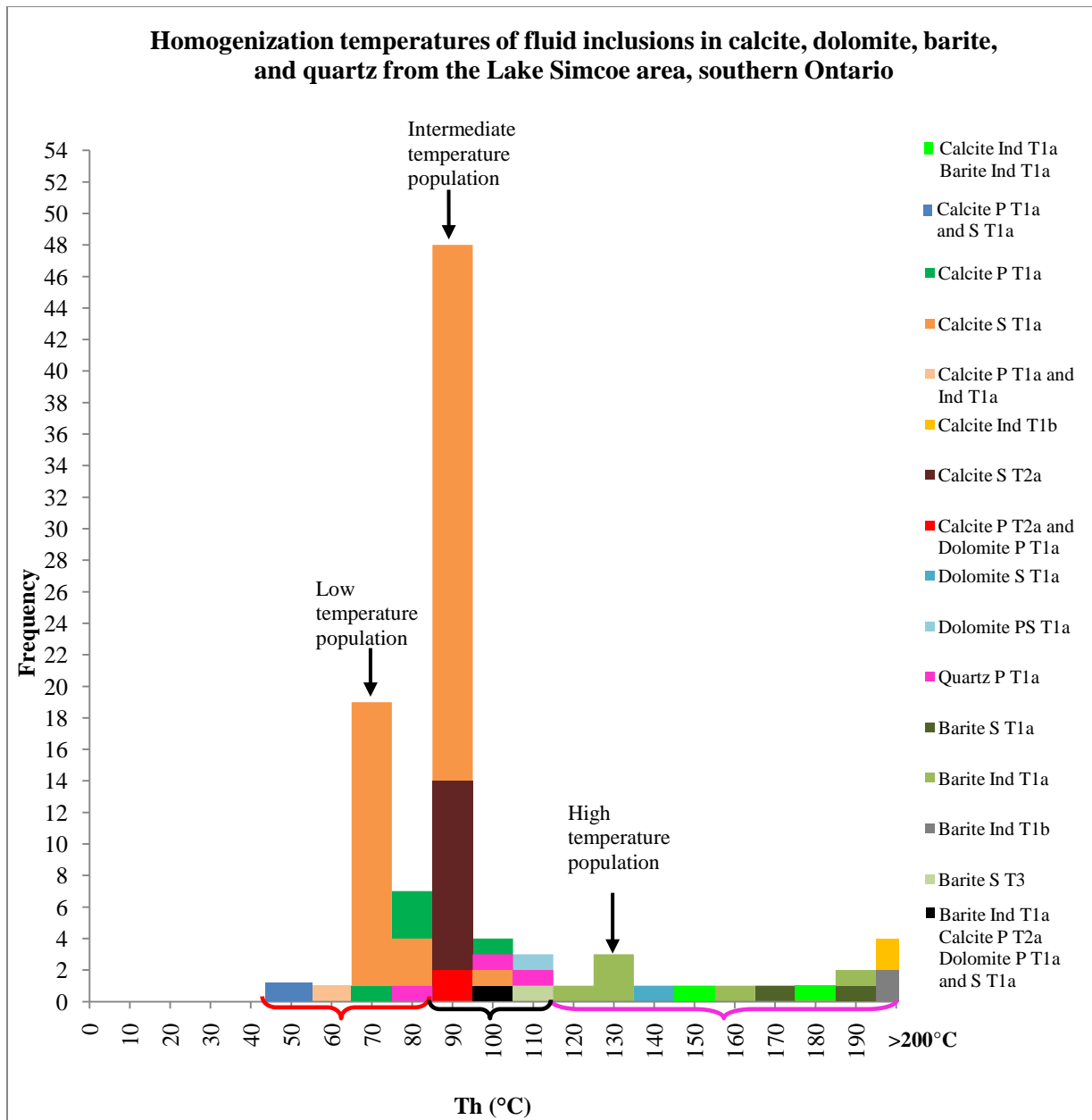


Fig.34 Histogram of T_h values for all types and origins of fluid inclusions in samples from the Lake Simcoe area, southern Ontario. Calcite had the majority of inclusions analyzed for this study therefore, shows the widest range in T_h values. Three populations of T_h values are seen on the histogram: 1) 40s to low 70s°C (red bracket); 2) high 70s to 100°C (black bracket); and 3) > 100°C (pink bracket).

P=Primary, S=Secondary, PS= Pseudosecondary, Ind=Indeterminate, T=Inclusion type. The a-b designations (T1a, T2b) are explained later in the final ice melting temperatures and salinity section below (following eutectic temperatures section).

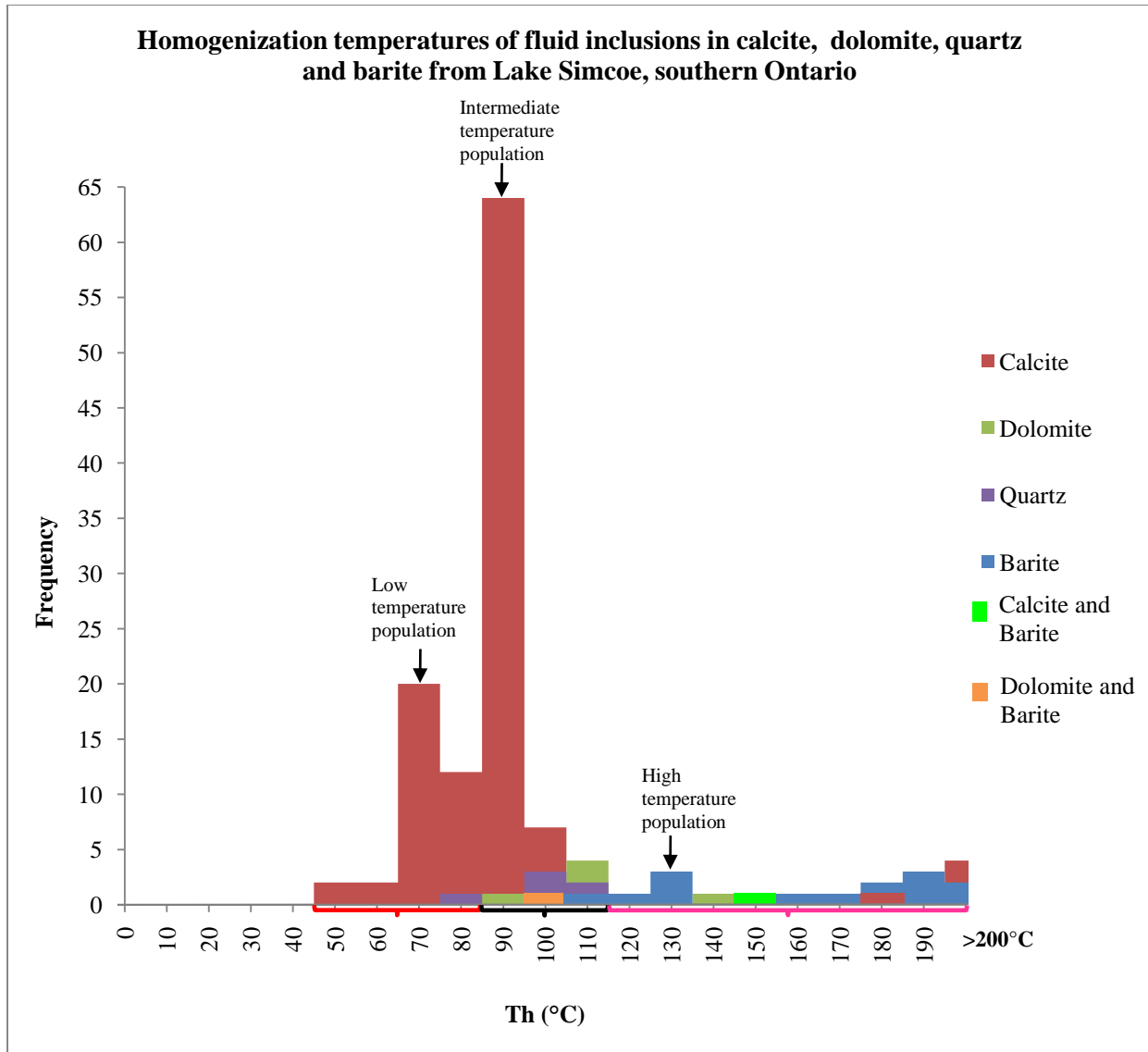


Fig. 35 Histogram of T_h values by mineral only for fluid inclusions in samples from the Lake Simcoe area, southern Ontario. Calcite had the majority of inclusions analyzed for this study therefore, shows the widest range in T_h values. Three populations of T_h values are seen on the histogram: 1) 40s to low 70s°C (red bracket); 2) high 70s to 100°C (black bracket); and 3) >100°C (pink bracket). The majority of inclusions in calcite have the lowest T_h ranging from 65-95°C. The majority of inclusions in dolomite and quartz range from 91-110°C and are distinctly higher than inclusions in calcite.

First Ice Melting Temperatures

First ice melting temperatures (eutectic, T_e) for type 1 fluid inclusions ($n=79$) range from -67 to -47°C (Fig.36) with the majority between -65 and -55°C (Table 3). These T_e values indicate

the presence of NaCl+CaCl₂ plus possibly MgCl₂ (Goldstein and Reynolds, 1994; Oakes et al, 1996). There is one type 1 inclusion with an anomalously high T_e value of -17°C. This may be due to either there being very little CaCl₂ in the fluid or from alteration (e.g. decrepitation and refilling). This inclusion has a T_h >200°C possibly from leaking or necking down (Goldstein and Reynolds, 1994).

Eutectic temperatures for type 2 inclusions (n=49) range from -60 to -35°C (Table 3). This range overlaps with the T_e range of type 1 inclusion (Fig. 36) indicating that the two types of inclusions have a similar composition.

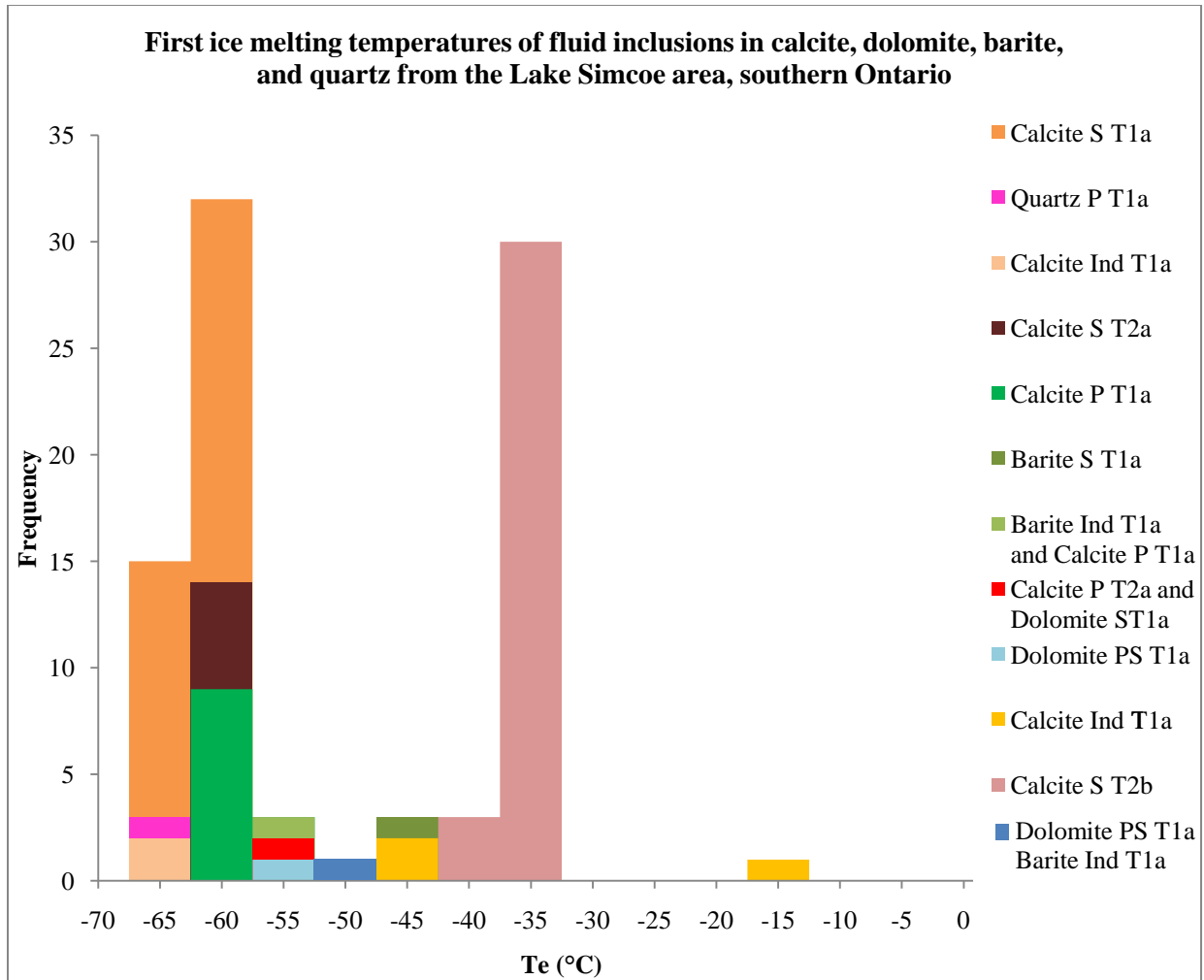


Fig. 36 Histogram of T_e values for all types and origin of inclusions from the Lake Simcoe area, southern Ontario. Type 1 and type 2 inclusions have similar low eutectic temperatures indicating $\text{CaCl}_2 + \text{MgCl}_2(?)$ rich fluids. P=Primary, S=Secondary, PS= Pseudosecondary, Ind=Indeterminate, T=Inclusion type. The a-b designations (T1a, T2a) are explained later in the final ice melting temperatures and salinity section below.

Final Ice Melting Temperatures and Salinity of Fluid Inclusions

There is a wide range over all of final ice melting temperatures, from -52.7 to 0°C (Table 3); however, quartz, barite, and saddle dolomite have relatively narrow $T_{m(\text{ice})}$ ranges. Ice was the only product that was observed to have melted in this study. There are two populations of $T_{m(\text{ice})}$ values consisting of both type 1 and type 2 inclusions. Type 1a and 2a (T1a and T2a) represent

population 1 and range from -52.7 to -6.5°C. Type 1b and 2b (T1b and T2b) represent population 2 and range from -2 to 0°C. The ice in the majority of T1b and T2b inclusions melted very close to or at 0°C (Table 3) implying fluid compositions close to pure water (Goldstein and Reynolds, 1994).

Final ice melting temperatures were used to calculate salinities which are reported as weight percent CaCl₂ (wt% CaCl₂). Salinity was determined using the equations and computer program of Bakker et al. (1996). Fluid composition was determined from the Oakes et al. (1990) NaCl-CaCl₂-H₂O ternary phase diagram.

Type 1:

The T1a fluid inclusions (n=85) have a wide range in final ice melting temperatures from -52.7°C to -16°C with a composition of 18.7 to 33.4 wt%_{CaCl₂} (Fig 37). The T1a inclusions in dolomite (n=2), barite (n=7), and quartz (n=3) have similar T_{m(ice)} ranges (-40 to -29°C) whereas calcite (n=73) has a wider T_{m(ice)} range from -52.7 to -16°C. The majority of inclusions in all four minerals have similar compositions (Fig. 37). No significant difference in T_{m(ice)} values was seen between T1a primary (n=12), pseudosecondary (n=2), secondary (n=60) or the majority of indeterminate (n=6) inclusions (Fig. 36). There are two out of eight inclusions of indeterminate origin that have higher T_{m(ice)} values (-23 and -16°C) with lower salinities (22.8 and 18.7 respectively) than the rest of the T1a inclusions (Fig. 37). The T1a secondary inclusions (n=60) have the widest range in salinities (Fig. 37); however, no significant difference was seen between

T1a inclusions of primary (n=15), pseudosecondary (n=2), and indeterminate (n=6) origin (Fig. 37).

The T1b fluid inclusions are of indeterminate origin in calcite (n=3) and have a $T_{m(\text{ice})}$ range of -0.2 to 0°C (Table 3). The salinities of the T1b inclusions range from 0 to 0.5 wt% CaCl_2 (Fig. 37).

Type 2:

The T2a inclusions (n=19) are in calcite and have a $T_{m(\text{ice})}$ range similar to T1a inclusions. Final ice melting temperatures (Table 3) for T2a inclusions range from -39 to -37.8°C and were determined from inclusions of primary (n=2) and secondary (n=17) origin (Fig. 36). There is one cluster of three T2a inclusions of secondary origin with a $T_{m(\text{ice})}$ value of -6.5°C . Salinities ranging from 10.5 to 29.4 wt% CaCl_2 were determined for seventeen T2a inclusions of primary (n=2) and secondary (n=17) origin (Fig.37).

The T2b inclusions (n=33) are of secondary origin in calcite with a $T_{m(\text{ice})}$ range of -2 to -0.5°C and a composition of 1.2 to 2.7 wt% CaCl_2 (Fig.37). Also, T2b inclusions have slightly higher T_e values (-35°C) compared to T2a inclusions (-60 to -40°C). It was very difficult to see low temperature phase changes in type 2 inclusions. Repeated cycling yielded no results in many inclusions even when frozen to -196°C .

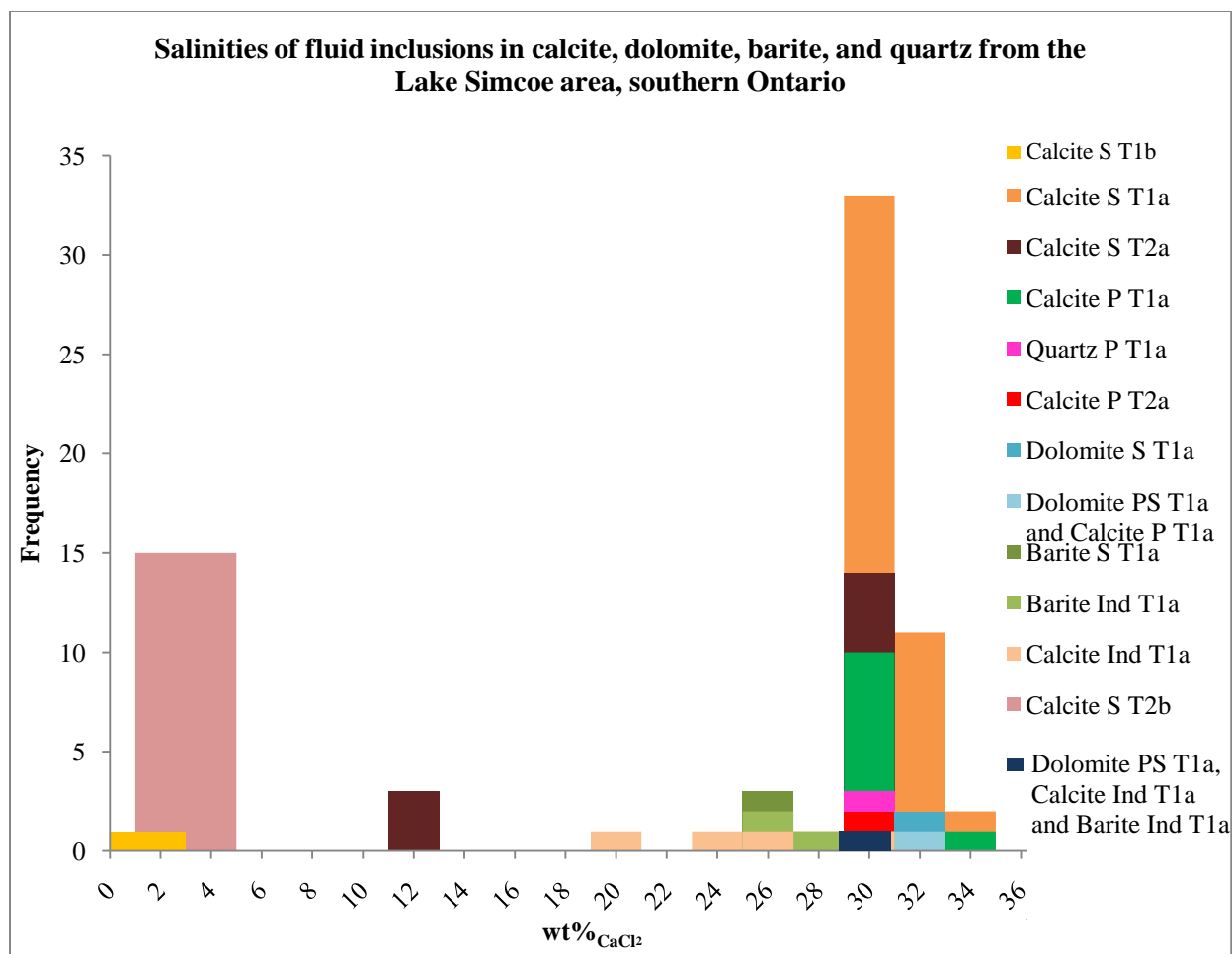


Fig. 37 Histogram of salinities for all types and origin of inclusions from the Lake Simcoe area, southern Ontario. The majority of type 1a and type 2a inclusions are clustered in the 23 to 35 wt% CaCl_2 range. In contrast type 1b and type 2b inclusions are much lower in salinity with the majority of inclusions in the 0 to 3 wt% CaCl_2 range. P=Primary, S=Secondary, PS= Pseudosecondary, Ind=Indeterminate, T=Inclusion type.

Homogenization Temperatures and Salinity

Saddle dolomite in sample 99-120 chip 1 (Appendix B) has a cluster of three T1a inclusions of pseudosecondary origin located in the interior of the crystal and a single primary inclusion located in a clear growth rim. Each of the inclusions in the cluster has a T_h value of 100.7°C and the single inclusion has a T_h value of 90.4°C. Also, saddle dolomite in sample 99-120 chip 3 (Appendix B) has three T1a inclusions (two primary and one secondary) located in a relatively

clear growth rim and are oriented parallel to the crystal boundaries (Fig 38). The primary inclusion located in the center of the growth rim has a T_h value of 137°C (Fig. 38) whereas the primary inclusions located closest to the crystal boundary has a T_h value of 83°C (Fig 38). The secondary inclusion has a T_h value of 109°C and is located in a fracture that is slightly closer to the crystal boundary than the high temperature primary inclusion (Fig 38). The salinities of six out of the seven inclusions described above are very similar (Fig. 39) indicating the inclusions could have formed from the same fluids. A $T_{m(\text{ice})}$ value was not obtained from the primary inclusions with a T_h value of 83°C . The similarity in salinity and the decreasing homogenization temperatures towards the crystal boundaries (Fig. 38) indicate cooling over time of the hydrothermal fluids from which the saddle dolomite precipitated.

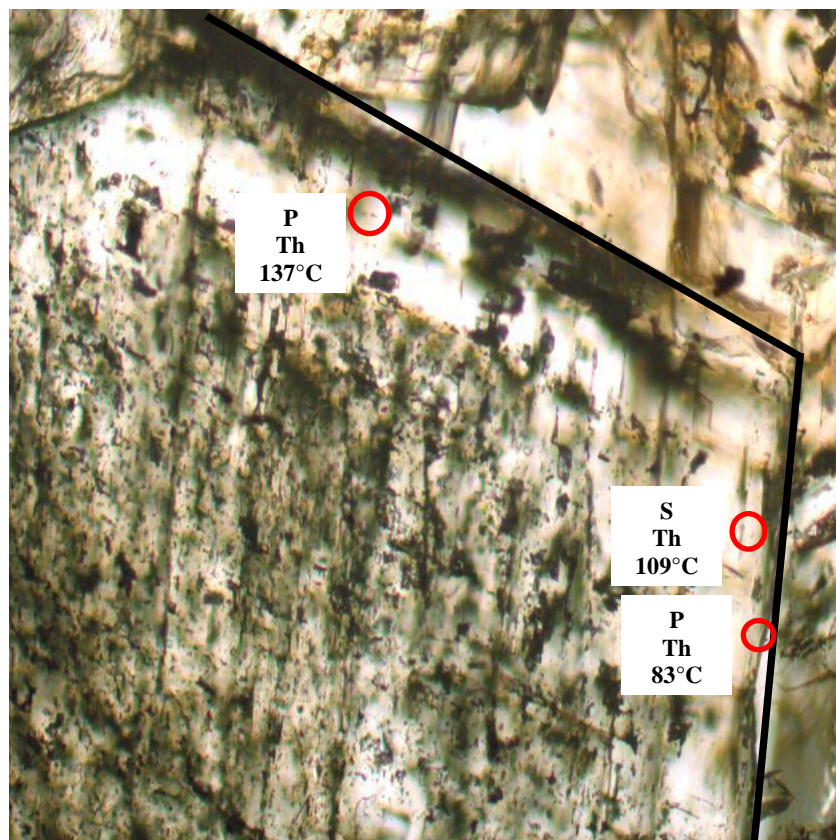


Fig. 38 Fluid inclusions (red circles) in saddle dolomite growth rims (ppl). Inclusion homogenization temperatures decrease towards crystal boundaries. Black lines highlight crystal boundaries. Sample 99-120.

Barite in sample LM-6 had T1a fluid inclusion clusters in chips 2 and 3 (Appendix B). Homogenization temperatures ranged from 130 to 181°C in chip 2 and 164 to 189°C in chip 3 (Figs. 34 and 35). However, given that the homogenization temperatures are anomalously high and that all inclusions from both chips had very similar salinities (Fig. 39), it is likely that these T1a inclusions have stretched at some point in time prior to analysis (Goldstein and Reynolds, 1994); therefore, these T_h values are discounted.

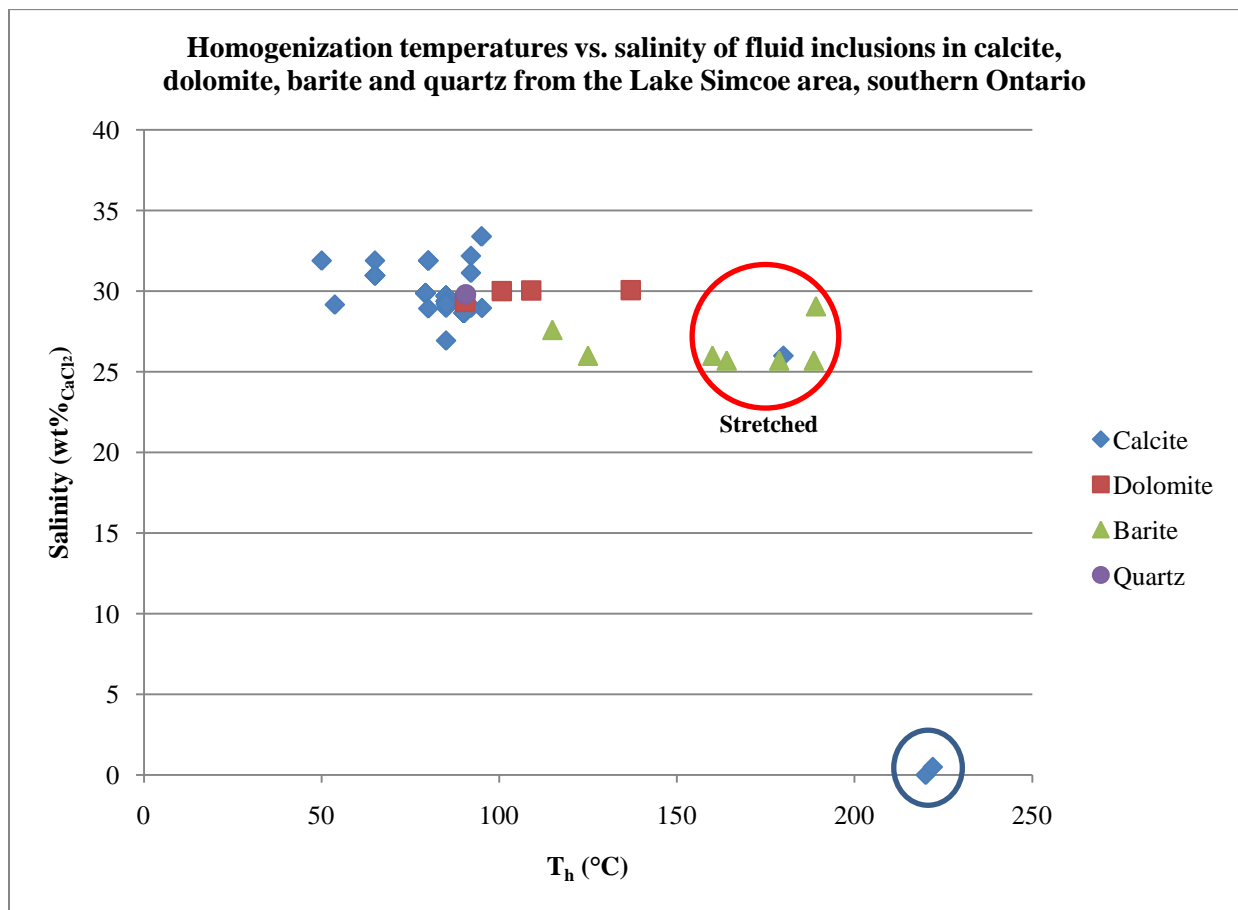


Fig. 39 Homogenization temperatures vs. salinity graph. The majority of T1a inclusions in calcite are grouped around 30 wt% CaCl_2 and 90 to 100°C. The T1a inclusions in calcite with $T_h < 150^\circ\text{C}$ are interpreted as having leaked. The inclusions in calcite with salinities between 0 and 1wt% CaCl_2 represent the T1b and T2b inclusions (blue circle). The T1a inclusion clusters in barite have a range of high T_h values and very similar salinities indicating stretching (red circle). Single T1a inclusions in dolomite have a range of T_h values and very similar salinities. Single T1a inclusions in quartz have similar T_h values and salinities as some T1a inclusions in dolomite. See text for details.

Table 3 Microthermometric data for type 1 and type 2 fluid inclusions from the Lake Simcoe area, southern Ontario. ND=No data

Type 1a				
Mineral	T_h °C	T_e °C	T_{m(ice)} °C	Salinity wt%_{CaCl2}
Calcite	43.1 to 180 ± 0.1 to 5	-66.6 to -47 ± 0.1 to 10	-52.7 to -16 ± 0.1 to 3	18.7 to 33.4
Saddle Dolomite	83 to 137 ± 0.1 to 3	-56 to -53 ± 5 to 10	-38.9 to -41.1 ± 0.1	29.3 to 30
Quartz	76 to 105 ± 0.2 to 1	-65 ± 1	-40.3 ± 0.1	29.8
Barite	115 to 189.1 ± 0.1 to 5	-59.9 to -49 ± 0.3 to 5	--34 to -29.3 ± 0.1 to 2	25.7 to 29.1
Origin	T_h °C	T_e °C	T_{m(ice)} °C	Salinity wt%_{CaCl2}
Primary	43.1 to 137 ± 5	-63 to -40.3 ± 1 to 10	-37 to -48.1 ± 0.2 to 2	28.7 to 32.2
Secondary	65 to 188 ± 5	-61 to -49 ± 1 to 10	-29.3 to -52.7 ± 0.1 to ± 3	25.7 to 33.4
Pseudosecondary	90 to 100.7 ± 0.1	-55 and -53 ± 10	-38.9 to -40.9 ± 0.1	29.3 and 30
Indeterminate	55.2 to 189.1 ± 0.1 to 5	-66.6 to -47 ± 1 to 10	-16 to -38.1 ± 0.1 to ± 2	26 to 28.9
Type 1b				
Mineral/Origin	T_h °C	T_e °C	T_{m(ice)} °C	Salinity wt%_{CaCl2}
Calcite and barite/Indeterminate	>200	-17 ± 1 to 5	-0.2, 0 ± 0.1 to 1	0.5, 0
Type 2a				
Mineral	T_h °C	T_e °C	T_{m(ice)} °C	Salinity wt%_{CaCl2}
Calcite	85 and 92 ± 2 to 5	-60 to -40 ± 5	-39 to -6.5 ± 0.2 to 0.5	10.5 to 29.4
Origin	T_h °C	T_e °C	T_{m(ice)} °C	Salinity wt%_{CaCl2}
Primary	85 and 92 ± 2	-57 and -56 ± 5	-37.8 ± 0.2	29
Secondary	85 ± 5	-60 ± 5	-39 and -38.5 ± 0.5	29.2 and 29.4
Type 2b				
Mineral/Origin	T_h °C	T_e °C	T_{m(ice)} °C	Salinity wt%_{CaCl2}
Calcite/secondary	ND	-35 ± 5	-1.2, -0.5 ± 0.1 to 0.2	2.7, 1.2
Type 3				
Mineral/Origin	T_h °C	T_e °C	T_{fm} °C	Salinity wt%_{CaCl2}
Barite/secondary	98.1 and 104.3 ± 0.1	ND	ND	ND

Discussion

Fluid inclusion types 1 and 2 were subdivided into “a” and “b” groups based on final ice melting temperatures. These subtypes represent two fluid inclusion assemblages (FIA) from separate environments or events. The high salinity fluid inclusions T1a and T2a (FIA1) in this study are similar to highly saline fluids in inclusions analyzed in other studies on correlative carbonates in southern Ontario and the United States. These fluids are interpreted as reflecting saline basin brines from which the host minerals precipitated during burial diagenesis (e.g., Granath, 1991; Coniglio et al., 1994; Drzewiecki et al., 1994; and Yoo et al., 2000).

The low salinity fluid inclusions T1b and T2b (FIA 2) may reflect mineral precipitation in a meteoric environment such as a vadose or phreatic zone. Evidence of this is found in samples LM-9A, 99-101, and 99-132. Sample LM-9A has vapour-liquid T1b inclusions in calcite with a $T_{m(\text{ice})}$ value of 0°C, 0 wt% CaCl_2 and T_h values $>200^\circ\text{C}$ (T_e was undetermined). The sample has inclusions of different phases (liquid-only, vapour-liquid and vapour only) (Fig. 40), also the vapour-liquid inclusions have variable V:L (Fig. 40). The near pure water composition of the inclusions, the presence of several phases of inclusions and the variable V:L are indicative of fluid inclusions trapped in a vadose zone (Goldstein et al., 1991). Vadose zones have a mixture of atmospheric gases and meteoric waters that allow for several different phases and variable V:L in inclusions trapped during mineral precipitation (Goldstein et al., 1991). Also, the anomalously high T_h values of the T1b inclusions may reflect trapping of atmospheric gases (Goldstein and Reynolds, 1994) and not leaking as first interpreted. If inclusions trapped in a vadose environment are heated the all-liquid inclusions will be the only ones affected (excluding

decrepitated, leaked/refilled or stretched inclusions) and will nucleate small vapour bubbles (Goldstein et al., 1991). Because of this the vadose zone characteristic of variable V:L in the inclusions will be preserved (Goldstein et al., 1991).

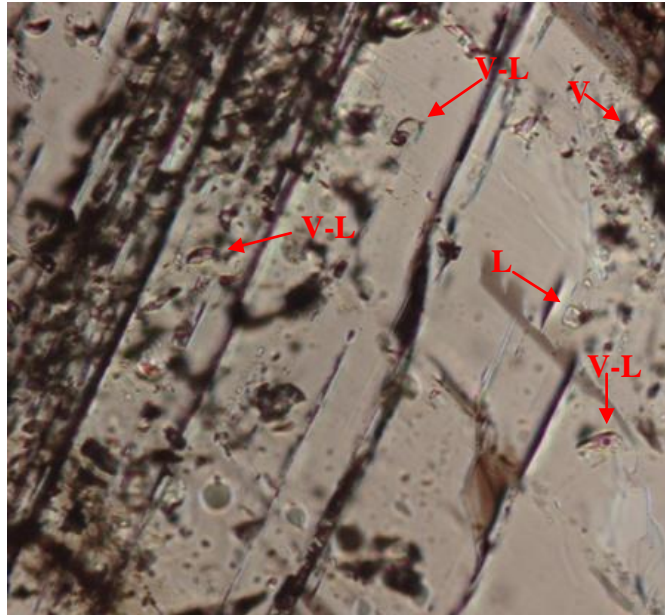


Fig. 40 Inclusions of various phases and V:L in calcite (cpl). V-L= vapour-liquid, V= vapour-only, L= liquid-only. Sample LM-9A

Samples 99-101 and 99-132 have liquid-only T2b inclusions in calcite with a T_e value of -35°C (both samples), $T_{m(ice)}$ values of -1.2 and -0.5°C and salinities of 1.2 and 2.7 wt% $CaCl_2$. These inclusions never nucleated vapour bubbles; therefore, homogenization temperatures could not be determined. The persistent single phase nature of these inclusions and their near pure water composition indicate these inclusions were trapped in a phreatic zone (Goldstein et al., 1991). The phreatic environment is constantly saturated so very little or no atmospheric gases are present allowing for only single phase (liquid-only) inclusions to be trapped during mineral precipitation (Goldstein and Reynolds, 1994). If inclusions trapped in a phreatic environment

are heated they will not nucleate a vapour bubble unless a volume change occurs (leaking, decrepitation or stretching) (Goldstein 1986).

An alternative explanation of the low salinity inclusions is alteration from an influx of meteoric fluids during periods of basement uplift. If this is the case establishing a timing relationship between the formation of FIA 1 and FIA 2 is difficult with the samples in this study because there are very few spatial relationships between fluid inclusion types in a single sample or sample location. Stable oxygen isotopes analysis was performed on carbonates extracted from the same samples as the polished sections containing the type 'a' and 'b' inclusions. The stable isotope analysis did not reveal any difference between the two events. Samples containing T1b and T2b inclusions have similar carbonate $\delta^{18}\text{O}$ values as samples containing T1a and T2a inclusions.

Although stable oxygen isotopes for samples that contain type 'b' inclusions do not reflect an influx of meteoric fluids, the very low salinities of the inclusions do suggest an involvement of meteoric fluids. For alteration of the type 'b' inclusions by these fluids to be a reasonable interpretation, the minerals hosting the inclusions had to be continuously bathed in or near a constant source of meteoric water without actually being in a vadose or phreatic environment.

The sites where the samples containing the T1b and T2b inclusions were taken from lie directly on faults and terrain boundaries (Fig. 41) that potentially are good conduits for descending meteoric fluids. Boyce et al., (2002) performed seismic and high-resolution magnetic surveys in Kempenfelt Bay (Lake Simcoe) and Hamilton Harbor (Lake Ontario) to

better understand the association of near-surface faulting with basement structural features. The Lake Simcoe survey revealed a 3 km wide zone of northwest-trending high-amplitude magnetic anomalies across the center of the bay (Boyce et al., 2002). These high-amplitude anomalies mark the boundaries of the Alliston-Go Home shear zone (Fig. 41). The shear zone is offset by 500 m from a left-lateral strike-slip fault. Normal faults, localized thrust faults, slumping, and gas-escape structures in post-glacial lake bottom sediments are interpreted as being associated with west-east strike-slip movement along pre-existing basement faults (Boyce et al., 2002). The deformation of post-glacial lake bottom sediments is evidence of recurrent reactivation of pre-existing basement faults by tectonic stresses emanating from plate margins (Boyce et al., 2002).

Evidence from reconstruction of Paleozoic tectonic and depositional processes along the east margin of the Michigan Basin and surrounding areas of the Canadian Shield, indicates periodic recurrence of basement uplift during the Paleozoic and Mesozoic (Sanford et al., 1985). This interpretation is supported by satellite imagery (Sanford et al., 1985). The recurring basement uplift caused reactivation of basement faults and vertical movement of fault-bounded megablocks (Sanford et al., 1985). These periodic fault and megablock reactivations could allow for the movement of ascending fluids from basement rocks and descending meteoric fluid.

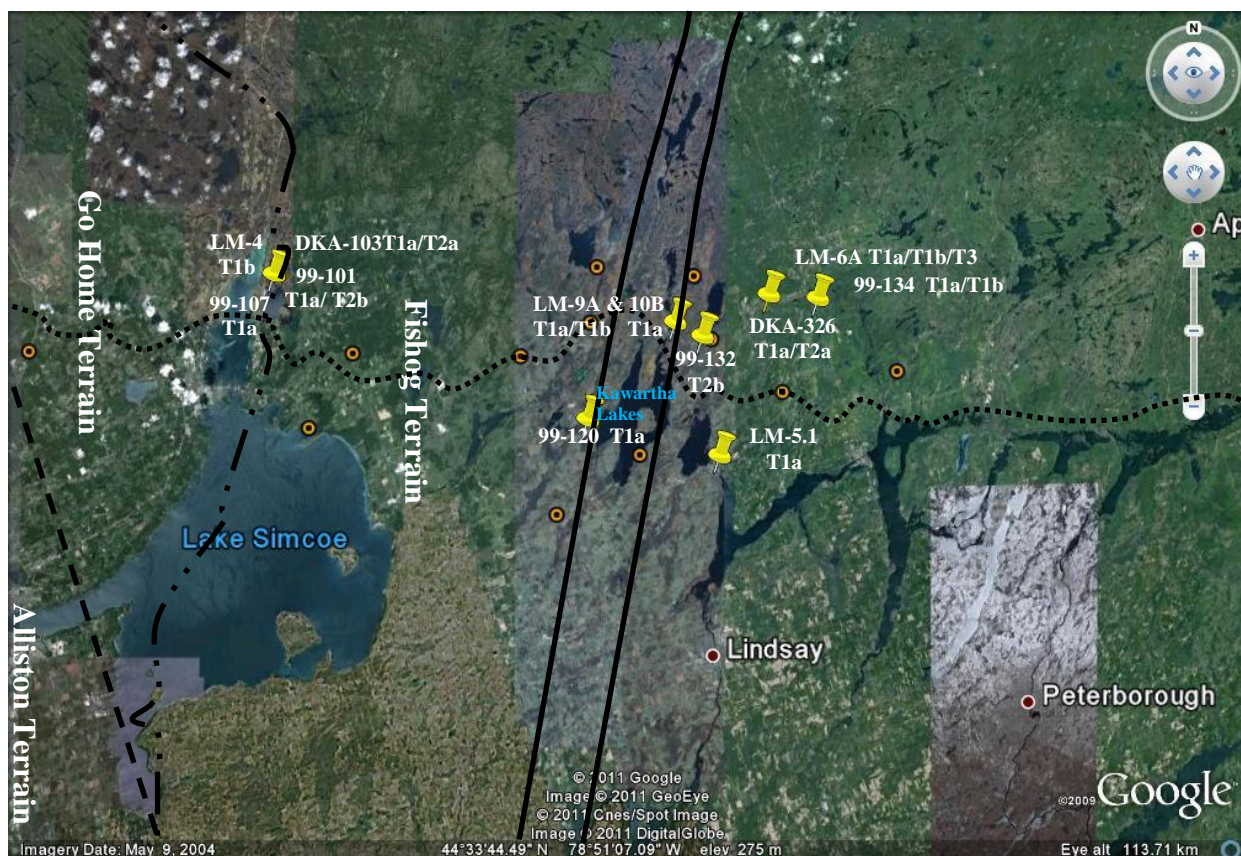


Fig. 41 Satellite image of the Lake Simcoe area taken from Fig.1 with fluid inclusion types added to sample numbers. The location of the samples containing T1b and T2b inclusions have a roughly linear occurrence across the study site. These sample sites lie directly on basement structural features that run through the Lake Simcoe area. The Central Metasedimentary Belt Boundary Zone (CMBBZ) is one such feature that runs through the Kawartha Lakes. The Precambrian contact runs above and through the sample site. All linear features are roughly positioned from Boyce et al. (2002). - - - = Alliston-Go Home shear zone, · · · = Boundary between Alliston Terrain and Fishog Terrain, ······· = PreCambrian-Paleozoic contact, **=====** = CMBBZ

A timing relationship can be determined for type 3 inclusions from petrographic observations of sample LM-6 (Figs. 27-30). Calcite precipitation was followed by barite as seen by barite replacement of the calcite (calcite inclusions were observed in barite laths). The type 3 inclusions are found in fractures in the barite (Fig. 29) which indicates that the oil-bearing fluid migrated through the rock after barite precipitation. Type 3 inclusions were also observed in sample 99-120 (Fig. 31) in the rims and interior of saddle dolomite crystals that are associated with calcite crystals. This implies the oil-bearing fluid was late during the dolomite precipitation

event and before or at the start of calcite precipitation, and is earlier than the type 3 inclusions in the barite. The type 3 inclusions in barite are a rusty color and fluoresced pale orange (Fig. 27-30) whereas the inclusions in the dolomite are redder (Fig. 31) and did not fluoresce, therefore, the hydrocarbons may be of a different composition to those in barite in sample LM-6. This suggests oil-bearing fluids of different compositions may have been present in the area at different times over an extended period or that the different samples have been heated to different temperatures causing the hydrocarbons to mature differently (Goldstein and Reynolds, 1994).

Conclusion

Microthermometry revealed 2 populations of fluid inclusions: FIA 1 composed of high salinity type 'a' inclusions, and FIA 2 composed of low salinity type 'b' inclusions. The majority of inclusions in FIA 1 have homogenization temperatures between 65 to 95°C and salinities of ~30 wt%_{CaCl₂} which suggest fluids of deep basinal brine composition. FIA 2 has homogenization temperatures >200°C and salinities close to pure water suggesting fluids of meteoric composition as the anomalously high homogenization temperatures can reflect the trapping of atmospheric gases. Carbonate $\delta^{18}\text{O}$ values are similar between the two FIAs and suggest deep burial.

The very low salinity of FIA 2 is indicative of meteoric fluids, not deep basinal brines as seen with FIA 1. The fluid inclusions in FIA 2 may have leaked and refilled with meteoric fluids under atmospheric pressure. Samples containing the fluid inclusions that make up FIA 2 were

collected from areas right on or adjacent to fault zones, fractures and terrain boundaries. These potentially could have acted as conduits for meteoric fluids during periods of basement uplift and resulting episodic fault reactivations. The lack of a distinct meteoric oxygen isotope signature in the carbonates containing FIA 2 could reflect the small number of samples used for stable oxygen isotope analysis. A larger collection of samples could potentially reveal an involvement of meteoric fluids through stable oxygen isotope analyses.

CHAPTER 5: INTERPRETATION AND DISCUSSION OF STABLE OXYGEN ISOTOPE AND MICROTHERMOMETRIC RESULTS

Introduction

Oxygen isotope and fluid inclusion data from FIA 1 can be interpreted in two different ways: (1) the $\delta^{18}\text{O}$ and T_h values are consistent with deep burial diagenesis, not a hydrothermal event or, (2) the $\delta^{18}\text{O}$ and T_h values reflect a regional hydrothermal event. The $\delta^{18}\text{O}$ values from samples containing FIA 2 are very similar to the $\delta^{18}\text{O}$ values from samples containing FIA 1 and are interpreted to reflect deep burial based on the presence of mainly low carbonate $\delta^{18}\text{O}$ values from these samples. However, the $\delta^{18}\text{O}$ values from the carbonates containing FIA 1 and FIA 2 are not low enough to indicate carbonate precipitation from hydrothermal fluids (Mario Coniglio personal communication, 2011; Arthur et al., 1983). The composition of FIA 2 is almost that of pure water, which indicates trapping of meteoric water potentially under atmospheric pressure in a vadose or phreatic environment. A second possibility is alteration of FIA 2 fluid inclusions possibly through leaking and refilling with meteoric water percolating down through faults and fractures in the bedrock.

Burial Diagenesis

The $\delta^{18}\text{O}$ values (-11 to -5‰) for the majority of carbonates in this study (Fig. 42) are too negative to reflect an original Ordovician seawater ^{18}O signature assuming Ordovician seawater surface temperatures were between 15 and 20°C. According to Tobin and Walker (1997) and

Muehlenbachs et al. (2003), the Ordovician seawater $\delta^{18}\text{O}$ value was $0\text{‰} \pm 2\text{‰}$ (SMOW). In this study, Ordovician hardground $\delta^{18}\text{O}$ values were evaluated as potential proxies for a local marine baseline $\delta^{18}\text{O}$ by comparing them with assumed Ordovician seawater $\delta^{18}\text{O}$ values from -8 to 0‰ (SMOW) under a range of seawater temperatures from 15 to 30°C (Fig. 20). One hardground $\delta^{18}\text{O}$ value of -3‰ produced a seawater $\delta^{18}\text{O}$ value of -2‰ at 20°C (Fig. 20). The hardground $\delta^{18}\text{O}$ values of -3 and -4‰ produced seawater $\delta^{18}\text{O}$ values in the -2 to 0‰ range with surface temperatures of 25 and 30°C (Fig. 20). The currently accepted Ordovician environment for south-central Ontario is tropical (Brookfield, 1988) with seawater temperatures between 20 and 25°C . Brookfield (1988) and Grimwood (1998) suggested the Trenton and Black River sediments were deposited in a temperate (≤ 13 to 18°C) carbonate shelf environment. Regardless of whether the Ordovician was tropical or temperate, the majority of hardground $\delta^{18}\text{O}$ values from this study produced Ordovician seawater $\delta^{18}\text{O}$ values more negative than the values (-2 to 0‰) suggested by Tobin and Walker (1997) and Muehlenbachs et al. (2003) (Fig. 20). Also, the $\delta^{18}\text{O}$ values from the carbonates in this study are progressively more negative from early to late-stages (Fig. 42). This implies both early and late-stage carbonates from this study precipitated from ^{18}O -depleted pore fluids and/or at progressively higher temperatures accompanying deeper burial.

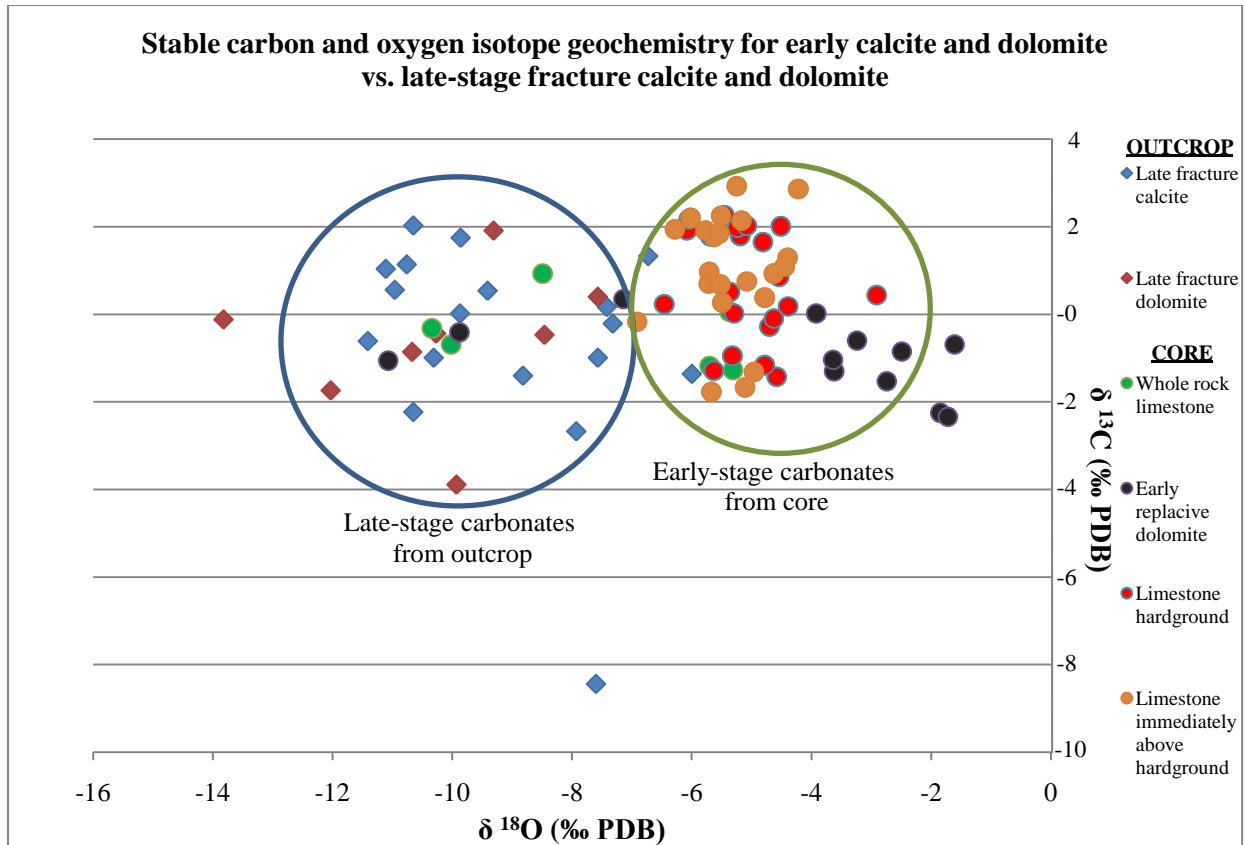


Fig. 42 Graph of $\delta^{18}\text{O}$ and $\delta^{13}\text{C}$ values of early and late-stage carbonates. The circle on the right contains data from core. The left circle contains data from outcrop. The late-stage carbonates have more negative $\delta^{13}\text{C}$ and $\delta^{18}\text{O}$ values than the early-stage carbonates.

Evaluation of homogenization temperatures in support of burial diagenesis

Burial temperatures were calculated (Tables 4 and 5) to determine if FIA 1 homogenization temperatures support burial diagenesis. In Table 4 FIA 1 T_h values do support burial diagenesis if for example, it is assumed the rocks were buried 2 km, the surface temperature was 20°C and the geothermal gradient was between 23 to 30°C/km. The resulting burial temperatures of 66 to 80°C (Table 4) are in the range of FIA 1 T_h values (Table 3). Increasing or decreasing either the surface temperature, burial depth or geothermal gradient can affect the other two parameters. For example in Table 4 a burial depth of 1.5 km and surface temperature of 20°C require

geothermal gradients of 30-45°C/km to produce burial temperatures in the range of FIA 1 T_h values.

Table 4 List of calculated burial temperatures for Ordovician carbonates of southern Ontario using surface temperatures of the Ordovician tropical seawater environment. Geothermal gradients marked with * are from Hogarth and Sibley (1985); Drzewiecki et al. (1994); Wang et al.(1994); and Gerard and Barnes (1995). Shading indicates burial temperatures in the range of the majority of FIA 1 T_h values in this study. Geothermal gradient X burial depth + surface temperature = burial temperature (BT°C).

Geothermal Gradient °C	Tropical Environment					
	Burial Depth 1.5 km		Burial Depth 2km		Burial Depth 3 km	
	Surface Temperature °C		Surface Temperature °C		Surface Temperature °C	
	20	25	20	25	20	25
	BT °C	BT °C	BT °C	BT °C	BT °C	BT °C
*23	54.5	59.5	66	71	89	94
*26	59	64	72	77	98	103
30	65	70	80	85	110	115
35	72.5	77.5	90	95	125	130
40	80	85	100	105	140	145
45	87.5	92.5	110	115	155	160
*50	95	100	120	125	170	175
*55	102.5	107.5	130	135	185	190

In Table 5 the assumed surface temperature is kept at a constant 15°C whereas the assumed burial depth and geothermal gradient can increase or decrease. For example burial diagenesis is supported by FIA 1 T_h values if the assumed burial depth is 2 km and geothermal gradient is 26 to 35°C/km. The resulting burial temperatures of 67 to 85°C (Table 5) are well within range of the majority of FIA 1 T_h values (Table 3).

Table 5 List of calculated burial temperatures for Ordovician carbonates of southern Ontario using surface temperatures of the Ordovician temperate seawater environment. Geothermal gradients marked with * are from Hogarth and Sibley (1985); Drzewiecki et al. (1994); Wang et al. (1994); and Gerard and Barnes (1995). Shading indicates burial temperatures in the range of the majority of FIA 1 T_h values in this study. Geothermal gradient X burial depth + surface temperature = burial temperature (BT °C)

Geothermal Gradient °C	Temperate Environment	
	Surface Temperature 15 °C	
	Burial Depth km	
	2	3
	BT °C	BT °C
*23	61	84
*26	67	93
30	75	105
35	85	120
40	95	135
45	105	150
*50	115	165

Support for estimated geothermal gradients, burial depths and temperatures

To determine if estimates of surface temperatures, geothermal gradients and burial depths used in Tables 4 and 5 are reasonable it is useful to compare them with those determined from independent methods, such as vitrinite reflectance and organic maturation. The four studies discussed below were chosen because they each use different methods other than stable isotope and fluid inclusion microthermometry to estimate burial depths and geothermal gradients of strata in the Michigan basin.

Cercone (1984) investigated the thermal history of the Michigan Basin using vitrinite reflectance (% R_o), thermal alteration index (TAI) of sporopollen and kerogen, and the “oil window” (window of time for oil creation). According to Cercone (1984) approximately 1000 m of Carboniferous strata were eroded from the Michigan Basin. This approximation was based on the elevated maturity of organic matter in Michigan Basin strata as well as comparison of

stratigraphic sequences among the Michigan, Appalachian, and Illinois basins (Cercione, 1984). The center of the Michigan Basin has 700 m of preserved Carboniferous strata compared to the Appalachian and Illinois basins that have between 1700 and 1800 m of preserved strata which implies ~1000 m of Carboniferous strata were eroded from the Michigan Basin (Cercione, 1984). Several observations support this interpretation: (1) the present erosional surface in the Michigan Basin indicates extensive post-Carboniferous erosion in the basin (Cercione, 1984); (2) when the regional dip of the upper Mississippian Bayport Limestone is projected to the northern hinge line of the Michigan Basin, the extended base of the Bayport Limestone is 1000 m above the present day erosional surface. This implies 1000 m of post-Carboniferous erosion (Cercione, 1984); and (3) the level of organic thermal maturity of the near-surface lower Pennsylvanian Saginaw coals is significantly higher than comparative near-surface Pennsylvanian age coals from the Moscow Basin. Cercione (1984) used the Lopatin Method and assumed geothermal gradients from 25 to 50 °C/km to calculate a range in the amount of overburden eroded during the Paleozoic and Mesozoic. Cercione (1984) suggested that geothermal gradients in the Michigan Basin were between 35 to 45°C/km from the Cambrian to the Carboniferous. This range of geothermal gradients produced the best estimate of 1000 m of eroded Carboniferous strata which can account for the elevated levels of organic maturity (0.54 to 0.6% R_o and TAI of 2.6) in Michigan Basin strata that are too young to have achieved these levels of thermal maturity under just 1700 m of burial.

Hogarth and Sibley (1985) used conodont color alteration index (CAI) to examine the thermal history of the Michigan Basin. They found CAI values ranged from 1 at surface exposures and

shallow burial in the Upper Peninsula of Michigan to 2.5 at a depth of 3.2 km in the deepest part of the central Michigan Basin. By comparing their data to experimental CAI results, Hogarth and Sibley (1985) determined that burial temperatures in the Michigan Basin ranged from 20 to 80°C for a CAI of 1 for the surface exposures and 110 to 140°C for a CAI of 3 for the deepest central portion of the basin. Hogarth and Sibley (1985) used Lopatin's method and their CAI results to estimate paleogeothermal gradients which were then fitted to a burial history curve of the Michigan Basin created using the 1000 m of extra burial suggested by Cercone (1984). The paleogeothermal gradient of 23°C/km best fits the CAI results and burial history curve of the north and central Michigan Basin. In the southern part of the basin a geothermal gradient 31°C/km best fits the elevated levels of organic maturity observed in this portion of the Michigan Basin.

Wang et al. (1994) estimated the thermal history of the south-central and east-central Michigan Basin by examining the Ordovician St. Peter Sandstone using vitrinite reflectance and apatite fission-track analysis. The data formed four straight line segments when plotted on a %R_o vs. depth graph (Wang et al., 1994). The graph showed vitrinite reflectance increased with depth to a value of 0.2%R_o. By applying best fit lines to the data points on the graph, Wang et al. (1994) were able to determine that ~2 km of material were eroded from their study site. They evaluated three kinetic reaction models using the %R_o data and: (1) no additional burial and a geothermal gradient of 26.2°C/km which did not create any thermal maturation of organic matter in pre-Devonian strata (Wang et al., 1994); (2) additional burial of 1 km and a geothermal gradient of 40°C/km which resulted in a better fit for thermal maturation of the organic matter

(Wang et al., 1994); and (3) an additional burial of 1.8 km and a geothermal gradient of 26.2°C/km which resulted in a match for calculated and observed reflectance values for the Ordovician. From these models Wang et al. (1994) suggested that additional burial depths in the Michigan Basin ranged from less than 1 km in the center of the basin to greater than 2 km on the margins. According to Wang et al. (1994) apatite fission-track analysis confirmed that for surface temperatures of 20 and 30°C and a geothermal gradient of 26.2°C/km, an additional 1.6 to 2.7 km of burial were needed to attain the temperatures required for fission-track annealing observed in their study.

Gerard and Barnes (1995) examined illitization and paleothermal regimes of the St. Peter Sandstone in the central Michigan Basin. They obtained an age range of 367 to 327 Ma for authigenic illite formation using K-Ar dating. Gerard and Barnes (1995) combined this age range with the present burial depths (1.5 to 3.5 km) of illite to determine paleodepths for illitization of the St. Peter Sandstone. The paleodepths obtained ranged from 2.5 to 3.2 km and represent minimum depths because the effects of compaction and erosion were not considered in the paleodepth reconstruction (Gerard and Barnes, 1995). Homogenization temperatures of fluid inclusions in pre-illite saddle dolomite in the St. Peter Sandstone ranged from 90 to 150°C. Gerard and Barnes (1995) suggested that the fluid inclusions in the saddle dolomite were stretched or reequilibrated based on fluid inclusion evidence consisting of variable L:V, amount of leaked and decrepitated inclusions and the wide range in T_h values all observed in individual crystals. These observations are supported by a lack of petrographic evidence for multiple generations of inclusions (Gerard and Barnes, 1995). A more reliable T_h range of 90 to 100°C

for inclusions in saddle dolomite was determined by comparison of inclusions with T_h values from 80 to 100°C in coexisting quartz cement. Gerard and Barnes (1995) estimated formational temperatures of 115 to 135°C for the St. Peter sandstone by assuming a depth of formation of 3 km and a maximum hydrostatic pressure of 300 bars (25 to 45°C pressure correction) during entrapment. According to Gerard and Barnes (1995) the wide range in T_h values implies dolomite and illite formation in the St. Peter Sandstone occurred at temperatures of 150°C or more. Using the 150°C temperature of formation, paleodepths of 2.5 and 3.2 km, and estimated surface temperature of 20°C, Gerard and Barnes (1995) obtained paleogeothermal gradients from 38 to 48°C/km which agree with those of Cercone (1984).

The geothermal gradients of 23 to 35°C/km and burial depth of 2 km used in this study (Table 6) are similar to the geothermal gradients and burial depths suggested by Cercone (1984); Hogarth and Sibley, (1985); Wang et al. (1994); and Gerard and Barnes, (1995) (Table 6). Also, the 23 to 35°C/km gradients and 2 km burial depth produce burial temperatures of 66 to 80°C that correlate with T_h values in this study (Table 4). Assuming geothermal gradients ranging from 23 to 35°C/km and a burial depth of 2 km are reasonable (Table 6) then the burial temperatures they produce (Table 4) are also considered reasonable. Therefore, the fluid inclusion homogenization temperatures in this study can be interpreted to support the stable oxygen isotope data as reflecting burial diagenesis.

Table 6 Comparison of geothermal gradients and burial depths of Cercone (1984); Hogarth and Sibley (1985); Wang et al. (1994); Gerard and Barnes (1995); and this study. The geothermal gradients and burial depth from this study are similar to the range in geothermal gradients and burial depths from the four studies mentioned above. The 23 to 35°C/km gradients and 2 km burial depth produce burial temperatures that correlate with T_h values in this study. Assuming these geothermal gradients and burial depth are reasonable then the T_h values in this study can be interpreted to support the stable oxygen isotope values as reflecting burial diagenesis

Studies	Location	Geothermal gradients	Burial depth
Cercone (1984)	Michigan Basin Carboniferous	35 to 45°C/km	1.7 km
Hogarth and Sibley (1985)	Michigan Basin Ordovician	23 and 31°C/km	2 to 3 km
Wang et al. (1994)	Michigan Basin Carboniferous	26°C/km	Additional 1.6 to 2.7 km
Gerard and Barnes (1995)	Michigan Basin Ordovician	38 to 48°C/km	2.5 and 3.2 km
This study	Lake Simcoe area Ordovician	23-35°C/km	2 km

Hydrothermal Event

Burial diagenesis cannot explain the fluid inclusions with T_h values greater than 90°C unless geothermal gradients are higher than 35°C/km or burial depth is increased to 3 km or more under both the tropical and temperate environments. Research on the thermal history of the Michigan basin suggests that the Ordovician strata were never buried more than 2 km and maximum burial temperatures did not exceed 80°C. Vitrinite reflectance and CAI results from recent studies of the Ordovician Trenton-Black River dolomites in eastern Wisconsin, northwestern Ohio, and New York, indicated that the mid-Ordovician rocks at the margins of the Michigan Basin were

never buried more than 1 to 1.5 km and that the maximum burial temperatures did not exceed 45 to 50°C (Luczaj, 2006; Smith, 2006). Using the geothermal gradients (23 to 35°C) determined in the burial diagenesis section of this discussion, the 1 to 1.5 km maximum burial depths and an assumed surface temperature of 20°C, the maximum burial temperatures for the Lake Simcoe carbonates would have been between 43 and 72.5°C.

Assuming the conclusions of the above studies are realistic, the homogenization temperatures from 80°C and higher in this study can be interpreted to indicate alteration of carbonates by hydrothermal fluids during progressive burial of middle Ordovician strata over an area covering the Michigan and Appalachian basins as well as the Algonquin and Wisconsin arches.

Support for a Regional Hydrothermal Event

The four studies discussed below each examine Paleozoic strata in different areas of southern Ontario and bordering US states using several alternate methods to determine the cause of high temperature fluid inclusion homogenization temperatures and possible sources of hydrothermal fluids.

Coniglio et al. (1994) interpreted the Chatham Sag subsurface and Manitoulin Island outcrop carbonate $\delta^{18}\text{O}$ (-11.2 to -2.9‰ PDB) and T_h (most from 80 to 150°C) values as reflecting hydrothermal alteration of the carbonates during deep burial diagenesis. They further suggested

that fractures were important conduits for dolomitizing hydrothermal fluids in the Trenton and Black River formations.

Evans and Battles (1999) studied the Paleozoic section of the central Appalachian Valley and Ridge province located in Pennsylvania, Maryland and the southeast corner of West Virginia. They conducted microthermometric and stable carbon and oxygen isotope analyses on vein calcite and quartz to characterize the fluids present during the Alleghanian orogeny and to establish the fluid migration path through the fold and thrust belt (Evans and Battles, 1999). Calcite and quartz $\delta^{18}\text{O}$ values ranged from -3.8 to +11.7‰ and aqueous fluid inclusion T_h values ranged from 60 to 250°C. Evans and Battles (1999) observed that fluid inclusion homogenization temperatures decreased and salinities increased from the Meadow Branch syncline to the Nittany Anticline. Microthermometric and isotope data from vein calcite and quartz showed that the central Appalachian Valley and Ridge province hydrologic system operated at a formational scale (Evans and Battles 1999). The temperature, chemistry and isotopic composition of fluids in veins in the Devonian Oriskany to Chemung formations indicated regional fluid migration (Evans and Battles, 1999). These fluids were different from fluids in strata above and below that interval implying the fluids from the Oriskany to Chemung interval were exotic (Evans and Battles, 1999). Also, fluid inclusions in rocks that were affected by hydrothermal fluids had higher temperatures (60 to >110°C) than would be produced by the regional geothermal gradient (20 to 25°C/km) (Evans and Battles, 1999). The warm migrating fluids would have had very high flow rates of 10 m/yr which could have been possible if the fluids migrated along fractures, faults, decollements (Evans and Battles, 1999) and other highly

permeable pathways. These conduits would have allowed large amounts of the warm brine to travel large distances with minimal heat loss.

Luczaj (2006) interpreted that negative $\delta^{18}\text{O}$ and high T_h values from dolomite and high T_h values from sphalerite and quartz from eastern Wisconsin reflect hydrothermal activity in the Michigan Basin during the time of dolomitization of upper Ordovician strata. Luczaj (2006) compared the $\delta^{18}\text{O}$ and T_h values with CAI and % R_o values from the same area and concluded that the data reflected a hydrothermal event because organic maturity was too low for the high burial temperatures needed to produce those $\delta^{18}\text{O}$ and T_h values.

Smith (2006) investigated characteristics and origins of hydrothermal dolomite (HTD) reservoirs in the upper Ordovician in south-central New York. Fluid inclusion T_h values in Black River matrix and saddle dolomite ranged from 110 to 180°C and post-dolomite quartz had T_h values of 155 to >200°C (Smith, 2006). Black River limestone from all sample areas had a uniform $\delta^{18}\text{O}$ value of -6.5‰ whereas matrix and saddle dolomite had $\delta^{18}\text{O}$ values from -12.5 to -9‰. Trace element analyses showed that the Trenton-Black River dolomites are enriched in Fe and Mn relative to the limestone and presumed Ordovician seawater indicating that the dolomite had a subsurface origin (Smith, 2006). Dolomite from the Black River Formation had Sr values slightly higher than Ordovician seawater implying the dolomitizing fluids circulated through basement rocks or immature feldspar-rich siliclastics prior to dolomite formation. Smith (2006) compared this geochemical data with CAI data from the overlying Utica Shale (CAI of 4.5). Smith (2006) suggested this level of organic maturity in the Utica Shale implied that the Black

River Formation was buried to a depth where the burial temperature exceeded homogenization temperatures ($>180^{\circ}\text{C}$), however; it did not preclude the dolomite from being hydrothermal in origin (Smith, 2006). According to Smith (2006) the Trenton-Black River dolomites in New York were similar to the Trenton-Black River dolomites in Ohio and Michigan that had T_h values interpreted as indicating a hydrothermal event as they were higher than maximum burial temperatures. The Trenton-Black River dolomites from New York, Ohio and Michigan were all related to wrench-faulting (e.g. Albion-Scipio Trend, Bowling Green Fault off the Lima-Indiana Trend) and had the same appearance and geochemistry, therefore; they were interpreted to have formed at the same time from the same processes (Smith, 2006).

If these authors are correct in their interpretations, their results along with the results from this study can be interpreted as reflecting a regional hydrothermal event. The major faults, terrain boundaries and fractures (Fig. 38) could have made excellent conduits for ascending or cross-basinal hydrothermal fluid flow.

Proposed Models for Regional Fluid Flow Systems

The models discussed below demonstrate how hot fluids could migrate through a region and maintain a high temperature without necessarily requiring a deep seated magmatic heat source.

Garven and Freeze (1984a) created a mathematical and numerical model, using equations for fluid flow and heat, mass and geochemical transport, to determine the effect of groundwater flow

on ore deposits in sedimentary basins. They used a gravity-driven fluid-flow system in a mature sedimentary basin in which groundwater flowed from elevated foreland recharge areas to lower-elevation discharge areas (Garven and Freeze, 1984a and b). Simulations were run to demonstrate the numerical approach to modeling ore formation in a sedimentary basin (Garven and Freeze, 1984a). A sensitivity analysis was done to quantitatively evaluate the model using different parameters (basin shape and size) to examine factors that affect fluid flow and heat, mass and geochemical transport (Garven and Freeze, 1984b). This analysis showed that maximum temperatures near the edge of a 300 km long wedge-shaped basin could range from 50 to 95°C under less than 1000 m of burial (Garven and Freeze, 1984b). In larger basins the temperatures could reach 100°C under 1000 m of burial. According to Garven and Freeze (1984b) quantitative modeling showed gravity-driven flow gave a simple realistic explanation to the mechanics of epigenetic ore formation in sedimentary basins. They suggested the model could be used to understand other basin related geological processes such as diagenesis and petroleum migration and accumulation. Garven and Freeze (1984b) calculated maximum burial temperatures at basin margins using a representative range of continental heat flow (50 to 80 mW/m²) and surface temperatures of 10 to 30°C. The maximum temperatures attained were 50 to 150°C under less than 1000 m of burial depending on the size and shape of the basin (Garven and Freeze, 1984b). For example, a basin several kilometers in maximum thickness and several hundreds of kilometers in lateral extent would have had temperatures high enough under the gravity-driven fluid-flow system that a deep-seated heat source was not needed to explain the elevated temperatures (Garven and Freeze, 1984b).

The above model demonstrates how high temperature fluids could easily flow by gravity alone without the need for the strata to be deeply buried or a magmatic intrusion as a heat source for the migrating fluids. The ambient temperature of basement rocks and the amount of continental heat flow from these rocks and the presence of groundwater can be sufficient to create a gravity-driven flow system in basins.

Oliver (1986) developed a hypothetical model of tectonically-driven fluid flow (squeegee model). The model mechanism was based on convergent continental margins getting buried beneath thrust sheets. Fluids were expelled from margin sediments and migrated into foreland basins and continental interiors with the thrust sheet acting like a “squeegee” pushing the fluids ahead of it (Oliver, 1986). These fluids had several effects on the host rocks such as veins and dykes created by upwardly mobile fluids as is commonly seen in metamorphic mountain belts. Fluids could have emerged in hot springs along fault traces or stayed in the decollement zone aiding in continued thrusting (Oliver, 1986). Fluids may have been “injected” into the hydrologic system of a foreland basin or platform bringing with them minerals, hydrocarbons and heat. The hot fluids also may have affected the geothermal regime of the basin or platform (Oliver, 1986).

Oliver’s (1986) study indicates a potential source for hydrothermal fluids and a mechanism for regional fluid flow in a basin, such as the Appalachian Basin. The folding and thrusting that occurred during the Taconic Orogeny could have been a mechanism for regional fluid migration from the Appalachian Basin into the Michigan Basin through the Algonquin Arch.

Machel and Cavell (1999) examined the “squeegee” model of Oliver (1986) by looking at data from stratigraphic, geochemical (Sr, C, O, T_h), petrographic and hydrological studies of Devonian aquifers and aquitards in the Western Alberta basin. They determined there was a brief influx of “squeegee-type” fluid flow from tectonic thrusting which Machel and Cavell (1999) termed a “hot flash”. Their research supported the conclusions of Oliver (1986) and suggests that “squeegee-type” flow through the Appalachian Basin is a realistic mechanism for regional hydrothermal fluid migration.

Coniglio et al. (1994) suggested a regional flow model to support their hydrothermal alteration interpretation for the high temperature carbonates in Manitoulin Island and Chatham Sag areas of southern Ontario. They found late-stage calcite with homogenization temperatures of $\sim 200^\circ\text{C}$ in Manitoulin Island area and cooler T_h values in late-stage calcite as well as a saddle dolomite sample from the Chatham sag area that had progressively cooler T_h values in successive growth zones. Coniglio et al (1994) suggested the variation in temperatures was caused by changing hydrothermal fluid circulation. Coniglio et al. (1994) proposed convection cells circulated descending basinal brines through fractures. The heat source for the high temperature fluid was unknown, possibly a deep seated intrusion (Coniglio et al., 1994).

Coniglio et al.’s (1994) convection cell model relies on buoyancy differences between hot and cool fluids as a mechanism for hydrothermal fluid flow. Though a deep seated heat source is required the model does not need tectonic activity to inject hot fluids into a region. The convection cell model allows regional fluid flow to be continuous over an extended period.

Davies and Smith (2006) developed a regional fluid flow model based on a structurally controlled hydrothermal system. Principle conduits for mobile deep basinal or basement brines were fault and fracture systems particularly extensional and strike-slip faults (Davies and Smith, 2006). The system was influenced by fluid pressure and shear stress and was very dynamic with episodic high-rate fluid flow. Advection was the main process for heat and solute transport in this system (Davies and Smith, 2006). A pore-fluid pressure gradient that decreased away from the fault conduit drove the hydrothermal fluid flow, dolomitization and leaching of the host limestone away from the main advective fault zone (Davies and Smith, 2006). Constraints on hydrothermal fluid flow were underlying overpressured sandstone aquifers that acted as lateral conduits or episodic feeders of high temperature and pressure fluids into faults, overlying and internal shales that acted as aquitards, and basement highs (Davies and Smith, 2006).

The main mechanism of fluid flow described in the model above is a temperature gradient that allows heated fluids migrating up from higher temperature basement rocks that are under greater pressure. The heated fluid can flow regionally into basins and arches through faults, fractures and pore-fluid pressure gradients.

Discussion

The four different models described above present possible sources of hydrothermal fluids and mechanisms that can drive a regional hydrothermal fluid flow system. The gravity-driven mathematical model proposed by Garven and Freeze (1984a and b) relies on assumed surface temperatures, fluid flow, heat and mass transport, and geochemical mass transfer equations to

predict maximum temperatures of strata at different depths in various basin configurations. Applying this model to a basin such as the Michigan Basin requires a better understanding of the above parameters than is currently available for the Michigan Basin. Surface temperatures and maximum burial temperatures at the time of mineral precipitation in the Michigan Basin during the Ordovician need to be known for comparison with the gravity-driven model. The question of what these two temperatures were during the Ordovician remains unresolved.

Oliver's (1986) fluid flow (squeegee) model is problematic when applied to a basin such as the Michigan Basin for two reasons: 1) the model relies on pulses of tectonic activity to expel or inject fluids into continental strata ahead of the thrust sheet. With this model the timing of mineral precipitation needs to be known to correlate it with the timing of tectonic activity. The timing of mineral precipitation in the Michigan Basin is not known; therefore, cannot be correlated to any tectonic pulses that occurred during basin formation. Evidence of 'squeegee-type' fluid flow was found by Machel and Cavell (1999) in the Western Alberta Basin by examining petrographic, hydrologic, stratigraphic and geochemical data. Increasing the abundance of data for these four analytical methods may help to resolve the timing of mineral precipitation in the Michigan Basin with regard to the timing of tectonic pulses; 2) the "squeegee-type" fluid flow model does not explain the pervasive regional dolomitization observed in the Michigan and Appalachian basins. Pulses of tectonically expelled fluids would not produce the volume of hydrothermal fluids need for such extensive dolomitization.

Coniglio et al.'s (1994) convection cell fluid flow model may explain the extent of dolomitization in the Michigan Basin. However, evidence of a deep seated heat source which is

required for circulation of hydrothermal fluids to occur has yet to be discovered (Coniglio et al., 1994).

Davies and Smith (2006) structurally controlled hydrothermal fluid flow model was developed based on structural, geochemical and temperature data acquired from research in the Appalachian Basin. Sudden changes in temperature gradients over short distances between limestone and dolostone, along with forced maturation of kerogens indicate advection is the main process for heat and solute transportation in the Appalachian Basin (Davies and Smith, 2006). The substantial amount of structural data in the Michigan Basin from research such as the reconstruction of the east margin of the Michigan Basin and surrounding areas of the Canadian Shield by Sanford et al. (1985) and the geophysical surveys of Lake Simcoe performed by Boyce et al. (2002) support the structural component of Davies and Smith's (2006) model. However, evidence supporting temperature differences between limestones and dolostones in the Michigan Basin is inconclusive. Whether advection is a key process for heat and mass transport in the Michigan Basin remains undetermined.

Potential Paragenetic Sequence of Events in the Lake Simcoe Area

A potential paragenetic sequence of events for the Lake Simcoe area study site (Fig. 43) can be created from the data in this study and the previous studies discussed earlier.

Deposition of the Simcoe Group occurred during the Tiptecanoe transgression in the Ordovician. The overall deepening-upward stratigraphic succession is punctuated with minor

stratigraphic units that indicate short regressive cycles (Fig. 43). These cycles are evident from the transitioning of near-shore siliclastics to deep-shelf lime mudstones back to near-shore siliclastics, etc. Periods of low to no sedimentation also occurred during deposition of the Simcoe Group as evidenced by abundant hardgrounds in the Gull River and Bobcaygeon formations (Fig. 43).

The early-stage calcite $\delta^{18}\text{O}$ values of -6.5 to -4.3‰ (PDB) and early-stage dolomite $\delta^{18}\text{O}$ values of -4 to -2‰ indicate deposition of the Simcoe Group was followed by shallow burial lithification by coeval microcrystalline calcite and dolomite. The early-stage dolomite $\delta^{18}\text{O}$ values of -11.1 to -6.6‰ indicate some of the early-stage calcite cement was diagenetically replaced by microcrystalline dolomite during progressive burial. The $\delta^{18}\text{O}$ values of -13.8 to -6.1‰ from late-stage fracture calcite and dolomite and T_h values of 60 to 90°C from the late-stage calcite indicate these minerals precipitated in deep burial conditions.

Homogenization temperatures of 90 to 150°C from late-stage fracture saddle dolomite and quartz indicate that at some point hydrothermal fluids migrated through the region. Hydrocarbon inclusions in barite suggest the hydrothermal fluids may have carried hydrocarbons into the area or helped rapidly mature kerogens in the host rocks. The precipitation sequence of the late-stage minerals is indeterminate.

The final sequence of events is uplift and erosion (Fig. 43). This is evident from the very low salinity FIA 2 fluid inclusions in this study and amount of missing strata in the Lake Simcoe area

(Fig. 43) when compared to areas such as the Michigan and Appalachian basins. Both basins have preserved strata into the Carboniferous (Cercone, 1984).

Simcoe Group south-central Ontario		Depositional Environment and Lithologies	Simcoe group Lake Simcoe Study Site	Paragenetic sequence
	Collingwood member	Deep shelf Petroliiferous, argillaceous lime mudstone		Uplift and erosion
	Lindsay Formation	Deep shelf Bioclastic lime mudstone-wackestone		
	Verulam Formation	Shallow shelf Bioclastic wackestone-packstone, bioclastic grainstone		Not readily accessible in the study site
	Bobcaygeon Formation	Shallow shoal intra-bioclastic grainstone		
	Gull River Formation	Shoal-shallow shelf Bioclastic packstone-grainstone		Very low salinity fluid inclusions indicate influx of meteoric water possibly through reactivated faults and fractures during periods of uplift Carbonate $\delta^{18}O$ values indicate progressive burial diagenesis Fluid inclusion homogenization temperatures of 90-150°C indicate influx of hydrothermal fluids. Appearance of hardgrounds indicate periods of low to no sedimentation
	Shadow Lake Formation	Deep shelf Bioclastic wackestone-grainstone calcareous shale		
	Bobcaygeon Formation	Shallow shelf Bioclastic grainstone Shallow shelf wacke-grainstone + shale		Carbonate $\delta^{18}O$ values indicate progressive burial diagenesis
	Gull River Formation	Shoal Intra-peloidal wacke-grainstone bioclastic wackestone		
	Gull River Formation	Lagoon-tidal flat Lime mudstone		Transgression of the sea Deposition of the Simcoe Group begins
	Shadow Lake Formation	Dolostone		
	Shadow Lake Formation	Nearshore-supratidal Arkosic siltstone, argillaceous sandstone conglomerate		

Fig. 43 An interpreted sequence of events for the Lake Simcoe area, south-central Ontario. The sequence begins with deposition of the Shadow Lake Formation over Precambrian basement. Short sea transgressive-regressive cycles are evident from the repetitive near-shore siliclastics to deep shelf mudstones back to near-shore sediments in an overall deepening-upward stratigraphic succession. The Lindsay Formation and Collingwood member are not found in the study site possibly due to uplift and erosion of these strata. The black lines in the Bobcaygeon Formation represent hardgrounds. They are not accurately located or to scale. (Modified from Armstrong, 2000).

CHAPTER 6: CONCLUSIONS

Deciding which of the interpretations discussed above best explains the isotope and fluid inclusion data is challenging for several reasons: (1) the amount of eroded material from the basins and arches discussed in this study remains unknown; therefore, burial depths and paleogeothermal gradients used in the burial diagenesis interpretation to calculate burial temperatures can only be estimated; (2) surface temperatures for the Ordovician are also unknown, hence the two conflicting proposed environments of tropical with surface temperatures from 20 to 25°C or temperate with surface temperatures from 13 to 18°C; and (3) data used to support the burial diagenesis interpretation can be used to support the hydrothermal event interpretation as well.

Hardground $\delta^{18}\text{O}$ values revealed the hardgrounds in the Lake Simcoe area did not retain an original Ordovician seawater signature and that they have been altered by early burial diagenesis. Late-stage calcite and dolomite $\delta^{18}\text{O}$ values are consistent with deeper burial diagenesis than the hardgrounds. Oxygen isotopes showing deep burial are supported by %Ro, CAI and T_h values, yet homogenization temperatures showing a hydrothermal event also are supported by %Ro and CAI. However, the support for deep burial depends upon assumptions made on surface temperatures, geothermal gradients, and burial depths. Also, deep burial does not explain the high temperature fluid inclusions.

Petrographic evidence indicates that T1a and T2a fluid inclusion T_h values greater than 150°C most likely are caused by stretched or leaked and/or refilled inclusions; therefore, can be discounted. The T1a and T2a inclusions with T_h values between 90 and 150°C are not so easily discounted and are interpreted to represent a true high temperature hydrothermal event. Furthermore, it is suggested here that the hydrothermal event had a regional impact particularly with regards to the extent of dolomitization observed in the Michigan and Appalachian basins, and into the Algonquin Arch.

For a regional hydrothermal event to occur, the fluids would need to retain their heat while migrating great distances which is possible. Considering the very high fluid inclusion temperatures recorded at major fault zones and trends such as the Albion-Scipio as well as numerous other faults and fractures, it is feasible that hot fluids entered the region (basins and arches) from several conduits concurrently during episodic reactivation of basement faults and fracture systems in response to intracratonic stresses created by the continuous interaction of tectonic plates. The relatively low thermal conductivity of carbonates (~ 1.2 to $5 \text{ W m}^{-1} \text{ K}^{-1}$) (Thomas et al., 1973; Clauser and Huenges, 1995; Canakci et al., 2007) allowed the hot fluids to retain much of their heat as the fluids migrated through the region. On the other hand tectonic events at plate margins (e.g. subduction-orogenesis) may have resulted in intracratonic deep seated intrusions that locally elevated geothermal gradients causing elevated fluid inclusion temperatures at these sites. A deep seated intrusion does not explain the elevated temperatures at basin margins and well up onto arches such as in the Lake Simcoe area. Regional hydrothermal

fluid migration through basement fault and fracture systems potentially is a better explanation for the elevated temperatures in the Lake Simcoe area and along basin margins.

Future Work

Research projects tend to focus on relatively small areas (square meters to square kilometers) due to funding, time, and labor constraints or simply because the questions being asked focus on a small part of a bigger, sometimes incompletely articulated question. Unfortunately, this approach often reveals new uncertainties associated with the problem or question. The reason for this may be the problem or question being asked cannot be resolved by one discipline or analytical technique alone. What is needed to address this conundrum is a collaborative multi-disciplinary research project covering geology (e.g. boreholes and outcrop sampling, geochemistry and petrography), geophysics (e.g. GPR, airborne magnetic and seismic surveys), and hydrogeology (e.g. defining basin catchment areas, basin flow modeling, and heat, mass and chemical transport processes).

This collaborative research project could involve researchers from different disciplines to do regional, systematic surface and subsurface investigative transects of the Michigan and Appalachian basins and surrounding arches. This multi-disciplinary and systematic approach would provide much more integrated data than is currently available for analyses such as stable isotopes, fluid inclusions, organic maturation and fluid flow. The increased amount of data may reveal trends currently not visible. This would be a long term and costly undertaking hence the need for much collaboration nationally and with the United States.

REFERENCES

- Al-Aasm, I.S., Taylor, B.E. and South B. 1990. Stable isotope analysis of multiple carbonate samples using selective acid extraction. *Chemical Geology (Isotope Geoscience Section)*, v. 80 p. 119 – 125.
- Armstrong, D.K. and Anastas, A.S. 1992. Paleozoic mapping and alkali-reactive aggregate studies in the eastern Lake Simcoe area. *In: Summary of field work and other activities 1992.* Ontario Geological Survey, Miscellaneous Paper 160, p. 131 – 135.
- Armstrong, D.K. and Rheume, P. 1993. Paleozoic mapping and alkali-reactive aggregate studies in the Lake Simcoe area: preliminary mapping results for the Fenelon Falls and Penetanguishene map sheets. *In: Summary of field work and other activities 1993.* Ontario Geological Survey, Miscellaneous Paper 162, p. 149 – 153.
- Armstrong, D.K. 2000. Paleozoic Geology of the northern Lake Simcoe area, south-central Ontario. Ontario Geological Survey, Open File Report 6011, 52 p.
- Arthur, M.A., Anderson, T.F., Kaplan, I.R., Veizer, J., and Land, L.S. 1983. Stable isotopes in sedimentary geology. SEPM Short Course no. 10, 151 p.
- Bakker, R.J., Dubessy, J., and Cathelineau, M. 1996. Improvements in clathrate modeling: The H₂O-CO₂ system with various salts. *Geochim. Cosmochim. Acta*, v. 60, iss. 10, p. 1657 – 1681.
- Boyce, J.I., Pozza, M.R., Morris, W.A., Eyles, N., and Doughty, M. 2002. High-resolution magnetic and seismic imaging of basement faults in western Lake Ontario and Lake Simcoe, Canada. *Proceedings of SAGEEP Annual meeting, Environmental and Engineering Geophysical Society*, p. 1 – 12.
- Brett, C.E. and Brookfield, M.E. 1984. Morphology, faunas and genesis of Ordovician hardgrounds from southern Ontario, Canada. *Paleogeography, Paleoclimatology, Paleoecology*, v. 46, p. 233 – 290.
- Brookfield, M.E. and Brett, C.E. 1988. Paleoenvironments of the mid-Ordovician (upper Caradocian) Trenton limestones of southern Ontario, Canada: storm sedimentation on a shoal-basin shelf model. *Sedimentary Geology*, v. 57, p. 75 – 105.
- Brookfield, M.E. 1988. A mid-Ordovician temperate carbonate shelf-the Black River and Trenton groups of southern Ontario, Canada. *Sedimentary geology*, v. 60, p. 137 – 153.
- Brookfield, M.E. and Elgadi, M. 1998. Sedimentology and paleocommunities of the Black River and Trenton limestone groups (Ordovician), Lake Simcoe area, Ontario. *Geological Society of America, Annual Meeting, Field Trip Guidebook*, v. 6, 35 p.

- Burruss, R.C. 1981. Hydrocarbon fluid inclusions in studies of sedimentary diagenesis. *In*: Hollister, L.S. and Crawford, M.L. eds., Short Course in fluid inclusions: applications to petrology. Mineralogical Association of Canada, v. 6, p. 138 – 156.
- Burruss, R.C. 1991. Practical aspects of fluorescence microscopy of petroleum fluid inclusions. *In*: Barker, C.E. and Kopp, O.C., eds., and Colburn, H.Y. ass. ed., Luminescence microscopy and spectroscopy: qualitative and quantitative applications. SEPM Short Course no. 25, p. 1 – 8.
- Canakci, H., Demrboga, R., Karakoc, M.B., and Sirin, O. 2007. Thermal conductivity of limestone from Gaziantep (Turkey). *Building and Environment*, v. 42, p. 1777 – 1782.
- Carter, T.R., Trevail, R.A., and Easton, R.M., 1996. Basement controls on some hydrocarbon traps in southwestern Ontario, Canada. *In*: van der Pluijm, B.A., and Catacosinos, P.A., eds., Basement and basins of eastern North America: Boulder, Colorado. GSA Special Paper 308, p. 95 – 107.
- Carter, T.R. and Trevail, R.A., 2000. Trenton-Black River oil and gas reservoirs in Ontario; the play goes on. *AAPG Bulletin*, v. 84, no. 9, p. 1381.
- Cercone, K.R. 1984. Thermal history of the Michigan Basin. *AAPG Bulletin*, v. 68, no. 2, p. 130 – 136.
- Clauser, C. and Huenges, E. 1995. Thermal conductivity of rocks and minerals. *Rock Physics and Phase relations: A Handbook of Physical Constants*. AGU Reference Shelf 3, p. 105 – 126.
- Coniglio, M., 1990. Dolomitization of Ordovician limestone in the Manitoulin Island area: preliminary results. *Ontario Petroleum Institute 28th Annual Conference*, v. 28, 13p.
- Coniglio, M. and William-Jones, A.E. 1992. Diagenesis of Ordovician carbonates from the north-east Michigan Basin, Manitoulin Island area, Ontario: evidence from petrography, stable isotopes and fluid inclusions. *Sedimentology*, v. 39, p. 813 – 836.
- Coniglio, M., Sherlock, R., William-Jones, A.E., Middleton, K., and Frape, S.K. 1994. Burial and hydrothermal diagenesis of the Ordovician carbonates from the Michigan Basin, Ontario, Canada. *Special Publications, International Association of Sedimentology*, v. 21, p. 231 – 254.
- Coniglio, M. 2000. Diagenetic history of Ordovician carbonates from hydrocarbon reservoirs and outcrops in southern Ontario: unanswered questions. *AAPG Bulletin*, v. 84, no. 7 – 12, p. 1381.
- Davies, G. R., and L. B. Smith, Jr., 2006. Structurally controlled hydrothermal dolomite reservoir facies: An overview. *AAPG Bulletin*, v. 90, no. 11, p. 1641–1690.

- Dix, G.R. and Robinson, G.W. 2002. The geochemical record of hydrothermal mineralization and tectonism inboard of the Appalachian Orogen: the Ottawa Embayment. *Chemical Geology*, v. 197, p. 29 – 53.
- Drzewiecki, P.A., Simo, J.A., Brown, P.E., Castrogiovanni, E., Nadon, G.C., Shepherd, L.D., Valley, J.W., Vandrey, M.R., and Winter, B.L. 1994. Diagenesis, diagenetic banding, and porosity evolution of the Middle Ordovician St. Peter Sandstone and Glenwood Formation in the Michigan Basin. *AAPG Memoirs*, v. 61, p. 179 – 199.
- Evans, M.A. and Battles, D.A. 1999. Fluid inclusion and stable isotope analyses of veins from central Appalachian Valley and Ridge province: implications for regional synorogenic hydrologic structure and fluid migration. *GSA Bulletin*, v. 111, no. 12, p. 1841 – 1860.
- Friedman, I. and O'Neil, J.R. 1977. Data of geochemistry: compilation of stable isotope fractionation factors of geochemical interest. *US Geol. Surv., Paper 440-KK*, p. 1 – 12.
- Garven, G. and Freeze, R. A. 1984a. Theoretical analysis of the role of groundwater flow in the genesis of stratabound ore deposits. 1. Mathematical and numerical model. *American Journal of Science*, v. 284, p. 1085 – 1124.
- Garven, G. and Freeze, R.A. 1984b. Theoretical analysis of the role of groundwater flow in the genesis of stratabound ore deposits. 2. Quantitative results. *American Journal of Science*, v. 284, p. 1125 – 1174.
- Gerard, J.P., Barnes, D.A., 1995. Illitization and Paleothermal regimes in the Middle Ordovician St. Peter Sandstone, Central Michigan Basin: K-Ar, oxygen isotope, and fluid inclusion data. *AAPG Bulletin*, v. 79, p. 49-69.
- Goldstein, R.H. 2001. Fluid inclusions in sedimentary diagenetic systems. *Lithos* v. 55, p. 159 – 193.
- Goldstein, R.H. and Reynolds, T.J. 1994. Systematics of fluid inclusions in diagenetic minerals. *SEPM Short Course no. 31*, 199 p.
- Goldstein, R.H.; Anderson, J.E.; and Bowman, M.W. 1991. Diagenetic responses to sea-level change; integration of field, stable isotope, paleosol, paleokarst, fluid inclusion, and cement stratigraphy research to determine history and magnitude of sea-level fluctuation. *In: Franseen, E.K.; Watney, W.L.; Kendall, C.G.St.C.; and Ross, W., eds., Sedimentary modeling; computer simulations and methods for improving parameter definition. Kansas Geological Survey, Bulletin, no. 233*, p. 139 – 162.
- Goldstein, R.H. 1986. Reequilibration of fluid inclusions in low-temperature calcium-carbonate cement. *Geology*, v. 14, p. 792 – 795.

Granath, V.C., 1991. Geochemical constraints on the origin of dolomite in the Ordovician Trenton and Black River Limestones, Albion-Scipio Area, Michigan. *AAPG Bulletin*, v. 75, pp.584 – 585.

Grimwood, J.L., 1998. Storm sedimentation, hardgrounds, and lithofacies of the Black River Group, Lake Simcoe area, Ontario. Unpublished MSc. Thesis, University of Waterloo, Waterloo, Ontario, 109 p.

Grimwood, J.L., Coniglio, M., and Armstrong, D.K. 1999. Blackriverian carbonates from the subsurface of the Lake Simcoe area, southern Ontario: stratigraphy and sedimentology of a low-energy carbonate ramp. *Canadian Journal of Earth Science*, v. 38, p. 871 – 889.

Hogarth, C.G., Sibley, D.F., 1985. Thermal history of the Michigan Basin: evidence from conodont coloration index. *In: Cercone, K.R. and Budai, J.M., eds., Ordovician and Silurian Rocks of the Michigan Basin and its Margins. Michigan Basin geol. Soc. Special Paper, no. 4, p. 45 – 58.*

Hutton, A.C. 1991. Fluorescence Microscopy in oil shale and coal studies *In: Barker, C.E. and Kopp, O.C., eds., and Colburn, H.Y. ass. ed., Luminescence microscopy and spectroscopy: qualitative and quantitative applications. SEPM Short Course no. 25, p.107 – 116.*

Johnson, M.D., Armstrong, D.K., Sanford, B.V., Telford, P.G., and Rutka, M.A. 1992. Paleozoic and Mesozoic geology of Ontario. *In: Thurston, P.C., Williams, H.R., Sutcliffe, R.H, and Stout, G.M., eds., Geology of Ontario. Ontario Geological Survey, Special Volume 4, Part 2, p. 907 – 1008.*

Land, L.S. 1985. The origin of massive dolomite. *Journal of Geological Education*, v. 33, p. 112 – 125.

LeBaron, P.S. and Williams, D.S. 1990. Carbonate building stone resources of the lake Simcoe-Kingston area, southeastern Ontario. Ontario Geological Survey, Open File Report 5730, 65 p.

Liberty, B.A., 1969. Paleozoic geology of the Lake Simcoe area, Ontario. Geological Survey of Canada, Memoir no. 355, 201 p.

Luczaj, J.A., 2006. Evidence against the dorag (mixing-zone) model for dolomitization along the Wisconsin Arch: a case for hydrothermal diagenesis. *APG Bulletin*, v.90, p. 1719-1738.

Machel, H.G. and Cavell, P.A. 1999. Low-flux, tectonically-induced squeegee fluid flow (“hot flash”) into the Rocky Mountain Foreland Basin. *Bulletin of Canadian Petroleum Geology*, v. 47, no. 4, p. 510 – 533.

McLimans, R.K., 1987. Application of fluid inclusions to migration of oil and diagenesis in petroleum reservoirs. *Applied Geochemistry*, v. 2, p. 585 – 604.

- Melchin, M.J.; Brookfield, M.E.; Armstrong, D.K.; and Coniglio, M., 1994. Stratigraphy, sedimentology and biostratigraphy of the Ordovician rocks of the Lake Simcoe area, south-central Ontario. Geological Association of Canada, Mineralogical Association of Canada Joint Annual meeting Field Trip A4 Guidebook, 101 p.
- Middleton, K., Coniglio, M., Sherlock, R., and Frappe, S.K. 1993. Dolomitization of middle Ordovician carbonate reservoirs, southwestern Ontario. *Bulletin of Canadian Petroleum Geology*, v. 41, no. 2, p. 150 – 163.
- Crude oil and natural gas resources. Oil, gas and salt resources. Ministry of Natural Resources. Government of Ontario, Canada. 13 April 2011
http://www.mnr.gov.on.ca/en/Business/OGSR/2ColumnSubPage/STEL02_167105.html
- Muehlenbachs, K., Furnes, H., Fonneland, H.C., and Hellevang, B. 2003. Ophiolites as faithful records of the oxygen isotope ratio of ancient seawater: the Solund-Stavfjord Ophiolite Complex as a late Ordovician example. *In: Dilek, Y. and Robinson, P.T., eds, Ophiolites in Earth History. Geological Society of London, Special Publication no. 218, p. 401 – 414.*
- Mukherji, K.K., and Young, G.M. 1973. Diagenesis of the Black River (middle Ordovician) limestones in southern Ontario, Canada. *Sedimentary Geology*, v. 9, p. 21 – 51.
- Munz, I.A. 2001. Petroleum inclusions in sedimentary basins: systematics, analytical methods and applications. *Lithos*, v. 55, p. 193 – 210.
- Noor, I. 1989. Lithostratigraphy, environmental interpretation, and palaeogeography of the middle Ordovician Shadow Lake, Gull River and Bobcaygeon formations in parts of southern Ontario; unpublished Ph.D. thesis, University of Toronto, Toronto, Ontario, 262 p.
- Oakes, C.S., Bodnar, R.J., and Simons, J.M. 1990. The system NaCl-CaCl₂-H₂O: I. The ice liquidus at 1 atm total pressure. *Geochimica et Cosmochimica Acta*, v. 54, p. 603 – 610.
- Oliver, J. 1986. Fluids expelled tectonically from orogenic belts: their role in hydrocarbon migration and other geologic phenomena. *Geology*, v. 14, p. 99 – 102.
- Reimer, J.D., Hudema, T., and Viau, C. 2001. TSR-HTD ten years later: an exploration update, with examples from western and eastern Canada. Rock the Foundation Convention, Canadian Society of Petroleum Geologists, p. 043-1 – 043-4.
- Rosenbaum, J., and Sheppard, S.M.F., 1986. An isotopic study of siderites, dolomites and ankerites at high temperatures. *Geochimica Cosmochimica Acta*, v. 50, p. 1147 – 1150.
- Sanford, B.V., Thompson, F.J., and McFall, G.H. 1985. Plate tectonics: a possible controlling mechanism in the development of hydrocarbon traps in southwestern Ontario. *Bulletin of Canadian Petroleum Geology*, v. 33, no. 1, p. 52 – 71.

Sangster, P.J., Laidlaw, D.A., Le Baron, P.S., Steele, K.G., Lee, C.R., Carter, T.R. and Lazorek, M.R. 2008. Report of Activities 2007, Resident Geologist Program, southern Ontario Regional Resident Geologist Report: southeastern and southwestern Ontario District, Mines and Minerals Information Centre, and Petroleum Resources Centre; Ontario Geological Survey, Open File Report 6222, 60 p.

Simo, J.A., Johnson, C.M., Vandery, M.R., Brown, P.E., Castrogiovanni, E., Drzewiecki, P.E., Valley, and Bayer, J., 1994. Burial dolomiteization of the Middle Ordovician Glenwood Formation by evaporitic brines, Michigan Basin. *In: Spec. Publs Int. Ass. Sediment.*, v. 21, p. 169 – 186.

Smith, L. B. Jr., 2006. Origin and reservoir characteristics of Upper Ordovician Trenton–Black River hydrothermal dolomite reservoirs in New York: *AAPG Bulletin*, v. 90, p. 1691– 1718.

Taylor, T.R. and Sibley, D.F., 1986. Petrochemical and geochemical characteristics of dolomite types and the origin of ferroan dolomite in the Trenton Formation, Ordovician, Michigan Basin, U.S.A. *Sedimentology*, v. 33, p. 61 – 86.

Thomas, J. Jr., Frost, R.R., and Harvey, R.D. 1973. Thermal conductivity of carbonate rocks. *Engineering Geology*, v. 7, iss. 1, p. 3 – 12.

Tobin, K.J. and Walker, K.R. 1997. Ordovician oxygen isotopes and paleotemperatures. *Palaeogeography, Palaeoclimatology, Palaeoecology*, v. 129, pp. 269 – 290.

Toole, P.L. 2001. Ordovician hardgrounds of the Lake Simcoe Area, southern Ontario, Canada; unpublished BSc. Thesis, University of Waterloo, Waterloo, Ontario, 36 p.

Wang, H.F., Crowley, K.D., Nadon, G.C., 1994. Thermal history of the Michigan Basin from apatite fission-track analysis and vitrinite reflectance. *In: AAPG Memoir*, v. 61, p. 167 – 177.

Wilkinson, B.H., Janecke, S.U. and Brett, C.E. 1982. Low-magnesian calcite marine cement in middle Ordovician hardgrounds from Kirkfield, Ontario. *Journal of Sedimentary Petrology*, v. 52, no. 1, p. 0047 – 0057.

Yoo, C.M., Gregg, J.M., and Shelton, K.L., 2000. Dolomitization and dolomite neomorphism: Trenton and Black River Limestones (Middle Ordovician) northern Indiana, U.S.A. *Journal of Sedimentary Research*, v. 70, no. 1, p. 265 – 274.

APPENDIX A

*Stable carbon and oxygen isotope data of early-stage and late-stage carbonates
in samples from the Lake Simcoe area, south-central Ontario*

Early-stage calcite in packstone from OGS cores			
Sample No.	$\delta^{18}\text{O}$	$\delta^{13}\text{C}$	Core No.
102	-8.49	0.93	93-10-3.89
105	-5.37	0.06	93-11-17.07
123	-5.32	-0.95	93-1224A
139	-4.63	-0.1	93-4-21.09
148	-5.67	-1.77	93-422.2

Early-stage calcite in mudstone from OGS cores			
Sample No.	$\delta^{18}\text{O}$	$\delta^{13}\text{C}$	Core No.
176	-10.02	-0.69	93-1-43.74
177	-10.34	-0.32	93-11-28.48

early-stage calcite in mixed rock types from OGS cores				
Sample No.	$\delta^{18}\text{O}$	$\delta^{13}\text{C}$	Core No.	Rock type
146	-4.96	-1.32	93-0503.1	Gst/Pkst
119	-4.58	-1.43	93-12-27.65	Pkst/Gst
122	-5.71	0.97	93-1222A	Gst/Pkst
137	-4.7	-0.28	93-9-8.09	Wkst/Pkst

Early-stage dolomite from OGS core			
Sample No.	$\delta^{18}\text{O}$	$\delta^{13}\text{C}$	Field No.
104	-1.61	-0.69	93-10-22.85a
107	-2.49	-0.85	11-34-34
108	-2.74	-1.53	11-36-80
125	-3.62	-1.30	93-1240
133	-3.64	-1.04	4--29--14
134	-1.85	-2.25	93-0512
149	-3.92	0.02	11-28-48
150	-3.24	-0.60	10-11-73
157	-1.72	-2.34	5-37-11
160	-11.07	-1.06	3-104-66
161	-7.14	0.35	3-101-33
162	-9.88	-0.41	2-54-55

Early-stage calcite in grainstone from OGS cores				
Sample No.	$\delta^{18}\text{O}$		$\delta^{13}\text{C}$	Core No.
103	-5.63		1.77	93-10-3.89
109	-5.19		1.79	11--13-99
110	-5.77		1.91	11--13-99
111	-5.45		2.26	93-11-9.19
112	-5.51		2.25	93-11-9.19
113	-6.08		1.92	93-11-8.10A
114	-6.28		1.94	93-11-8.10A
117	-4.51		2.01	93-12-22.72
118	-4.22		2.86	93-12-22.72
120	-4.78		0.38	93-12-27.65
124	-5.49		0.27	93-1224A
126	-5.7		-1.18	93-1224A
129	-5.24		1.98	2-36-84
130	-4.4		1.29	2-36-84
131	-4.81		1.65	2-36-84
132	-5.25		2.93	2-36-84
135	-6.05		2.17	93-10-1.66
136	-6.02		2.2	93-10-1.66
140	-4.45		1.09	93-4-21.09
141	-6.46		0.23	93-3-17.01
142	-4.63		0.93	93-3-17.01
143	-5.36		0.51	93-3-17.01
144	-5.52		0.68	93-3-17.01
145	-5.63		-1.29	93-0503.1
147	-4.78		-1.16	93-422.2
151	-5.08		2.02	(93)-10-2-47
152	-5.17		2.14	(93)-10-2-47
153	-5.69		1.78	(93)-10-2-29
154	-5.54		1.85	(93)-10-2-29
158	-5.31		-1.27	(93)-5-31-07
159	-5.11		-1.67	(93)-5-31-07

Isotope data for hardgrounds from OGS cores		
HG	13C	18O
93-10-3.89	0.85	-4.54
11--13-99	1.79	-5.19
93-11-9.19	2.26	-5.45
93-11-8.10A	1.92	-6.08
93-11-23.16	0.44	-2.91
93-12-22.72	2.01	-4.51
93-12-27.65	-1.43	-4.58
93-1222A	0.18	-4.39
93-1224A	-0.95	-5.32
2-36-84	1.98	-5.24
2-36-84	1.65	-4.81
93-10-1.66	2.17	-6.05
93-9-8.09	-0.28	-4.70
93-4-21.09	-0.10	-4.63
93-3-17.01	0.23	-6.46
93-3-13.92	0.51	-5.36
93-0503.1	-1.29	-5.63
93-422.2	-1.16	-4.78
10-2-47	2.02	-5.08
10-2-29	1.78	-5.69
7-7-78	0.02	-5.29
5-31-07	-1.27	-5.31

Isotope data for sediments above hardgrounds from OGS cores		
Above HG	13C	18O
93-10-3.89	1.77	-5.63
11--13-99	1.91	-5.77
93-11-9.19	2.25	-5.51
93-11-8.10A	1.94	-6.28
93-11-23.16	0.75	-5.08
93-12-22.72	2.86	-4.22
93-12-27.65	0.38	-4.78
93-1222A	0.97	-5.71
93-1224A	0.27	-5.49
2-36-84	1.29	-4.40
2-36-84	2.93	-5.25
93-10-1.66	2.20	-6.02
93-9-8.09	0.70	-5.72
93-4-21.09	1.09	-4.45
93-3-17.01	0.93	-4.63
93-3-13.92	0.68	-5.52
93-0503.1	-1.32	-4.96
93-422.2	-1.77	-5.67
10-2-47	2.14	-5.17
10-2-29	1.85	-5.54
7-7-78	-0.17	-6.91
5-31-07	-1.67	-5.11

BMB= brown marker bed, biocls=bioclastic, Do=dolostone, FF=fracture fill, Gst=grainstone, GMB=green marker bed, Ls=limestone, Mdst=mudstone, ool=oolitic, Pkst=packstone, pel=peloidal, Wkst=wackestone
 Bob= Bobcaygeon Formation, GR=Gull River Formation, MHB=Moore Hill Bed
 u=upper, l=lower, m=middle

Late-stage ferroan calcite cement 99-series					
Sample No.	$\delta^{18}\text{O}$	$\delta^{13}\text{C}$	Location	Formation	Rock type
101	-10.31	-0.99	FF	uGR	?
117	-9.86	1.75	FF	lBob	biocls Gst
130	-11.41	-0.61	FF	lBob	sucrosic Do
133	-10.65	2.03	FF	lBob	Gst
135	-10.76	1.14	FF	lBob MHB	biocls pel Gst

Late-stage non-ferroan calcite cement 99-series					
Sample No.	$\delta^{18}\text{O}$	$\delta^{13}\text{C}$	Location	Formation	Rock type
105	-7.32	-0.21	Brec fault area	uGR/lBob	peloidal Mdst
108	-6	-1.36	Vugs	GR	BMB Wkst/Pkst
113	-7.42	0.17	FF	lBob	pel (ool?) Gst
116	-6.73	1.33	biomoldic pore fill	lBob	pel biocls Gst/Pkst
118	-7.93	-2.67	FF	l&mBob	pel biocls Gst
132	-7.57	-0.99	FF	lBob	Gst

Late-stage ferroan to non-ferroan calcite cement 99-series					
Sample No.	$\delta^{18}\text{O}$	$\delta^{13}\text{C}$	Location	Formation	Rock type
107	-10.65	-2.23	FF	lGR	BMB Wkst/Pkst
112	-9.87	0.02	FF	uGR	micropelite Ls (Gst?)
123	-7.6	-8.44	breccia cement	uBob	?
137	-9.41	0.54	FF	uGR/lBob	?

Late-stage slightly to very slightly ferroan calcite cement 99-series					
Sample No.	$\delta^{18}\text{O}$	$\delta^{13}\text{C}$	Location	Formation	Rock type
120	-8.82	-1.4	FF	uBob	Do
134	-11.11	1.04	FF	lBob MHB	biocl pel Gst
111	-10.96	0.56	FF107	uGR	shear zone in Do?

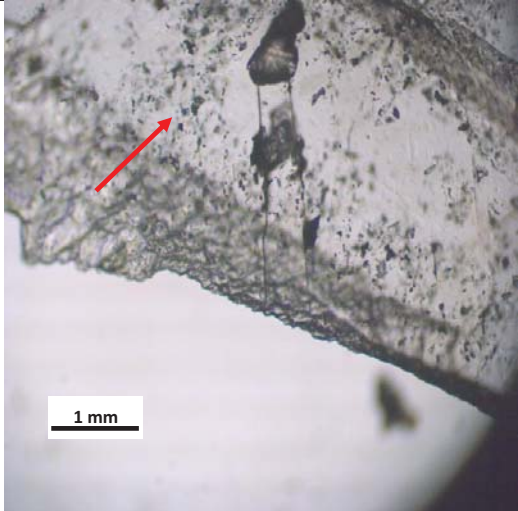
Late-stage ferroan dolomite 99-series					
Sample No.	$\delta^{18}\text{O}$	$\delta^{13}\text{C}$	Type of Do	Formation	Rock type
104	-8.46	-0.47	SD	IGR	GMB
120A	-10.27	-0.44	SD	uBob	Do
123	-12.03	-1.74	Repl zoned SD	uBob	?
125	-13.82	-0.12	ReplSD	uBob	Do
128	-9.31	1.91	ReplSD	lBob	Do
130	-10.67	-0.86	Microxst Do	lBob	Do


Late-stage non-ferroan dolomite 99-series					
Sample No.	$\delta^{18}\text{O}$	$\delta^{13}\text{C}$	Type of Do	Formation	Rock type
102	-7.57	0.4	Microxst	IGR	GMB
110	-9.93	-3.89	Microxst	l(?)GR	Gst(?)

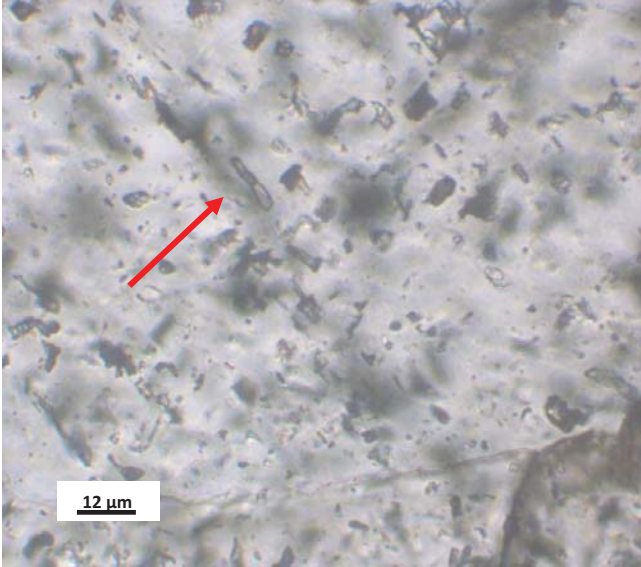
APPENDIX B

Fluid inclusion microthermometry data of late-stage calcite, dolomite, barite and quartz in samples from the Lake Simcoe area, south-central Ontario

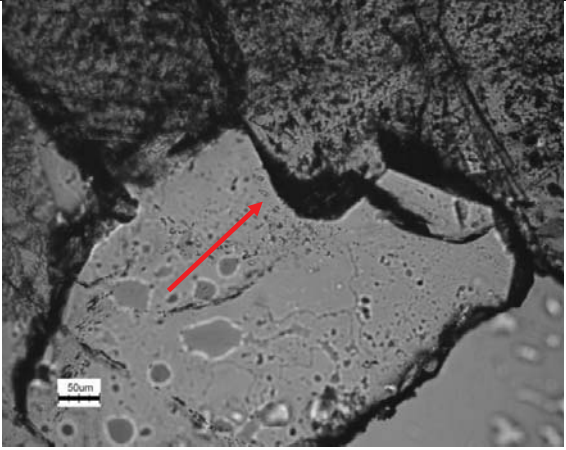
Microthermometry data and photomicrographs of fluid inclusions analyzed in this study

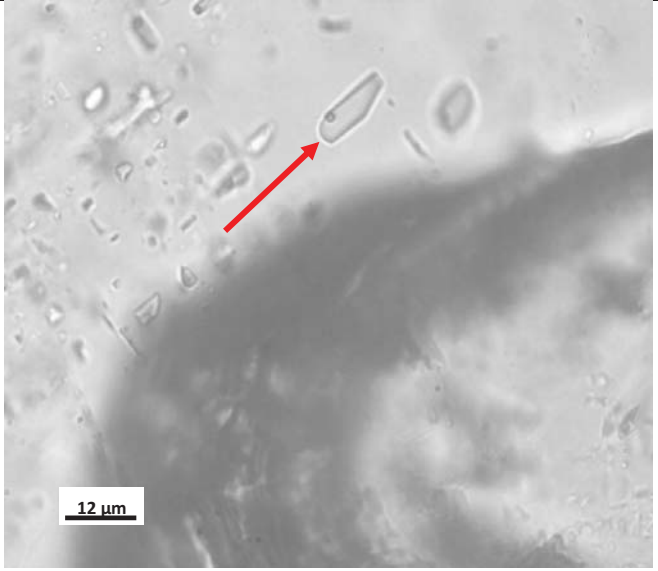
Date: m/d/y	Sample #	Chip #	Host Mineral	Lens X	Res	Picture LM-4 Chip1 calcite
06/24/09	LM-4	1 Low V:L Practice chip since sample very fragile. Lost most of the calcite	Calcite	10	1280 x 1024	

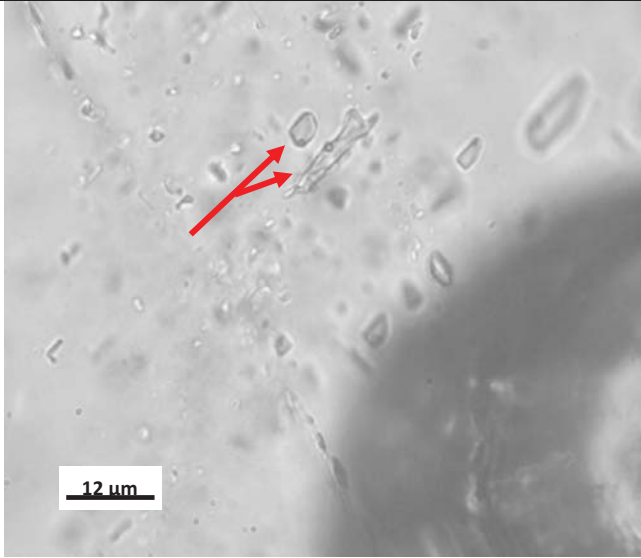
Incl #	Lens X	Incl Size	FI Type	Origin	Picture: LM-4 Chip 1 L-rich
1	60	12 um	1	indeter	

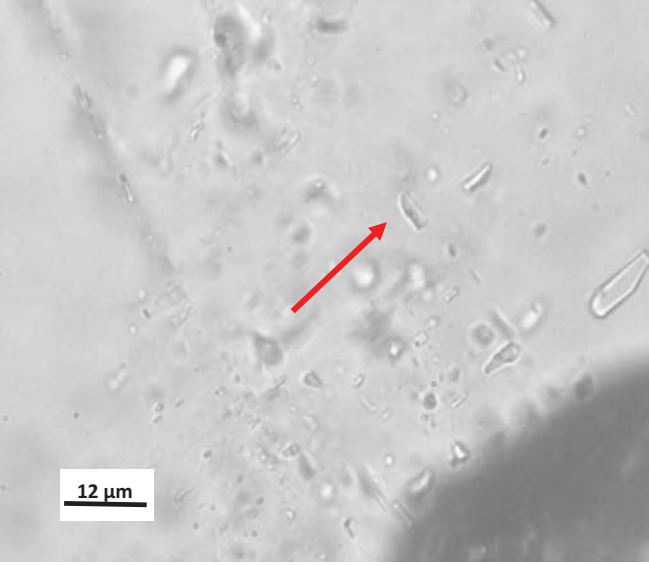
Incl #	Lens X	Incl Size	FI Type	Origin	Picture: LM-4 Chip 1 L-rich
2	60	~ 12 um	1	indeter	

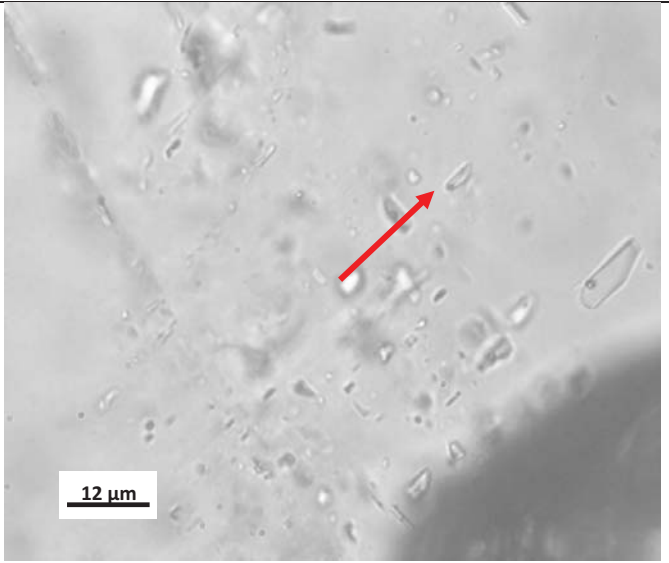
Incl #	T _{freeze} (°C)	T _e (°C)	T _{m(ice)} (°C)	LM-4 Chip 1 Comments
1	-87 ±1	-47 ±1	-16 ±1	Used to practice freezing experiments. Did Th second >120 C
2	-66.6 ±.1	-47.5 ±2.5	-23 ±1	Used to practice freezing experiments. Did Th second >120 C

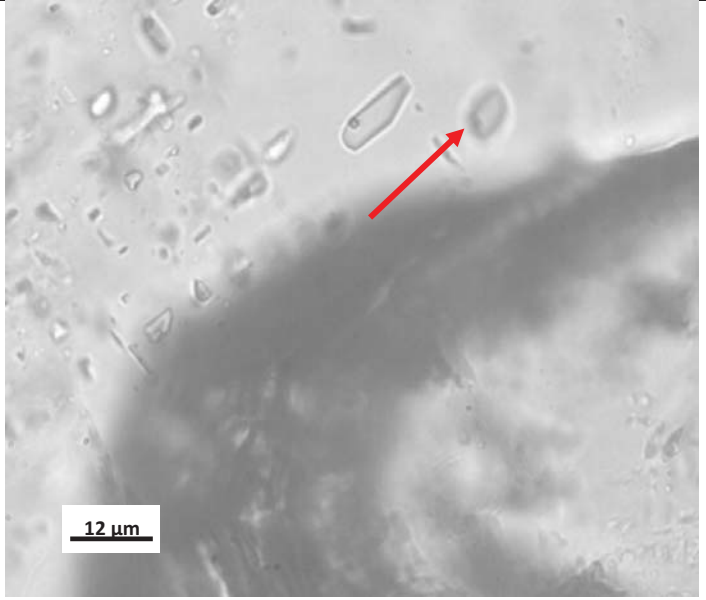
Date: m/d/y	Sample #	Chip #	Host Mineral	Lens X	Res	Picture LM-5.1 Chip 1 quartz
07/02/09	LM-5.1	1 L-rich cluster Very low V:L	Quartz	20	1280 x 1024	

Incl #	Lens X	Incl Size	FI Type	Origin	Picture: LM-5.1 Chip 1 L-rich
1	100	12 µm	1	P (?)	

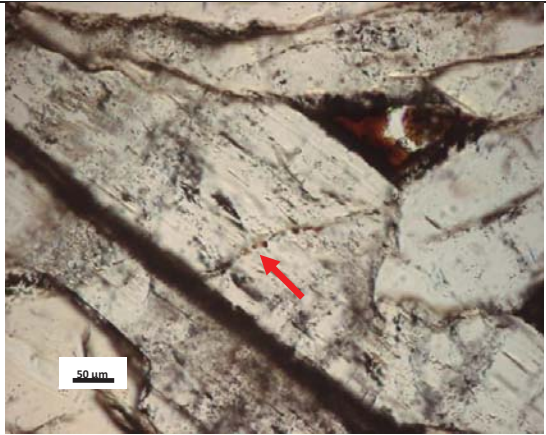
Incl #	Lens X	Incl Size	FI Type	Origin	Picture: LM-5.1 Chip 1 L-rich
2 and 3	100	12 um and 5 um	1	P (?)	


Incl #	Lens X	Incl Size	FI Type	Origin	Picture: LM-5.1 Chip 1 L-rich
4	100	7 um	1	P (?)	

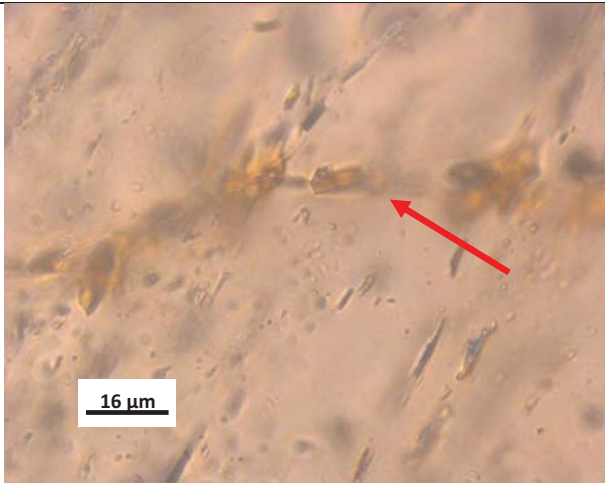
Incl #	Lens X	Incl Size	FI Type	Origin	Picture: LM-5.1 Chip 1 L-rich
5	100	5 um	1	P (?)	

Incl #	Lens X	Incl Size	FI Type	Origin	Picture: LM-5.1 Chip 1 L-rich
6	100	8 um	1	P (?)	

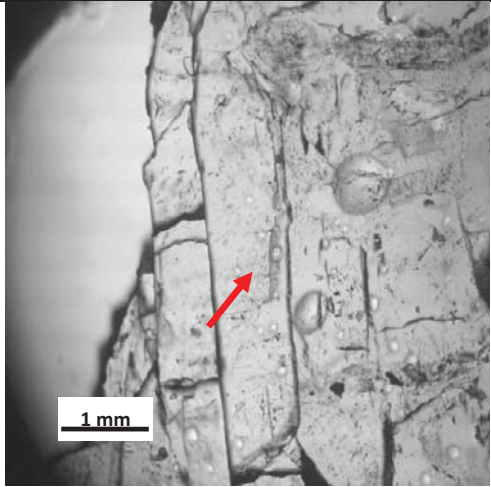
Incl #	T _{freeze} (°C)	T _e (°C)	T _{m(ice)} (°C)	T _H (°C)	LM-5.1 Chip 1Comments
1	-88±1	-65±1	-40.3	90.6±0.2	All the FIs were located in the same optic plane in a relatively clear crystal (potential primaries?)
2	-88±1	-65±1	-40.3	90.6±0.2	
3	-88±1	-65±1	-40.3	90.6±0.2	
4	ND	ND	ND	103.0±0.7	Could not see freeze or melt
5	ND	ND	ND	105.0±1	Could not see freeze or melt
6	ND	ND	ND	76.0±0.1	Could not see freeze or melt

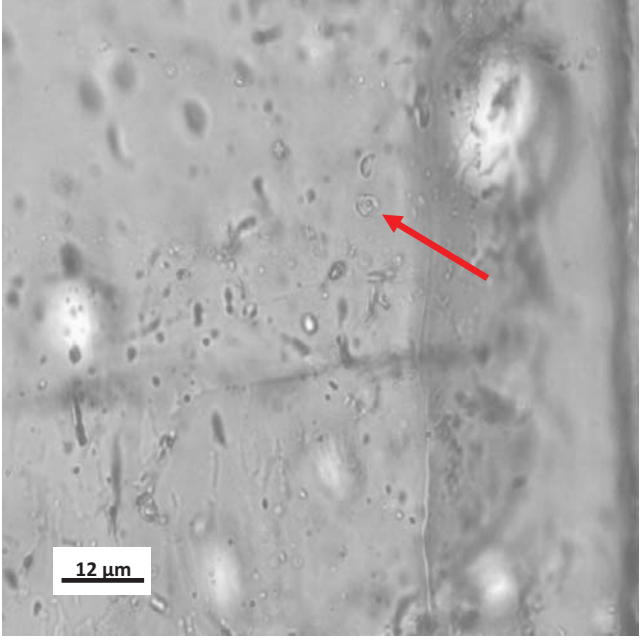
Date: m/d/y	Sample #	Chip #	Host Mineral	Lens X	Res	Picture LM-6 Chip 1 barite oil-bearing
09/8- 10/09	LM-6	1 L-rich Oil- bearing Very low V:L	Barite	20	1280 X 1024	

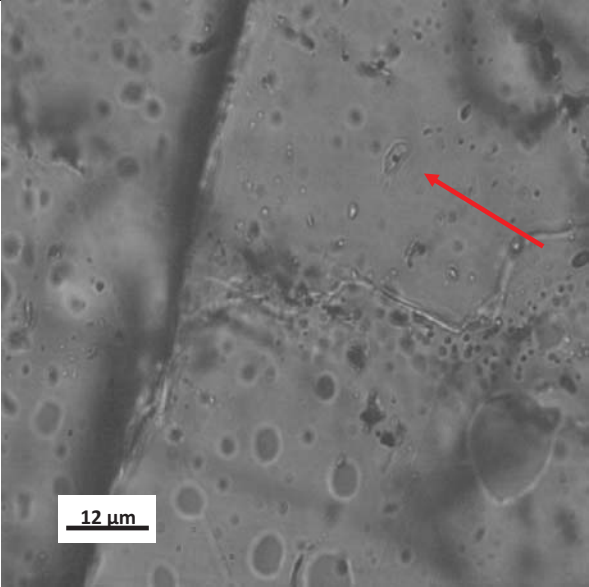
Incl #	Lens X	Incl Size	FI Type	Origin	Picture: LM-6 Chip 1 L-rich oil-bearing
1	100	~16 um	3	S	

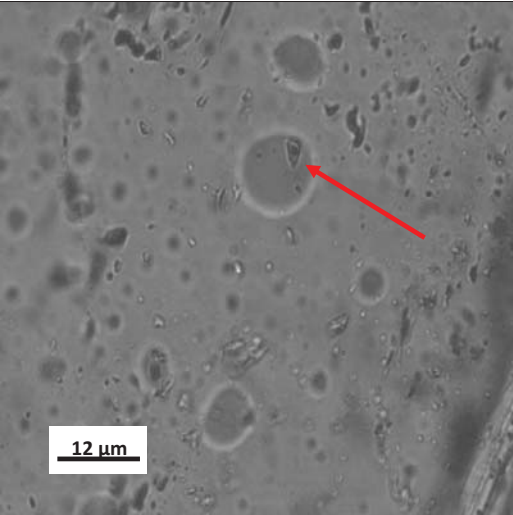
Incl #	Lens X	Incl Size	FI Type	Origin	Picture: LM-6 Chip 1 L-rich oil-bearing
2	100	~11 um	3	S	

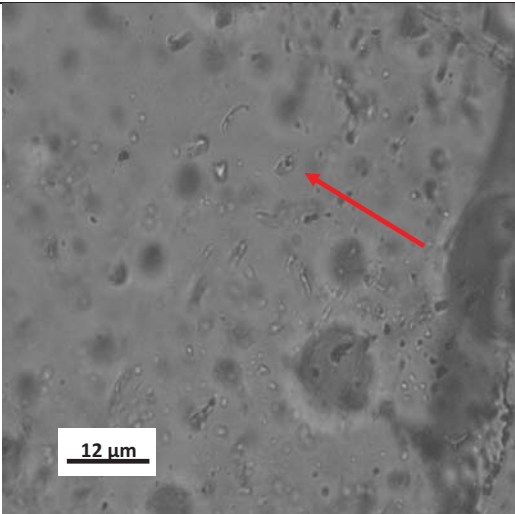
Incl #	T _{freeze} (°C)	T _e (°C)	T _{m(ice)} (°C)	T _H (°C)	LM-6 Chip 1 Comments
1	ND	ND	ND	104.3 ±.1	Could only obtain Th since oil-bearing. Freezing data would be meaningless without knowing what hydrocarb dealing with
2	ND	ND	ND	98.1 ±.1	Analyzed a third incl in fracture but had inconsistent Th. Took 9 measurements Th dropped from 120 to 79.6. Bob: possibly changes in chemistry due to overheating

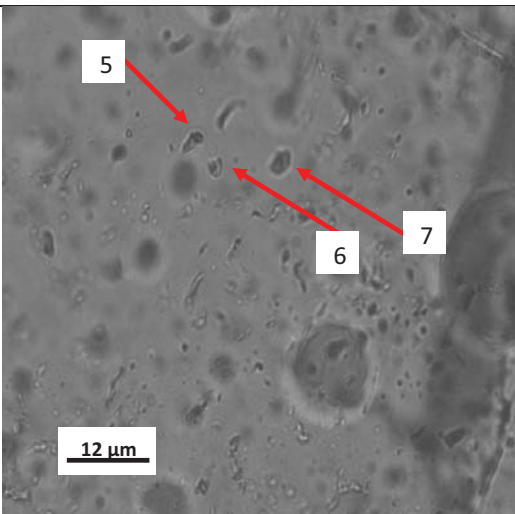
Date: m/d/y	Sample #	Chip #	Host Mineral	Lens X	Res	Picture LM-6 Chip 2 barite
09/8-10/09 and 11/18-20/09	LM-6	2 L-rich	Barite	10	1280 X 1024	

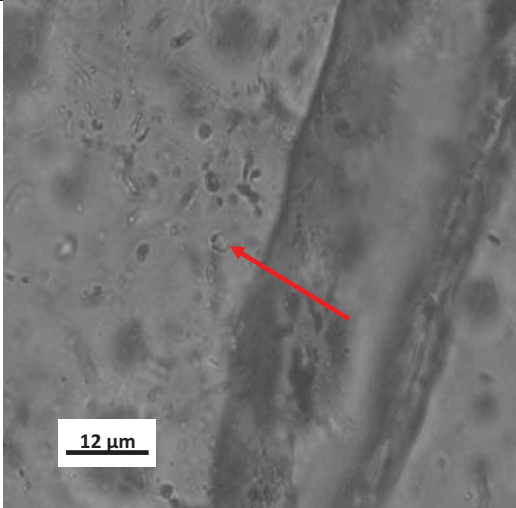
Incl #	Lens X	Incl Size	FI Type	Origin	Picture: LM-6 Chip 2 L-rich
1	100	~3 um	1	Indeter (S?)	

Incl #	Lens X	Incl Size	FI Type	Origin	Picture: LM-6 Chip 2 L-rich
2	100	~5 um	1	Indeter (PS?)	

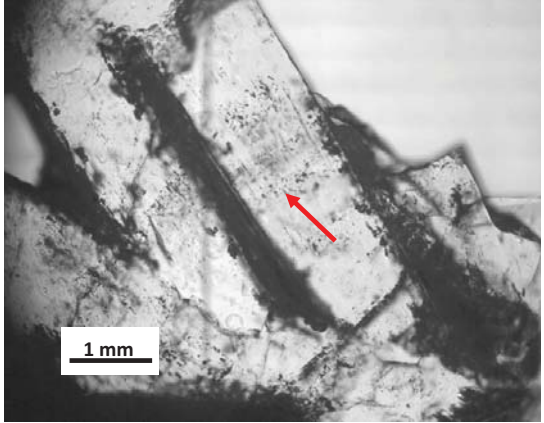
Incl #	Lens X	Incl Size	FI Type	Origin	Picture: LM-6 Chip 2 L-rich
3	100	~3 um	1	Indeter	


Incl #	Lens X	Incl Size	FI Type	Origin	Picture: LM-6 Chip 2 L-rich
4	100	~3 um	1	Indeter (PS?)	

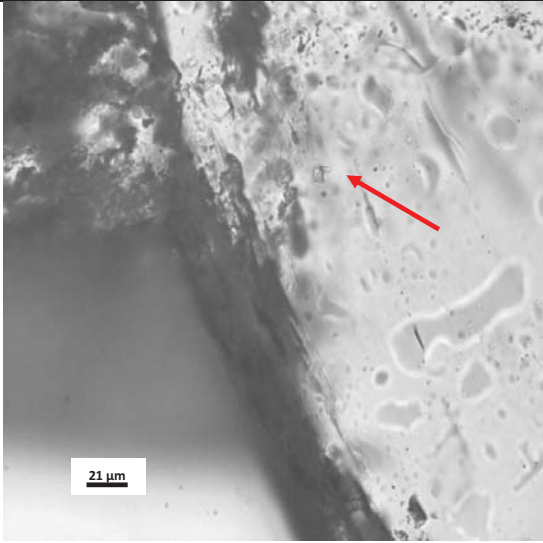
Incl #	Lens X	Incl Size	FI Type	Origin	Picture: LM-6 Chip 2 L-rich
5-7	100	~3-5 um	1	Indeter (PS?)	

Incl #	Lens X	Incl Size	FI Type	Origin	Picture: LM-6 Chip 2 L-rich
8	100	~3 um	1	PS	

Incl #	T _{freeze} (°C)	T _e (°C)	T _{m(ice)} (°C)	T _H (°C)	LM-6 Chip 2 Comments
1	ND	ND	~ -33 ±2	181 ±2	<p>The variation in Th could have been caused by stretching at some time.</p> <p>Inclusions 5-8 could not see freezing or melting.</p>
2	-105 ±5	-50 ±5	-34 ±0.1	115 ±5	
3	-100 ±5	-55 ±5	-30 ±0.1	125 ±5	
4	-90 ±5	-55 ±5	-30 ±1	160 ±5	
5	ND	ND	ND	130 ±5	
6	ND	ND	ND	130 ±5	
7	ND	ND	ND	145 ±5	
8	ND	ND	ND	180 ±5	

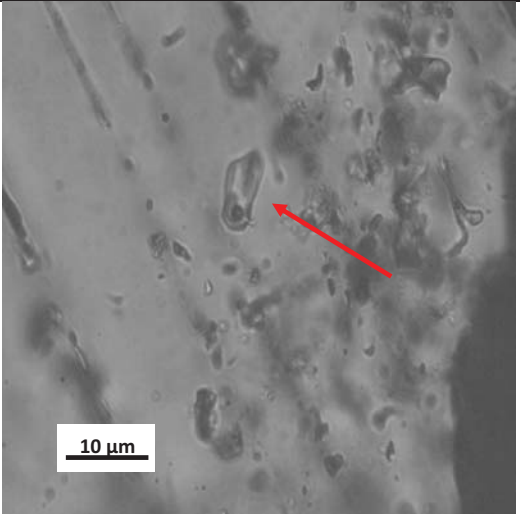
Date: m/d/y	Sample #	Chip #	Host Mineral	Lens X	Res	Picture LM-6 Chip 3 barite
09/8- 10/09	LM-6	3 L-rich Low V:L	Barite	10	1280 X 1024	

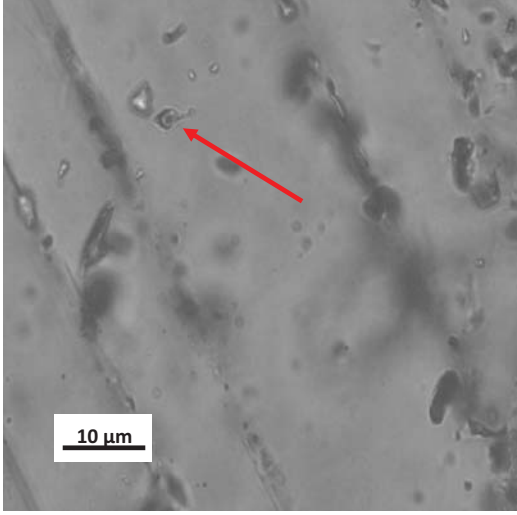
Incl #	Lens X	Incl Size	FI Type	Origin	Picture: LM-6 Chip 3 L-rich
incl1 and 2 (blk arrow) incl 3 (red arrow)	60	~9 um	1	S	

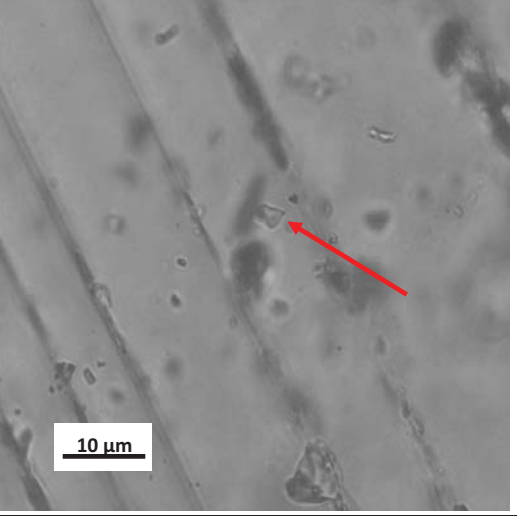
Incl #	Lens X	Incl Size	FI Type	Origin	Picture: LM-6 Chip 3 L-rich single
Single 1	100	~7 um	1	Indeter	

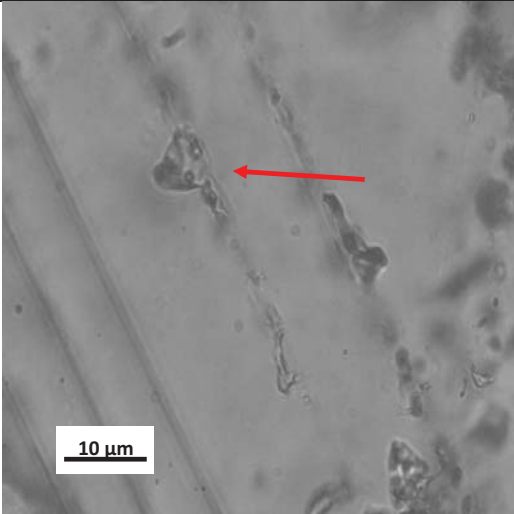
Incl #	T _{freeze} (°C)	T _e (°C)	T _{m(ice)} (°C)	T _H (°C)	LM-6 Chip 3 Comments
1	-92.6 ±2	-49 ±1	-29.3 ±.1	164 ±1	In cluster
2	-92.6 ±2	-49 ±1	-29.3 ±.1	178.8 ±1	In cluster
3	-92.6 ±2	-49 ±1	-29.3 ±.1	188.5 ±.2	In cluster
Single 1	-97.3 ±.1	-59.9 ±.3	-38.1 ±.2	189.1 ±.1	Not in cluster

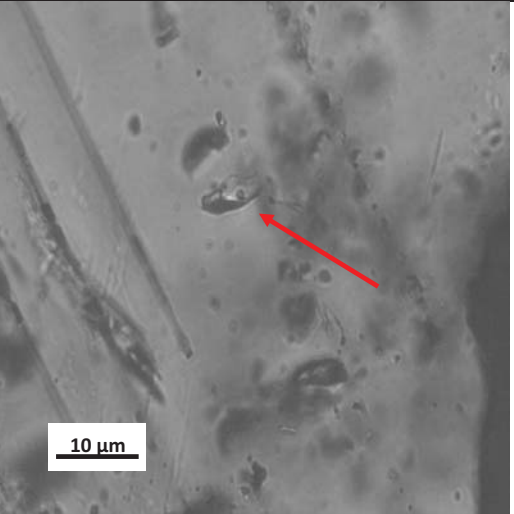
Date: m/d/y	Sample #	Chip #	Host Mineral	Lens X	Res	Picture LM-6 Chip 4 calcite
11/30/09 and 12/01/09	LM-6	4 L-rich	Calcite	10	1280 X 1024	NA

Incl #	Lens X	Incl Size	FI Type	Origin	Picture: LM-6 Chip 4 L-rich single
1	100	~10 um	1	S	

Incl #	Lens X	Incl Size	FI Type	Origin	Picture: LM-6 Chip 4 L-rich single
2	100	~5 um	1	S	

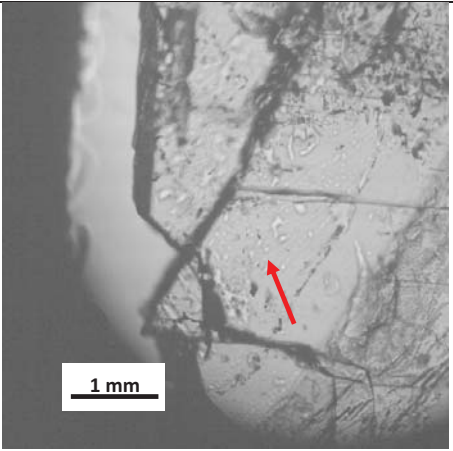
Incl #	Lens X	Incl Size	FI Type	Origin	Picture: LM-6 Chip 4 L-rich single
3	100	~3 um	1	S	

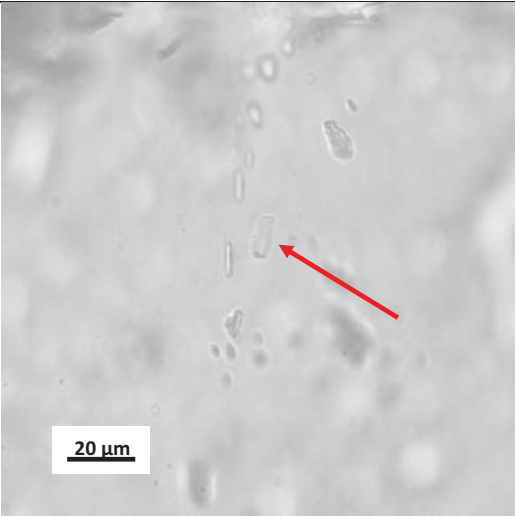
Incl #	Lens X	Incl Size	FI Type	Origin	Picture: LM-6 Chip 4 L-rich single
4	100	~9 um	1	S	

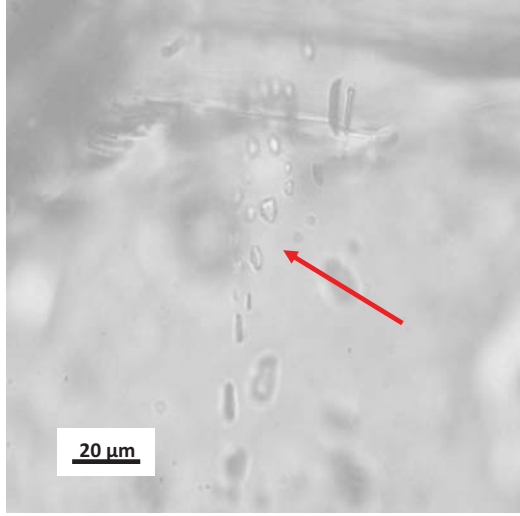
Incl #	Lens X	Incl Size	FI Type	Origin	Picture: LM-6 Chip 4 L-rich single
5	100	~10 um	1	S	

Incl #	Lens X	Incl Size	FI Type	Origin	Picture: LM-6 Chip 4 L-rich single
6 and 7	100	~2 um	1	S?	Could not get good picture

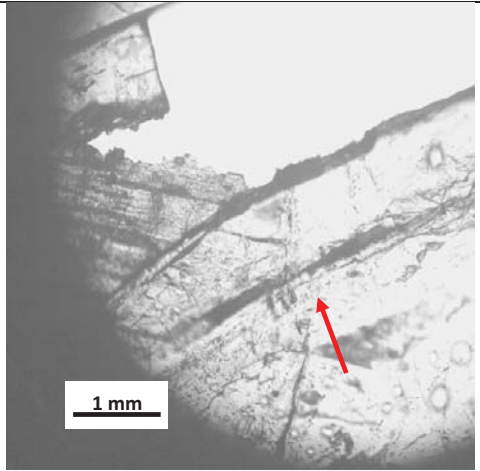
Incl #	T _{freeze} (°C)	T _e (°C)	T _{m(ice)} (°C)	T _H (°C)	LM-6 Chip 4 Comments
1	-66 ±10	-60 ±10	-47 ±3	65 ±5	Sample was frozen first from a previous analysis. Therefore Th are taken as maximums. These Th are in same range as other samples.
2	-66 ±10	-60 ±10	-47 ±3	80 ±5	
3	-66 ±10	-60 ±10	-47 ±3	80 ±5	
4	-66 ±10	-60 ±10	-47 ±3	50 ±5	
5	-66 ±10	-60 ±10	-47 ±3	80 ±5	
6	-69 ±0.1	-60 ±5	-52.7 ±0.5	95 ±5	
7	-69 ±0.1	-60 ±5	-52.7 ±0.5	95 ±5	

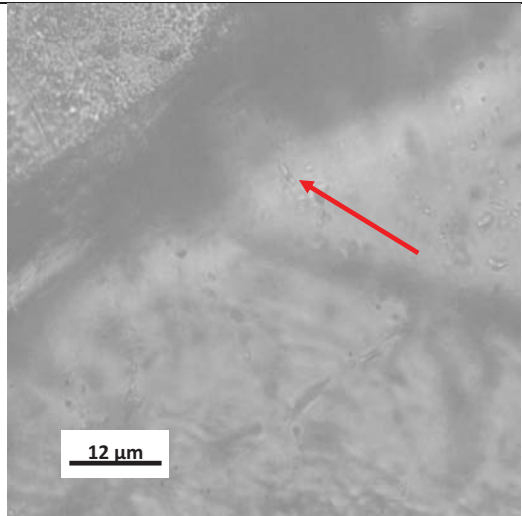
Date: m/d/y	Sample #	Chip #	Host Mineral	Lens X	Res	Picture LM-6 Chip 5 calcite
12/2 - 3/09	LM-6 clusters 1 and 2 (Same fracture different optic plains)	5 L-rich	Calcite	10	1280 X 1024	

Incl #	Lens X	Incl Size	FI Type	Origin	Picture: LM-6 Chip 5 L-rich cluster
cluster 1 1-3	100	~2-10 um	1	S	

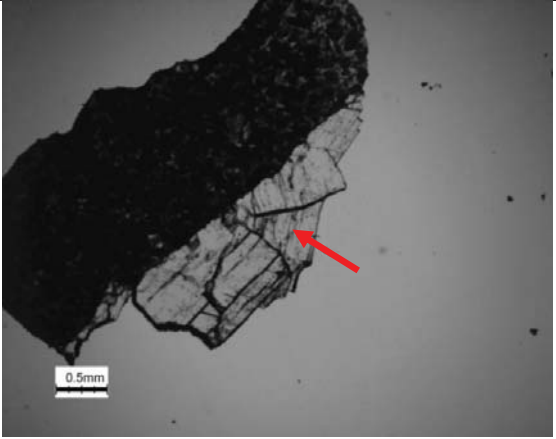
Incl #	Lens X	Incl Size	FI Type	Origin	Picture: LM-6 Chip 5 L-rich cluster
cluster 2 1-4	100	~2-10 um	1	S	


Incl #	T _{freeze} (°C)	T _e (°C)	T _{m(ice)} (°C)	T _H (°C)	LM-6 Chip 5 calcite Comments
cluster 1	-90s ±10	ND	-40s ±10	65 ±5	Both clusters were in the same fracture but slightly different optic planes. Could not see freezing and melting but know inclusions were frozen in the -90s and melted by the -40s.
cluster 2	-90s ±10	ND	-40s ±10	65 ±5	


Date: m/d/y	Sample #	Chip #	Host Mineral	Lens X	Res	Picture LM-6 Chip 5 barite
12/2 - 3/09	LM-6 Singles 1 and 2	5 L-rich	Barite	10	1280 X 1024	


Incl #	Lens X	Incl Size	FI Type	Origin	Picture: LM-6 Chip 5 L-rich
Singles 1 & 2	100	~3 um	1	Indeter	


Incl #	T _{freeze} (°C)	T _e (°C)	T _{m(ice)} (°C)	T _H (°C)	LM-6 Chip 5 Barite Comments
Singles 1 & 2	ND	ND	ND	>200	To small to see freezing or melting


Date: m/d/y	Sample #	Chip #	Host Mineral	Lens X	Res	Picture LM-9A Calcite LOST
07/23- 30/09	LM-9A	1 L-rich Very low V:L singles (white arrow) clusters (red arrow)	Calcite	2.5	3840 X 3072	

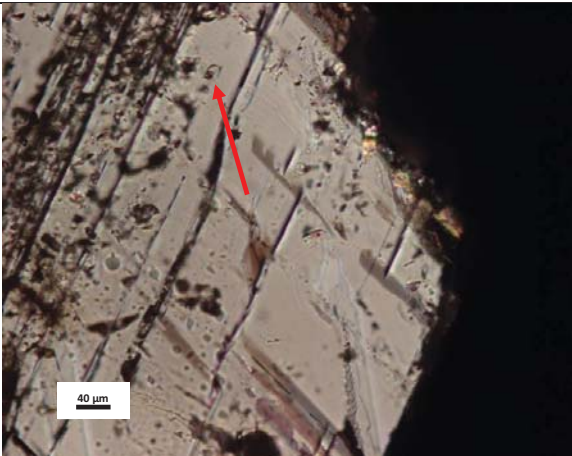
Incl #	Lens X	Incl Size	FI Type	Origin	Picture: LM-9A Chip 1 L-rich 1
1	100	7 um	1	P	

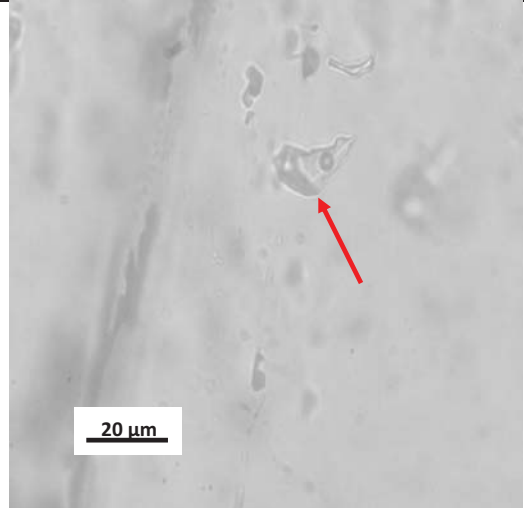
Incl #	Lens X	Incl Size	FI Type	Origin	Picture: LM-9A Chip 1 L-rich 2
2	100	5 um	1	P	

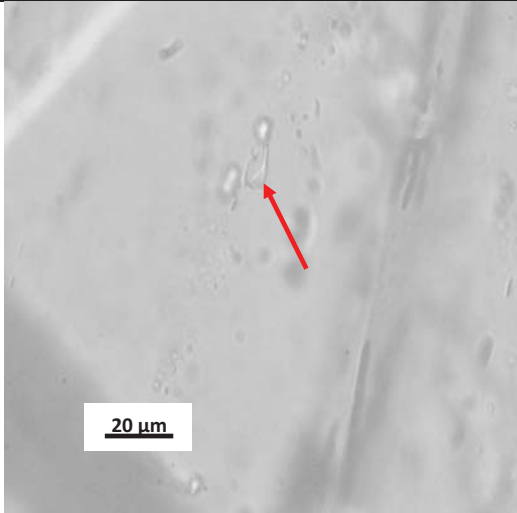
Incl #	Lens X	Incl Size	FI Type	Origin	Picture: LM-9A Chip 1 L-rich 3
3	100	12 um	1	P	

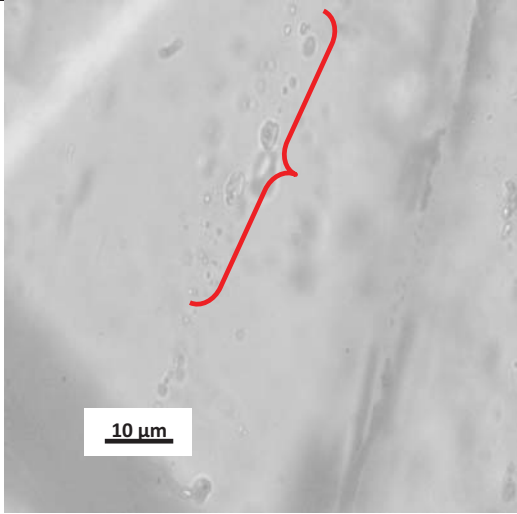
Incl #	Lens X	Incl Size	FI Type	Origin	Picture: LM-9A Chip 1 L-rich 4
4	100	7 um	1	Indeter (PS?)	

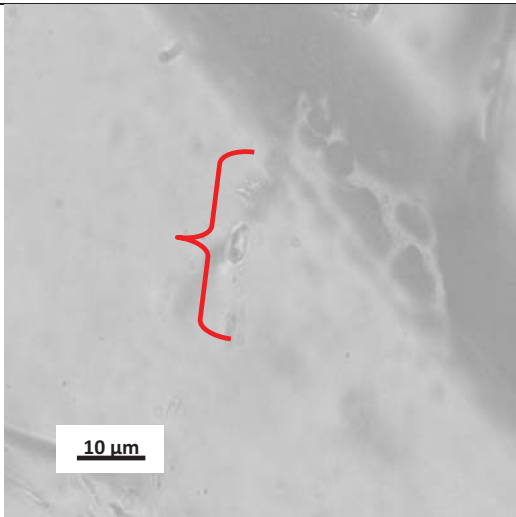
Incl #	Lens X	Incl Size	FI Type	Origin	Picture: LM-9A Chip 1 L-rich 5
5	100	8 um	1	Indeter (PS?)	

Incl #	Lens X	Incl Size	FI Type	Origin	Picture: LM-9A Chip 1 L-rich 6
6	20	20 um	1	Indeter (PS?)	

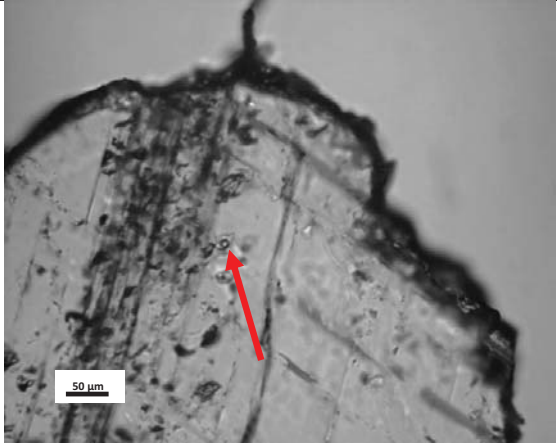
Incl #	Lens X	Incl Size	FI Type	Origin	Picture: LM-9A Chip 1 L-rich 7
7	100	~20 um	1	S	

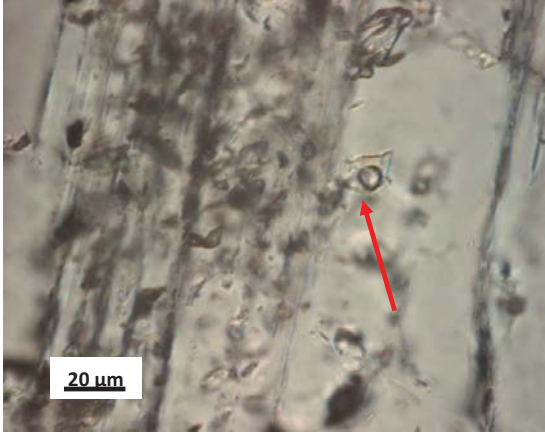
Incl #	Lens X	Incl Size	FI Type	Origin	Picture: LM-9A Chip 1 L-rich 8
8	100	~10 um	1	S	

Incl #	Lens X	Incl Size	FI Type	Origin	Picture: LM-9A Chip 1 L-rich clusters 1 and 2 (same fracture as single incl 1-8, but different optic plains)
9-11 and 12-14	100	~5 um	1	S	

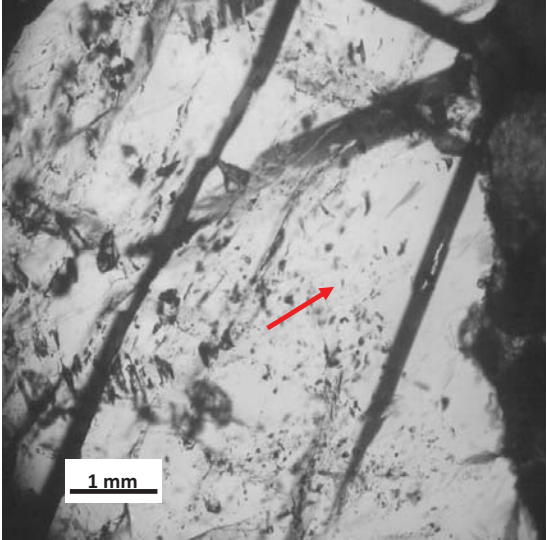
Incl #	Lens X	Incl Size	FI Type	Origin	Picture: LM-9A Chip 1 L-rich cluster 3 (same fracture as clusters 1 and 2 but different optic plains)
15-17	100	~5 μm	1	S	

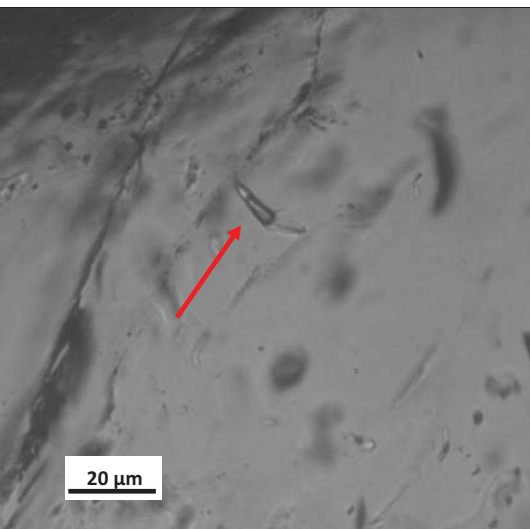
Incl #	$T_{\text{freeze}} (^{\circ}\text{C})$	$T_{\text{e}} (^{\circ}\text{C})$	$T_{\text{m(ice)}} (^{\circ}\text{C})$	$T_{\text{H}} (^{\circ}\text{C})$	LM-9A Chip1 Comments
1	ND	ND	ND	68.1 \pm 1	Could not see freezing even at -196 $^{\circ}$ C or with cycling
2	ND	ND	ND	43.1 \pm 1	Could not see freezing even at -196 $^{\circ}$ C or with cycling
3	-108.3 \pm 1	~ -63	-38.4 \pm 2	53.7 \pm 1	First melt very difficult to determine. Could be in -50s
4	ND	ND	ND	55.2 \pm 1	Could not see freezing even at -196 $^{\circ}$ C or with cycling
5	-102.8 \pm 1	~ -65	~ -36.7	80 \pm 5	Did not go over 100 $^{\circ}$ C b/c did not want to destroy other FIs. 1st melt could be in -50s, very hard to see
6	-86.6 \pm 1	~ -66.6 \pm 2	~ -30 \pm 2	180 \pm 5	1st melt could be in -50s, very hard to see
7	ND	ND	ND	85 \pm 5	Same problems as above
8	ND	ND	ND	85 \pm 5	“
clusters 1	ND	ND	ND	85 \pm 5	“
2	ND	ND	ND	85 \pm 5	“
3	ND	ND	ND	85 \pm 5	“
					Single FIs 1-3 where isolated in a clear growth rim potential P

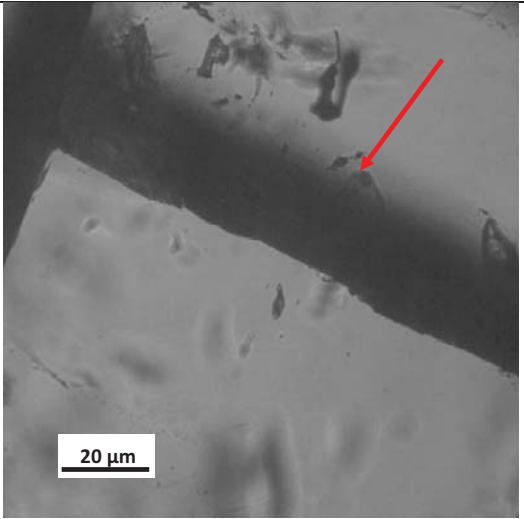
Date: m/d/y	Sample #	Chip #	Host Mineral	Lens X	Res	Picture LM-9A Chip 2 calcite LOST
08/4- 6/09	LM-9A	2 LOST L-rich Low V:L	Calcite	20	3840 X 3072	

Incl #	Lens X	Incl Size	FI Type	Origin	Picture: LM-9A Chip 2 L-rich 1 LOST on microtherm stage
1	50	20 µm	1	Indeter (S?) Leaked?	

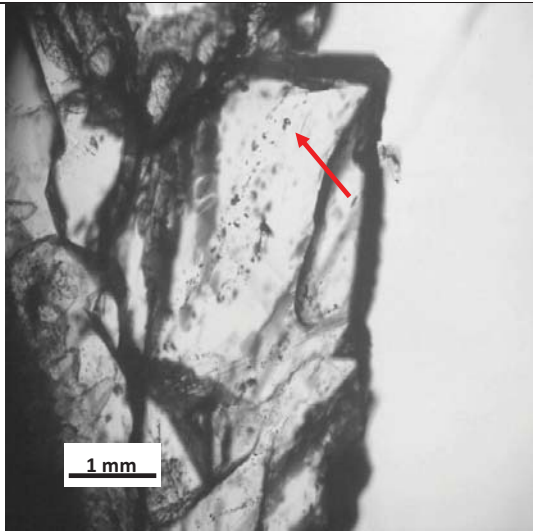
Incl #	T _{freeze} (°C)	T _e (°C)	T _{m(ice)} (°C)	T _H (°C)	LM-9A Chip2 Comments
1	-37.2 ±.1	ND	0.0 ±.1	>200	Started doing Th but stopped at 120°C b/c didn't want to lose chip. Tried to analyze other L-only FIs to no avail. Returned to incl 1 did freezing then tried Th. Sample disintegrated (lost) on microthermo stage before analysis completed (very tiny piece). However, the bubble did not increase or decrease in size (inclusion showed no sign of homogenizing) with increasing temperature. Same behavior as 4 other incl with Th >200°C from other chips.

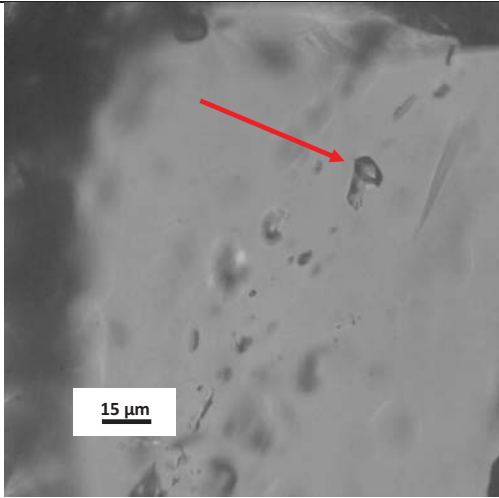
Date: m/d/y	Sample #	Chip #	Host Mineral	Lens X	Res	Picture LM-9A Chip 3 calcite
08/11/09	LM-9A	3 L-rich Low V:L	Calcite	10	1280 x 1024	

Incl #	Lens X	Incl Size	FI Type	Origin	Picture: LM-9A Chip 3 L-rich 1
1	60	~20 um	1	Indeter (S?)	

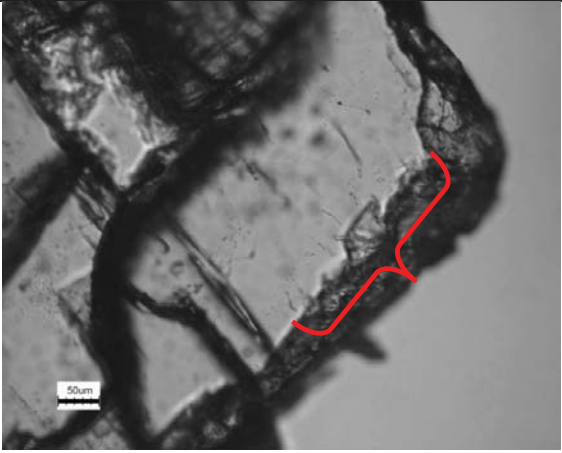
Incl #	Lens X	Incl Size	FI Type	Origin	Picture: LM-9A Chip 3 L-rich 2
2	60	~15 um	1	Indeter (S?)	

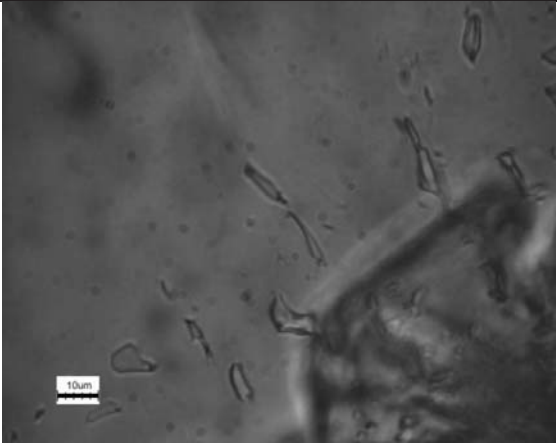
Incl #	T _{freeze} (°C)	T _e (°C)	T _{m(ice)} (°C)	T _H (°C)	LM-9A Chip3 Comments
1	-36.4 ±.1	~ -17 ±5	-0.2 ±.1	368.7 ±.1	
2	ND	ND	ND	356.1 ±.1	Could not see freezing down to 196°C


Date: m/d/y	Sample #	Chip #	Host Mineral	Lens X	Res	Picture LM-10B chip 1 calcite
08/11/09	LM-10B	1 L-rich Very low V:L	Calcite	10	1280 x 1024	

Incl #	Lens X	Incl Size	FI Type	Origin	Picture: LM-10B Chip 1 L-rich
1	60	~15 um	1	S	

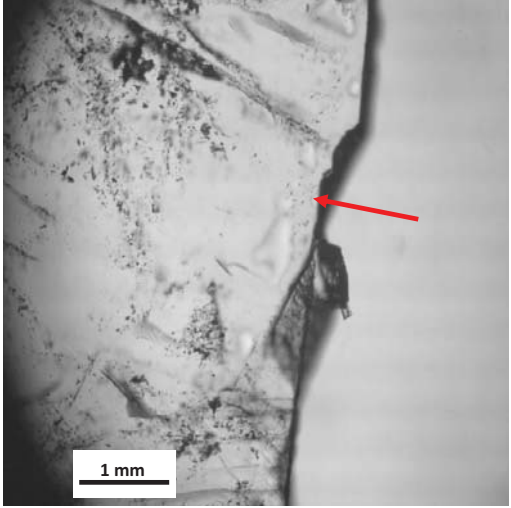
Incl #	T _{freeze} (°C)	T _e (°C)	T _{m(ice)} (°C)	T _H (°C)	LM-10B Chip 1 Comments
1	ND	ND	ND	71.4 ± 1	Could not see melting

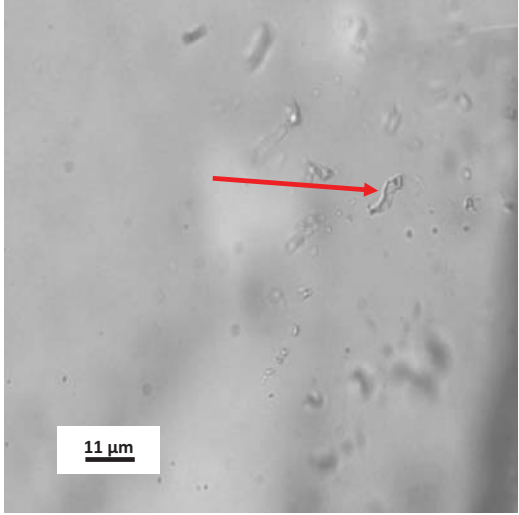
Date: m/d/y	Sample #	Chip #	Host Mineral	Lens X	Res	Picture LM-10B chip 2 cluster
08/12-13/09	LM-10B	2 L-rich cluster Very low V:L	Calcite	20	3840 X 3072	

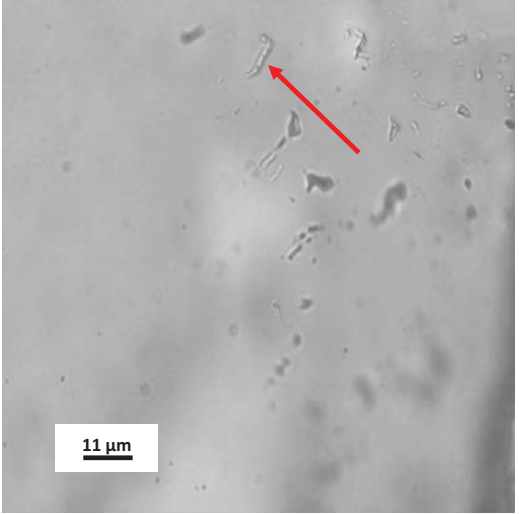
Incl #	Lens X	Incl Size	FI Type	Origin	Picture: LM-10B Chip 2 L-rich cluster
1-7	100	~10 - 15 µm	1	P	

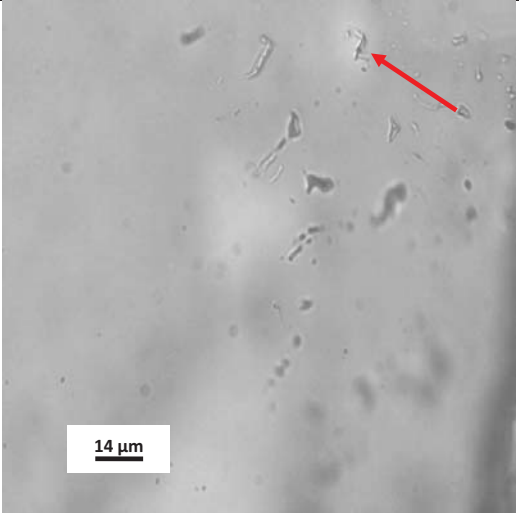
Incl #	Lens X	Incl Size	FI Type	Origin	Picture: LM-10B Chip 2 L-rich
8	100	~10 um	1	P	

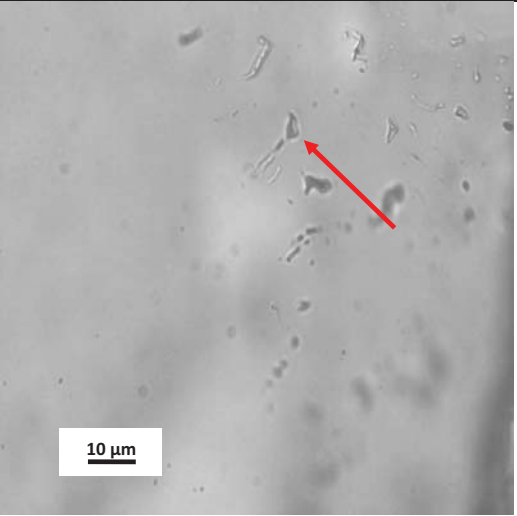
Incl #	T _{freeze} (°C)	T _e (°C)	T _{m(ice)} (°C)	T _H (°C)	LM-10B Chip 2 Comments
1-7	-77.7 ±.1	-60±10	-40.5 ±2	79.2 ±.1	CL candidate could be later overgrowth when fluids cooled a bit
8	-100 ±.1	-63 ±5	~ -37 ± 1	95.1 ±.1	CL candidate possible earlier phase with hotter fluids than above but 1 & 2 could be related

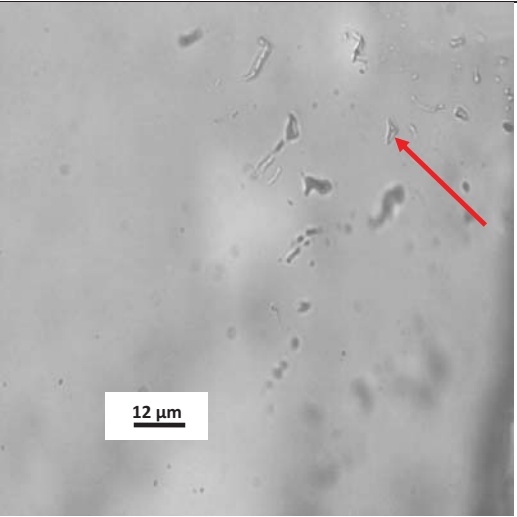
Date: m/d/y	Sample #	Chip #	Host Mineral	Lens X	Res	Picture DKA-103 chip 1 L-rich and L-only cluster
09/24/09	DKA-103	1 L- rich/L- only cluster L-rich has very low V:L	Calcite	10	1280 X 1024	

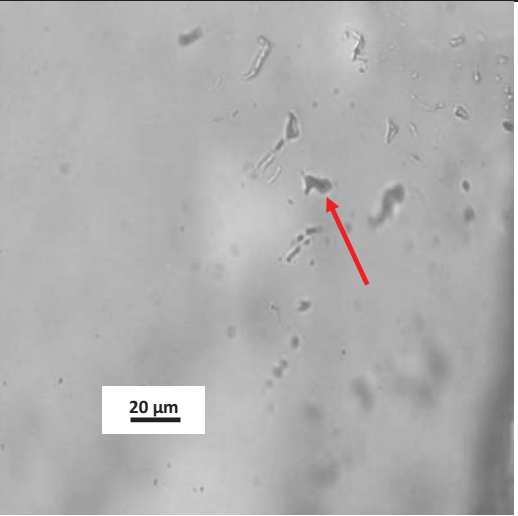
Incl #	Lens X	Incl Size	FI Type	Origin	Picture: DKA-103 Chip 1 L-rich in cluster
1	100	~11 μ m	1	P	

Incl #	Lens X	Incl Size	FI Type	Origin	Picture: DKA-103 Chip 1 L-rich in cluster
2	100	~11 um	1	P	

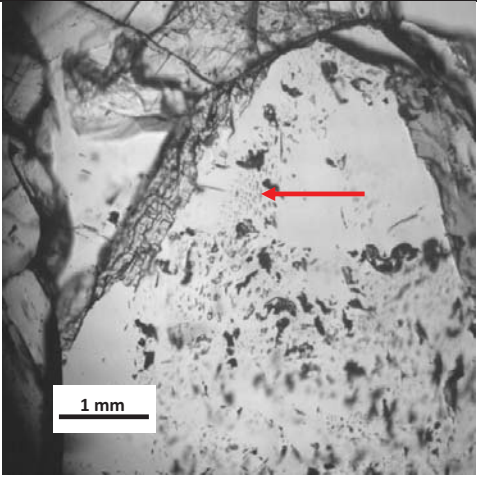
Incl #	Lens X	Incl Size	FI Type.	Origin	Picture: DKA-103 Chip 1 L-rich in cluster
3	100	~7 um	1	P	

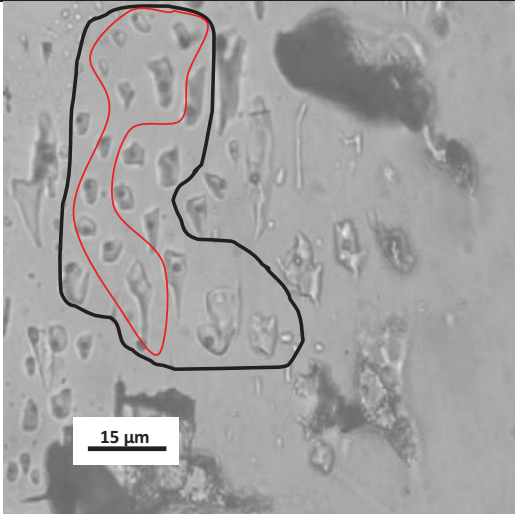
Incl #	Lens X	Incl Size	FI Type	Origin	Picture: DKA-103 Chip 1 L-only in cluster
4	100	~5 um	2	P	

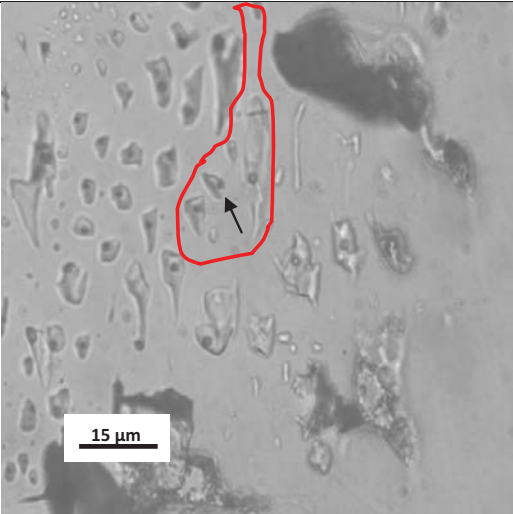
Incl #	Lens X	Incl Size	FI Type	Origin	Picture: DKA-103 Chip 1 L-only in cluster
5	100	~4 um	2	P	

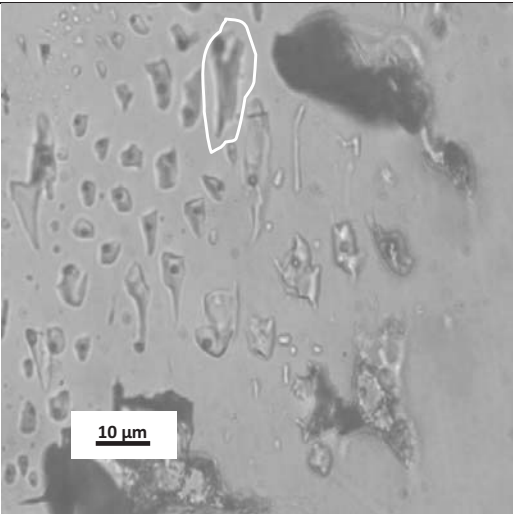
Incl #	Lens X	Incl Size	FI Type	Origin	Picture: DKA-103 Chip 1 L-only in cluster
6	100	~11 um	2	P	

Incl #	T _{freeze} (°C)	T _e (°C)	T _{m(ice)} (°C)	T _H (°C)	DKA-103 Chip 1 Comments
1 L-V	-120 ±5	-59 ±5	-44.5 ±.2	92 ±2	L-rich and L-only are in same plane. L-rich have very low V:L. L-only when cooled below zero nucleate tiny V-bubbles similar to L-rich therefore have similar very low V:L
2 L-V	-120 ±5	-56 ±5	-48.1 ±.2	92 ±2	
3 L-V	-120 ±5	-56 ±5	-38.1 ±.2	92 ±2	
4 L	-120 ±5	-56 ±5	-37.8 ±.2	85 ±2	
5 L	-120 ±5	ND	ND	85 ±2	
6 L	-120 ±5	-57 ±5	-37.8 ±.2	92 ±2	

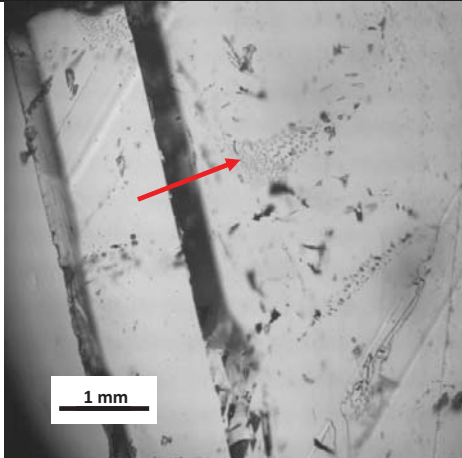
Date: m/d/y	Sample #	Chip #	Host Mineral	Lens X	Res	Picture DKA-326 Chip 1 calcite
09/29/09 to 10/01/09	DKA-326	1 L-rich/L- only cluster	Calcite	10	1280 x 1024	

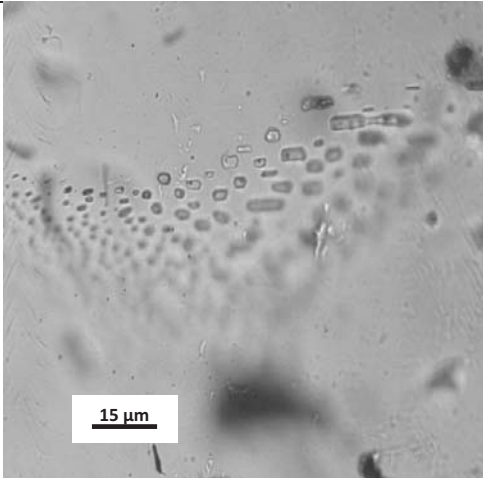
Incl #	Lens X	Incl Size	FI Type	Origin	Picture: DKA-326 Chip 1 L-rich/L-only clusters
1 - 21	100	~2 - 15 um	1 and 2 (inside red line)	S	

Incl #	Lens X	Incl Size	FI Type	Origin	Picture: DKA-326 Chip 1 L-rich/L-only cluster
22 -25	100	~5- 20 um	1(black arrow) and 2	S	

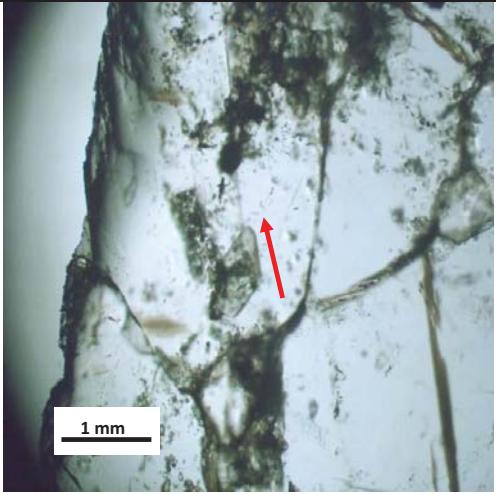
Incl #	Lens X	Incl Size	FI Type	Origin	Picture: DKA-326 Chip 1 L-rich/L-only cluster
26	100	~ 20 um	1	S	

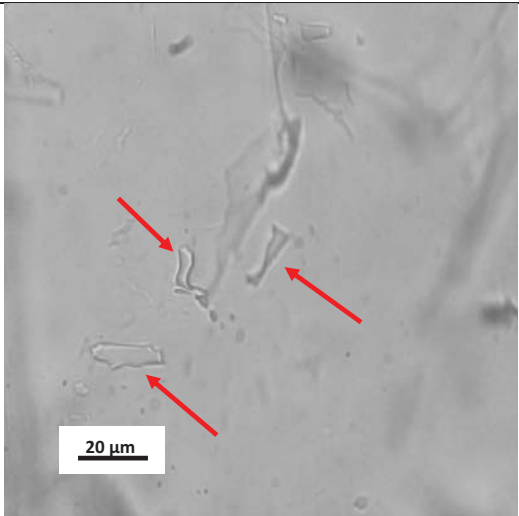
Incl #	T _{freeze} (°C)	T _e (°C)	T _{m(ice)} (°C)	T _H (°C)	DKA-326 Chip 1 Comments L-rich and L-only are in same optic plane therefore are an assemblage. L-rich have very low V:L. L-only when cooled below zero nucleate small V-bubbles similar to L-rich therefore have same low V:L
1-21	-80 ±5	-60 ±5	-39 ±.5	85 ±5	
22-25	-80 ±5	-60 ±5	-38.5 ±.5	85 ±5	
26	-80 ±5	-60 ±5	-32.3 ±.2	85 ±5	

Date: m/d/y	Sample #	Chip #	Host Mineral	Lens X	Res	Picture DKA-326 Chip 2 calcite
09/29/09 to 10/01/09	DKA-326	2 cluster ~10-15 are L-rich low V:L Rest are L-only	Calcite	10	1280 x 1024	

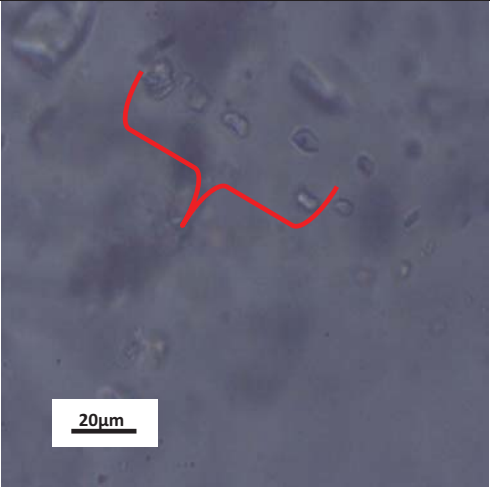
Incl #	Lens X	Incl Size	FI Type	Origin	Picture: DKA-326 Chip 2 L-rich/L-only cluster
50 + Monitored 15 then checked rest	100	~ 5-15 um	1 and 2	S	

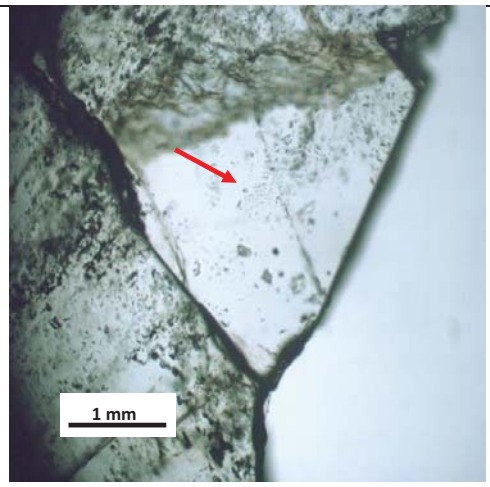
Incl #	T _{freeze} (°C)	T _e (°C)	T _{m(ice)} (°C)	T _H (°C)	DKA-326 Chip 2 Comments
50 +	-105 ±5	-65 ±5	-40 ±.5	85 ±5	L-rich have very low V:L. L-only when cooled below zero nucleate small V-bubbles similar to L-rich therefore have same low V:L. Was able to see ~15 inclusions react all at same time then checked rest of inclusions to see how many were in same phase at same time as the 15. It appeared the rest of the FIs in the cluster matched the 15 within a couple of degrees depending on depth into mineral.

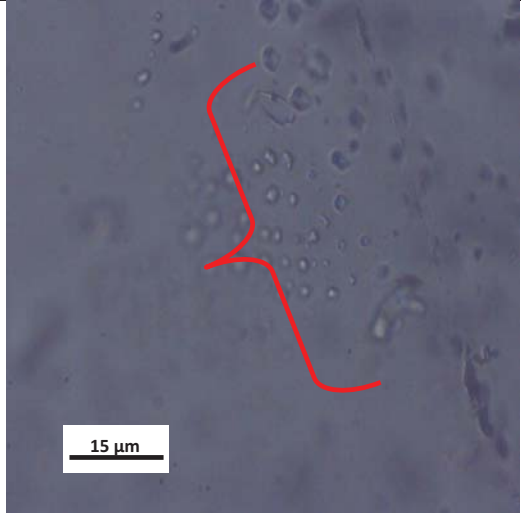
Date: m/d/y	Sample #	Chip #	Host Mineral	Lens X	Res	Picture 99-101 Chip 1 calcite
10/6-8/09	99-101	1 L-only cluster	Calcite	10	1280 x 1024	

Incl #	Lens X	Incl Size	FI Type	Origin	Picture 99-101 Chip 1 L-only cluster
1-3	100	~ 10- 20 um	2	S	

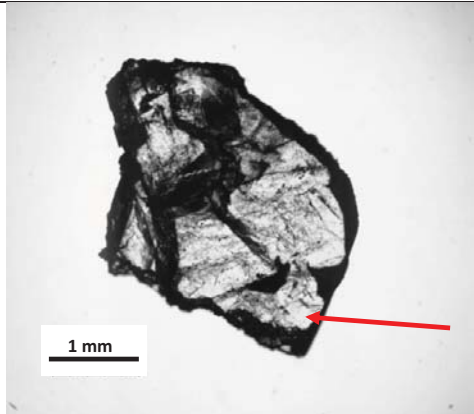
Incl #	T _{freeze} (°C)	T _e (°C)	T _{m(ice)} (°C)	T _H (°C)	99-101 Chip 1 Comments
1-3	-55 ±5	-40 ±5	-6.5 ±.1	NA L-only	Could not nucleate a bubble but could see freezing and melting


Incl #	Lens X	Incl Size	FI Type	Origin	Picture 99-101 Chip 2 L-only cluster 1
1-5	100	~5- 10 um	2	S	


Date: m/d/y	Sample #	Chip #	Host Mineral	Lens X	Res	Picture 99-101 Chip 2 calcite
10/6-8/09	99-101	2 L-rich/L-only clusters	Calcite	10	1280 x 1024	

Incl #	Lens X	Incl Size	FI Type	Origin	Picture 99-101 Chip 2 L-only cluster 2
1-5 L-rich 6+ L-only	100	~2- 10 um	2	S	

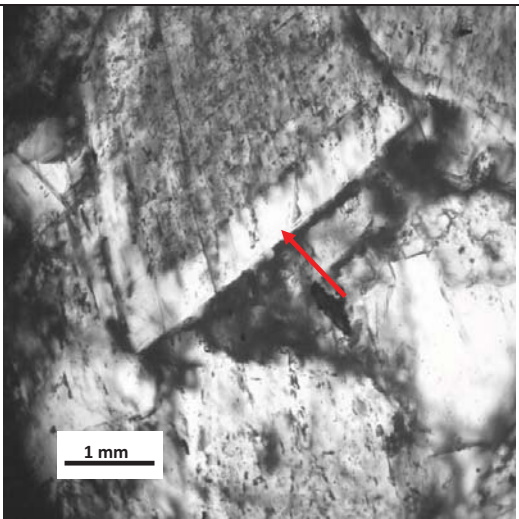
Incl #	T _{freeze} (°C)	T _e (°C)	T _{m(ice)} (°C)	T _H (°C)	99-101 Chip 2 Comments
cluster 1 1-5	ND	ND	ND	70 ±5	cluster 1 has two inclusions with bubbles others L-only. Could not see freezing or melting. cluster 2 had ~ 1 with bubble ~ 20 without bubbles. Bubbles returned after homogenization upon freezing. L-only eventually nucleated bubbles after several freezings.
cluster 2 1-6+	-100 ±5	-60 ±5	-44 ±1 (?)	65 ±5	

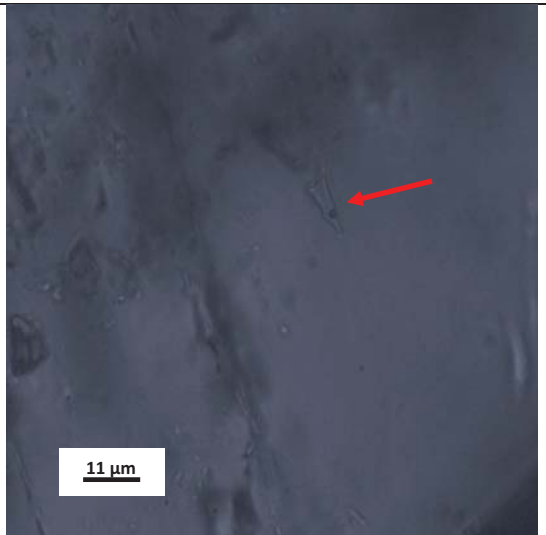
Date: m/d/y	Sample #	Chip #	Host Mineral	Lens X	Res	Picture 99-107 Chip 1 calcite
10/13- 15/09	99-107	1 L-rich cluster Low V:L	Calcite	10	3840 x 3072	

Incl #	Lens X	Incl Size	FI Type	Origin	Picture 99-107 Chip 1L-rich cluster
From right to left 1-4	50	~6-30 um	1	S	

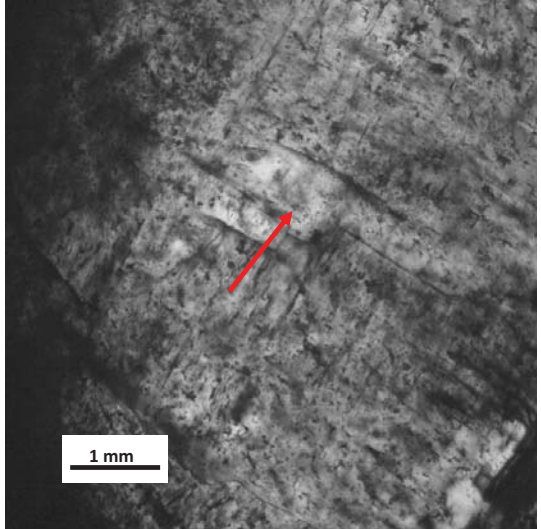
Incl #	Lens X	Incl Size	FI Type	Origin	Picture 99-107 Chip 1 L-rich cluster
Right to left 5-7	50	~6-10 um	1	S	


Incl #	T _{freeze} (°C)	T _e (°C)	T _{m(ice)} (°C)	T _H (°C)	99-107 Chip 1 Comments
1	-110 ±5	-61 ±2	-36.9 ±.1	90 ±2	Inclusions 1-4 are in a slightly different optical plane to 5-7 but results are the same.
2	-95 ±5	-61 ±2	-36.9 ±.1	90 ±2	
3	-100 ±5	-61 ±2	-36.9 ±.1	90 ±2	
4	-105 ±5	-61 ±2	-36.9 ±.1	90 ±2	
5	-95 ±5	-61 ±2	-36.9 ±.1	90 ±2	
6	-95 ±5	-61 ±2	-36.9 ±.1-	90 ±2	
7	-110 ±5	-61 ±2	36.9 ±.1	90 ±2	

Date: m/d/y	Sample #	Chip #	Host Mineral	Lens X	Res	Picture 99-120 Chip 1 oil-bearing saddle Do
09/16-18/09	99-120	1 L-rich single	Saddle Do	10	1280 X 1024	

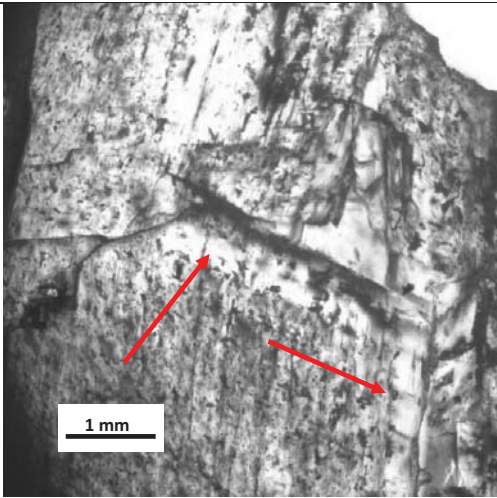
Incl #	Lens X	Incl Size	FI Type	Origin	Picture: 99-120 Chip 1 L-rich single
Single 1	100	11 um	1	PS	

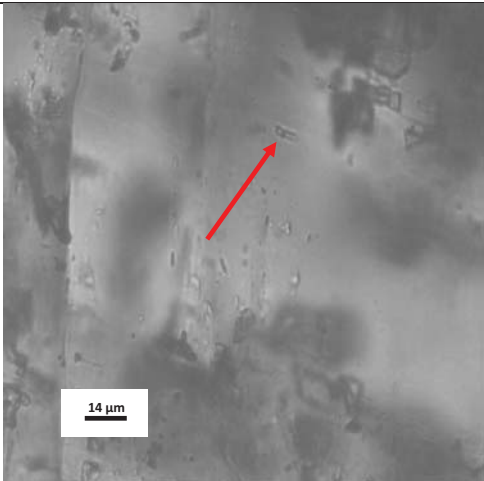
Incl #	T _{freeze} (°C)	T _e (°C)	T _{m(ice)} (°C)	T _H (°C)	99-120 Chip 1 Comments
Single 1	-93.8 ± 1	-53 ± 10	-38.9 ± 1	90.4 ± 1	Possible primary in Do growth rim.

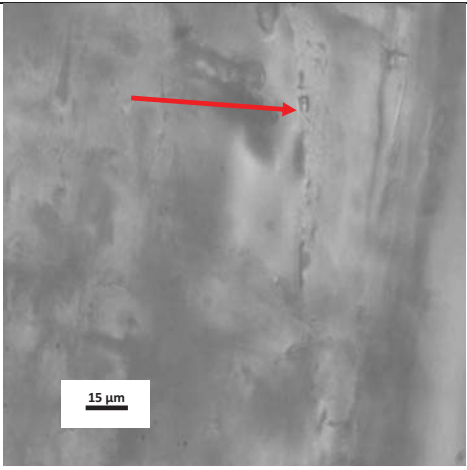
Date: m/d/y	Sample #	Chip #	Host Mineral	Lens X	Res	Picture 99-120 Chip 1 cluster oil-bearing saddle Do
09/16-18/09	99-120	1 L-rich cluster Low V:L	Saddle Dolomite	10	1280 X 1024	

Incl #	Lens X	Incl Size	FI Type	Origin	Picture: 99-120 Chip 1 L-rich cluster
1-3	100	8-10 um	1	PS	

Incl #	T _{freeze} (°C)	T _e (°C)	T _{m(ice)} (°C)	T _H (°C)	Chip 1 cluster Comments
1	-83.8 ±.1	-55 ±10	-40.9 ±.1	100.7 ±.1	Could only see largest of the three freeze and melt. All three had same Th.
2	ND	ND	ND	100.7 ±.1	
3	ND	ND	ND	100.7 ±.1	

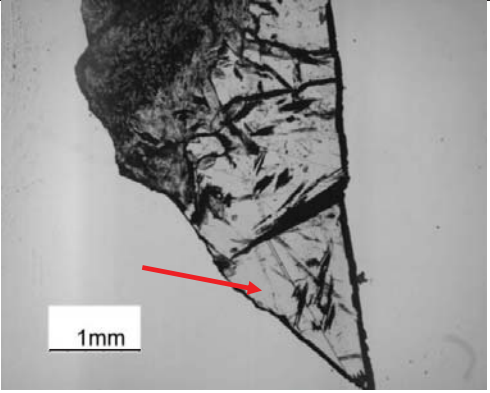
Date: m/d/y	Sample #	Chip #	Host Mineral	Lens X	Res	Picture 99-120 Chip 3 oil-bearing saddle Do
09/23/09	99-120	3 L-rich Low V:L	Saddle Dolomite	10	1280 X 1024	

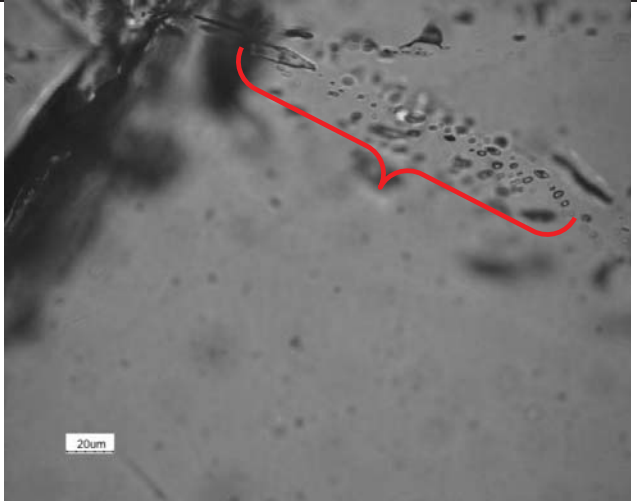
Incl #	Lens X	Incl Size	FI Type	Origin	Picture: 99-120 Chip 3 L-rich
1	100	~7 um	1	P	

Incl #	Lens X	Incl Size	FI Type	Origin	Picture: 99-120 Chip 3 L-rich
2	100	~5 um	1	S	

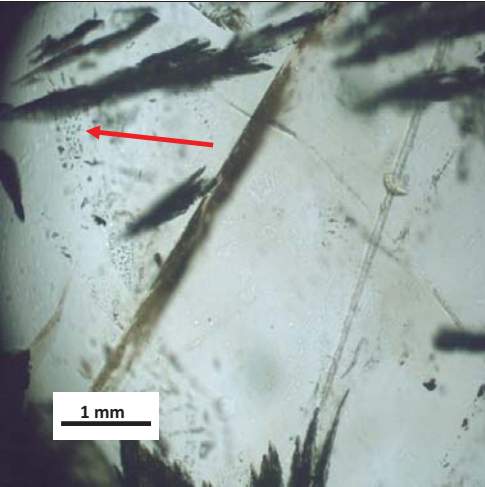
Incl #	Lens X	Inclu Size	FI Type	Origin	Picture: 99-120 Chip 3 L-rich
3	100	~7 um	1	P?	NA

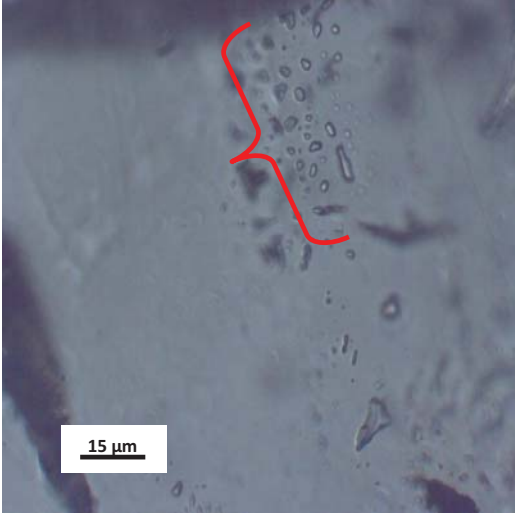
Incl #	T _{freeze} (°C)	T _e (°C)	T _{m(ice)} (°C)	T _H (°C)	99-120 Chip 3 Comments
1	-85 ± 5	-55 ± 5	-41.1 ± 1	137 ± 3	Found in Do growth rim parallel to cleavage
2	-79 ± 1	-56 ± 5	-41 ± 5	109 ± 3	In same growth rim as incl 1 but on side and definitely secondary
3	ND	ND	ND	83 ± 2	Could not see well but possible Primary b/c isolated along and parallel to crystal rim

Date: m/d/y	Sample #	Chip #	Host Mineral	Lens X	Res	Picture 99-132 Chip 1 calcite
10/13- 15/09	99-132	1 L-only cluster	Calcite	10	3840 x 3072	

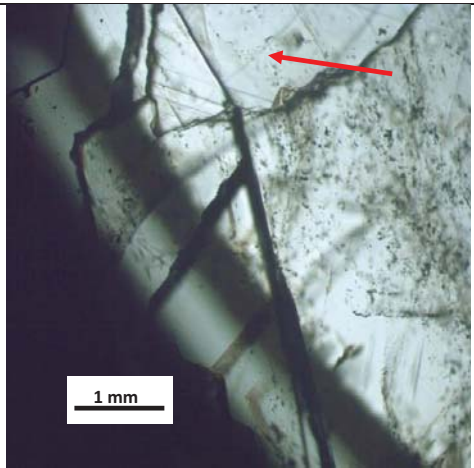
Incl #	Lens X	Incl Size	FI Type	Origin	Picture 99-132 chip 1 L-only cluster
1-15	50	~5 um 2 @ ~20um	2	S	


Incl #	T _{freeze} (°C)	T _e (°C)	T _{m(ice)} (°C)	T _H (°C)	99-132 Chip 1 Comments
cluster 1- 15	-50 ±5	-35 ±5	-0.5 ±.1	ND	Liquid only inclusions never nucleated bubbles

Date: m/d/y	Sample #	Chip #	Host Mineral	Lens X	Res	Picture 99-132 Chip 2 calcite
10/13-15/09	99-132	2 L-only cluster	Calcite	10	1280 x 1024	

Incl #	Lens X	Incl Size	FI Type	Origin	Picture 99-132 chip 2 L-only cluster
1-15	60	~2-10 um	2	S	

Incl #	T _{freeze} (°C)	T _e	T _{m(ice)}	T _H (°C)	99-132 Chip 2 Comments
cluster 1-15	-50 ±5	-35 ±2	-1.2 ±.2	ND	Liquid only inclusions never nucleated bubbles

Date: m/d/y	Sample #	Chip #	Host Mineral	Lens X	Res	Picture 99-134 Chip 1 calcite
10/13-15/09	99-134	1 L-rich cluster	Calcite	10	1280 x 1024	

Incl #	Lens X	Incl Size	FI Type	Origin	Picture 99-134 chip 1 L-rich
1	60	~20 um	1	S	

Incl #	T _{freeze} (°C)	T _e (°C)	T _{m(ice)} (°C)	T _H (°C)	99-134 Chip 1 Comments
1 T1	~-100 ±10	~-60 ±10	~-40 ±10	85 ±5	Could see sample freeze and thaw only once. Not well enough to get definitive data. Only Th is accurate. Tried several chips but very few useable inclusions

Incl #	T _{freeze} (°C)	T _e (°C)	T _{m(ice)} (°C)	T _H (°C)	99-134 Chip 2 Calcite Comments
1 & 2 S	ND	ND	ND	85 ±5	Inclusions were ~ 2 -4 um could not get photos of them. All T1
3 Indeter	ND	ND	ND	>200	
4 Indeter	ND	ND	ND	~150 ±10	

Fluid inclusion Microthermometry data

ND=No Data

LM-4 Chip 1 calcite L-V uBob Used as a practice chip						
Incl #	T_{Freeze}	T_e	T_{m(ice)}	T_H	Origin/Type	wt%CaCl₂
1	-87±0.1	-47±1	-16±1	ND	indeter/1a	18.69
2	-66.6±0.1	-47.7±2.5	-23±1	ND	indeter/1a	22.76
LM-5.1 Chip 1 cluster qtz L-V uBob						
Incl #	T_{Freeze}	T_e	T_{m(ice)}	T_H	Origin/Type	wt%CaCl₂
1	-88±1	-65±1	-40.3±0.1	90.6±0.2	P/1a	29.81
2	-88±1	-65±1	-40.3±0.1	90.6±0.2	P/1a	29.81
3	-88±1	-65±1	-40.3±0.1	90.6±0.2	P/1a	29.81
4	ND	ND	ND	103±0.7	P/1a	ND
5	ND	ND	ND	105±1	P/1a	ND
6	ND	ND	ND	76±0.1	P/1a	ND
LM-6 Chip 1 oil bearing barite L-V uGR-MHB-ulBob						
Incl #	T_{Freeze}	T_e	T_{m(ice)}	T_H	Origin/Type	wt%CaCl₂
1	ND	ND	ND	104.3±0.1	S/3	ND
2	ND	ND	ND	98.1±0.1	S/3	ND
3	ND	ND	ND	see below	S/3	ND
FI 3 went from: 120, 116, 104.5, 99.8, 92.5, 87.5, 82, 81.7, 79.6 where I stopped						
Bob: possible overheated hydrocarbs changing chemistry (PVT cond)and causing hydrocarb cracking						
LM-6 Chip 2 barite L-V uGR-MHB-ulBob						
Incl #	T_{Freeze}	T_e	T_{m(ice)}	T_H	Origin/Type	wt%CaCl₂
1	ND	ND	ND	181±2	Indeter (S?)/1a	ND
2	-105±5	-50±5	-34±0.1	115±5	Indeter (PS?)/1a	27.6
3	-100±5	-55±5	-30±0.1	125±5	Indeter/1a	26
4	-90±5	-55±5	-30±1	160±5	Indeter (PS?)/1a	26
5	ND	ND	ND	130±5	Indeter (PS?)/1a	ND
6	ND	ND	ND	130±5	Indeter (PS?)/1a	ND
7	ND	ND	ND	145±5	Indeter (PS?)/1a	ND
8	ND	ND	ND	180±5	Indeter (PS?)/1a	ND
LM-6 Chip 3 barite L-V uGR-MHB-ulBob						
Incl #	T_{Freeze}	T_e	T_{m(ice)}	T_H	Origin/Type	wt%CaCl₂
cluster incl 1	-92.6±0.1	-49±1	-29.3±0.1	164±1	S/1a	25.7
incl 2	-93±2	-49.4±1	-29.3±0.1	178.8±1	S/1a	25.7
incl 3	-93.2±2	-49.2±1	-29.3±0.1	188.5±0.2	S/1a	25.7
single 1	-97.3±0.1	-59.9±0.3	-38.1±2	189.1±0.1	indeter/1a	29.07

LM-6 Chip 4 calcite all single Fls L-V uGR-MHB-ulBob						
Incl #	T _{Freeze}	T _e	T _{m(ice)}	T _H	Origin/Type	wt%CaCl ₂
1	-66±10	-60±10	-47±3	65±5	S/1a	31.9
2	-66±10	-60±10	-47±3	80±5	S/1a	31.9
3	-66±10	-60±10	-47±3	80±5	S/1a	31.9
4	-66±10	-60±10	-47±3	50±5	S/1a	31.9
5	-66±10	-60±10	-47±3	80±5	S/1a	31.9
6	-69±0.1	-60±10	-52.7±0.5	95±5	S/1a	33.4
7	-69±0.1	-60±10	-52.7±0.5	95±5	S/1a	33.4
sample frozen previously so Th is max but is in range of others						
LM-6 Chip 5 calcite FI cluster L-V uGR-MHB-ulBob						
Incl #	T _{Freeze}	T _e	T _{m(ice)}	T _H	Origin/Type	wt%CaCl ₂
cluster 1 incl 1-3	-90s±10	ND	-40s±10	65±5	S/1a	20s-30s
cluster 2 incl 1-4	-90s±10	ND	-40s±10	66±5	S/1a	20s-30s
LM-6 Chip 5 barite L-V uGR-MHB-ulBob						
Incl #	T _{Freeze}	T _e	T _{m(ice)}	T _H	Origin/Type	wt%CaCl ₂
Singles 1 & 2	ND	ND	ND	>200	Indeter/1a (?)	ND
LM-9A Chip 1 calcite L-V MHB						
Incl #	T _{Freeze}	T _e	T _{m(ice)}	T _H	Origin/Type	wt%CaCl ₂
1	ND	ND	ND	68.1±0.1	P/1a	ND
2	ND	ND	ND	43.1±0.1	P/1a	ND
3	-108.3±0.1	-63±10	-38.4±0.2	53.7±0.1	P/1a	29.17
4	ND	ND	ND	55.2±0.1	Indeter (PS?)/1a	ND
5	-102.8±0.1	-65±10	-37.7±0.5	80 ±5	Indeter (PS?)/1a	28.93
6	-86.6±0.1	-66.6±0.2	-30±2	180 ±5	Indeter (PS?)/1a	26
7	ND	ND	ND	85 ±5	S/1a	ND
8	ND	ND	ND	85 ±5	S/1a	ND
cluster 1 incl 9-11	ND	ND	ND	85 ±5	S/1a	ND
cluster 2 incl 12-14	ND	ND	ND	85 ±5	S/1a	ND
cluster 3 incl 15-17	ND	ND	ND	85 ±5	S/1a	ND
LM-9A Chip 2 calcite L-V MHB						
Incl #	T _{Freeze}	T _e	T _{m(ice)}	T _H	Origin/Type	wt%CaCl ₂
1	-37.2±0.1	ND	0±0.1	>200	Indeter (S?)/1b	0
LM-9A Chip 3 calcite L-V MHB						
Incl #	T _{Freeze}	T _e	T _{m(ice)}	T _H	Origin/Type	wt%CaCl ₂
1	-36.4±0.1	-17±5	-0.2±0.1	>200 (368.7±0.1)	Indeter (S?)/1b	0.49
2	ND	ND	ND	>200 (356.1±0.1)	Indeter (S?)/1b (?)	ND

LM-10B Chip 1 calcite L-V MHB						
Incl #	T _{Freeze}	T _e	T _{m(ice)}	T _H	Origin/Type	wt%CaCl ₂
1	ND	ND	ND	71.4±0.1	S/1a	ND
LM-10B Chip 2 calcite cluster (1 to 7) single (8) L-V MHB						
Incl #	T _{Freeze}	T _e	T _{m(ice)}	T _H	Origin/Type	wt%CaCl ₂
1 to 7	-77.7±0.1	-60±10	-40.5±2	79.2±0.1	P/1a	29.88
8	-100±0.1	-63±5	-37±1	95.1±0.1	P/1a	28.69
DKA-103 Chip 1 calcite cluster L-V & L-only (L) uBob						
Incl #	T _{Freeze}	T _e	T _{m(ice)}	T _H	Origin/Type	wt%CaCl ₂
1 L-V	-120±5	-59±5	-44.5±0.2	92±2	P/1a	31.14
2 L-V	-120±5	-56±5	-48.1±0.2	92±2	P/1a	32.19
3 L-V	-120±5	-56±5	-38.1±0.2	92±2	P/1a	29.07
4 L	-120±5	-56±5	-37.8±0.2	85±2	P/2a	28.97
5 L	-120±5	ND	ND	85±2	P/2a	ND
6 L	-120±5	-57±5	-37.8±0.2	92±2	P/2a	28.97
DKA-326 Chip 1 calcite cluster L-V GR						
Incl #	T _{Freeze}	T _e	T _{m(ice)}	T _H	Origin/Type	wt%CaCl ₂
1-21	-80±5	-60±5	-39±0.5	85±5	S/1a (10) & 2a (11)	29.38
22-25	-80±5	-60±5	-38.5±0.5	85±5	S/1a (1) & 2a (3)	29.21
26	-80±5	-60±5	-32.3±0.2	85±5	S/1a	26.94
DKA-326 Chip 2 calcite cluster L-V GR						
Incl #	T _{Freeze}	T _e	T _{m(ice)}	T _H	Origin/Type	wt%CaCl ₂
1-15 for sure (50+)	-105±5	-65±5	-40±0.5	85±5	S/1a	29.71
99-101 Chip 1 calcite cluster L-only uGR						
Incl #	T _{Freeze}	T _e	T _{m(ice)}	T _H	Origin/Type	wt%CaCl ₂
1-3	-55±5	-40±5	-6.5±0.1	ND	S/2a	10.53
99-101 Chip 2 calcite cluster L-V uGR						
Incl #	T _{Freeze}	T _e	T _{m(ice)}	T _H	Origin/Type	wt%CaCl ₂
cluster 1 1-5	ND	ND	ND	70±5	S/1a	ND
cluster 2 1-6	-100±5	-60±5	-44±1	65±5	S/1 a	30.98
99-107 Chip 1 calcite cluster L-V GR						
Incl #	T _{Freeze}	T _e	T _{m(ice)}	T _H	Origin/Type	wt%CaCl ₂
1	-110±5	-61±5	-36.9±0.1	90±2	S/1a	28.65
2	-95±5	-61±5	-36.9±0.1	90±2	S/1a	28.65
3	-100±5	-61±5	-36.9±0.1	90±2	S/1a	28.65
4	-105±5	-61±5	-36.9±0.1	90±2	S/1a	28.65
5	-95±5	-61±5	-36.9±0.1	90±2	S/1a	28.65
6	-95±5	-61±5	-36.9±0.1	90±2	S/1a	28.65

99-107 Chip 1 calcite cluster L-V GR						
7	-110±5	-61±5	-36.9±0.1	90±2	S/1a	28.65
99-120 Chip 1 saddle dolomite L-V uBob						
Incl #	T _{Freeze}	T _e	T _{m(ice)}	T _H	Origin/Type	wt%CaCl ₂
Single 1	-93.8±1	-53±10	-38.9±0.1	90.4±0.1	PS/1a	29.34
cluster 1 incl 1	-83.8±0.1	-55±10	-40.9±0.1	100.7±0.1	PS/1a	30.01
cluster 1 incl 2	ND	ND	ND	100.7±0.1	PS/1a	ND
cluster 1 incl 3	ND	ND	ND	100.7±0.1	PS/1a	ND
could only see largest of the three freeze and melt clearly. All had identical Th						
99-120 Chip 3 saddle dolomite growth rim L-V uBob						
Incl #	T _{Freeze}	T _e	T _{m(ice)}	T _H	Origin/Type	wt%CaCl ₂
1	-85±5	-55±5	-41.1±0.1	137±3	S/1a	30.07
2	-79±1	-56±5	-41±0.1	109±3	S/1a	30.04
3	ND	ND	ND	83±2	P/1a	ND
99-132 Chip 1 calcite cluster L-only lBob						
Incl #	T _{Freeze}	T _e	T _{m(ice)}	T _H	Origin/Type	wt%CaCl ₂
1-15	-50±5	-35±5	-0.5±0.1	ND	S/2b	1.19
99-132 Chip 2 calcite cluster L-only lBob						
Incl #	T _{Freeze}	T _e	T _{m(ice)}	T _H	Origin/Type	wt%CaCl ₂
1-15	-50±5	-35±2	-1.2±0.2	ND	S/2b	2.68
99-134 Chip 1 calcite L-V lBob						
Incl #	T _{Freeze}	T _e	T _{m(ice)}	T _H	Origin/Type	wt%CaCl ₂
1	~-100±10	~-60±10	~-40±10	85±5	S/1a	~29
99-134 Chip 2 calcite L-only lBob						
Incl #	T _{Freeze}	T _e	T _{m(ice)}	T _H	Origin/Type	wt%CaCl ₂
1 and 2	ND	ND	ND	85 ±5	S/1a	ND
3	ND	ND	ND	>200	Indeter/1b (?)	ND
4	ND	ND	ND	150 ±10	Indeter/1a	ND